Characterization of Neuromuscular Disorders Using Quantitative Electromyographic Techniques

by

Meena AbdelMaseeh Adly Fouad

A thesis
presented to the University of Waterloo
in fulfilment of the
thesis requirement for the degree of
Doctor of Philosophy
in
Systems Design Engineering

Waterloo, Ontario, Canada, 2016

I hereby declare that I am the sole author of this thesis. This is a true copy of the thesis, including any required final revisions, as accepted by my examiners.

I understand that my thesis may be made electronically available to the public.

Abstract

This thesis presents a multifaceted effort to develop a system that allows electrodiagnostic clinicians to perform a quantitative analysis of needle detected electromyographic (EMG) signals for characterization of neuromuscular disorders. Currently, the most widely adopted practise for evaluation of patients with suspected neuromuscular disorders is based on qualitative visual and auditory assessment of EMG signals. The resulting characterizations from this qualitative assessment are criticized for being subjective and highly dependent on the skill and experience of the examiner.

The proposed system can be decomposed functionally into three stages: (1) *extracting* relevant information from the EMG signals, (2) *representing* the extracted information in formats suitable for qualitative, semi-quantitative and quantitative assessment, and (3) *supporting* the clinical decision, i.e., characterizing the examined muscle by estimating the likelihood of it being affected by a specific category of neuromuscular disorders.

The main contribution of the thesis to the extraction stage is the development of an automated decomposition algorithm specifically tailored for characterization of neuromuscular disorders. The algorithm focuses on identifying as many representative motor unit potential trains as possible in times comparable to the times needed to complete a qualitative assessment. The identified trains are shown to reliably capture important aspects of the motor unit potential morphology and morphological stability.

With regards to the representation stage, the thesis proposes ten new quantitative EMG features that are shown to be discriminative among the different disease categories. Along with eight traditional features, the features can be grouped into subsets, where each subset reflects a different aspect of the underlying motor unit structure and/or function. A muscle characterization obtained using a feature set in which every relevant aspect is included using the most representative feature is more structured, simple, and generalizable. All the investigated features are clinically relevant. An examiner can easily validate their values by visual inspection; interpret them from an anatomical, physiological, and pathological basis; and is aware of their limitations and dependence on the acquisition setup.

The second main contribution to the representation stage is the evaluation of the possibility of detecting neurogenic disorders using a newly proposed set of quantitative features

describing the firing patterns of the identified motor units. The last contribution to the representation stage is the development of novel methods that allow an examiner to detect contributions from fibres close to the detection surface of a needle electrode and to track them across a motor unit potential train.

The work in this thesis related to the decision support stage aims at improving existing methods for obtaining transparent muscle characterization. Transparent methods do not only estimate the likelihood of the muscle being affected by a specific disorder, but also induce a set of rules explaining the likelihood estimates. The results presented in this thesis show that remodelling the characterization problem using an appropriate binarization mapping can overcome the decrease in accuracy associated with quantizing features, which is used to induce transparency rules.

To attain the above mentioned objectives, different signal processing and machine learning methods are utilized and extended. This includes spectral clustering, Savitzky-Golay filtering, dynamic time warping, support vector machines, classification based on event association rules and Gaussian mixture models. The performance of the proposed methods has been evaluated with four different sets of examined limb muscles (342 muscles in total). Also, it has been evaluated using simulated EMG signals calculated using physiologically and anatomically sound models. A system capable of achieving the aforementioned objectives is expected to promote further clinical adoption of quantitative electromyographic techniques. These techniques have potential advantages over existing qualitative assessments including resolving equivocal cases, formalizing communication and evaluating prognosis.

Acknowledgements

First of all, I would like to express sincere appreciation to my adviser, Professor Daniel William Stashuk, for the opportunity he gave me to do research in the field of neuromuscular disorders. Professor Stashuk continually supported, guided and encouraged me. He carefully revised my results, reports and papers providing an insightful feedback. Without his persistent help, this work would have not been possible.

Professor Stashuk has also been a great career adviser. We were working together on a daily basis. His professionalism, enthusiasm and dedication have a lasting effect on me. During my PhD, he initiated and supported my engagement with two different industrial partners. This greatly enriched my PhD experience.

A thank you to my laboratory partner, Tsu-Wei Chen. I learnt a lot from the discussions I had with him. I always found working with him to be fun and fruitful.

A thank you to Professor Benn Smith of Mayo Clinic, for acquiring and annotating the clinical signals used in this thesis. I have also benefited significantly from his broad knowledge and encouraging research attitude.

A thank you to Professor Tim Doherty for his advice and assistance. He helped me appreciate the clinical utility of quantitative electromyographic techniques, and realize the impact of my research to the full.

My gratitude goes to the administrative staff of System Design Engineering department and the graduate studies office. In particular, many thanks to Vicky Lawrence and Janine Blair. They helped me sort out many dwelling situations.

I am deeply indebted to my parents, Beshoy and Sally for their support and love throughout my Ph.D. studies.

Dedication

To Nadia Rady
I am my mother's son.

Table of Contents

List of Tables

xiv

List of Figures

Abbreviations

μS	Microsecond
μV	Microvolt
	-A-
Amp	Amplitude
ANN	Artificial Neural Network
ANR	Amplitude to Noise Ratio
Ar	Area
AUC	Area under curve
avg	average
	-B-
BFS	Backward Feature Selection Algorithm
BJig	B Jiggle
	-C-
CI	Confidence Interval
Cont.MFR	Contraction Mean of Firing Rates
Cont.Range	Contraction Range of Firing Rates
Cont.SFR	Contraction Sum of Firing Rates
	-D-
DAG	Directed Acyclic Graph
DDAG	Decision Directed Acyclic Graph
DLT	Deltoid
DNA	Deoxyribonucleic acid
DQEMG	Decomposition Based Quantitative Electromyography

DTW	Dynamic Time Warping
Dur	Duration

<div align="center">-E-</div>

EAR	Event Association Rules
EFE	Error Filtered Estimation
EMG	Electromyographic

<div align="center">-F-</div>

FbrCnt	Fibre Count
FDI	First Dorsal Interosseous

<div align="center">-G-</div>

G.Cmpl	Global Complexity
GMM	Gaussian Mixture Model

<div align="center">-H-</div>

Hz	Hertz

<div align="center">-I-</div>

IDI	Interdischarge interval
IRB	Institutional Review Board

<div align="center">-K-</div>

KΩ	Kilo Ohms
KV	Kilo Volts
KNN	K-nearest neighbours

<div align="center">-L-</div>

L.Cmpl	Local Complexity
LB	Lower Bound
Ln	MUP Length
LnInd	Length Index
LOOCV	Leave One Out Cross Validation

<div align="center">-M-</div>

MFAP	Muscle Fibre Action Potential
MFP	Muscle Fibre Potential
mm	Millimetre

ms	Millisecond
MUP	Motor Unit Potential
MUPT	Motor Unit Potential Train
	-N-
NF	Near Fibre
NF-MUP	Near-Fibre MUP
NMD	Neuromuscular Disorders
	-O-
OAA	One-Against-All
	-P-
Ph	Number of Phases
PhAr	Phase Area
PhCmpl	Phase Complexity
PWC	Pairwise Coupling
PWD	Pairwise Decomposition
PWR	Pairwise Resemblance
	-Q-
QEMG	Quantitative Electromyographic
	-R-
RBF	Radial Basis Function
RDTW	Regional Dynamic Time Warping
RIR	Relative Irregularity Coefficient
	-S-
s	Second
SFEMG	Single Fibre EMG
SFS	Statistical Forward Feature Selection Algorithm
SG Filter	Savitzky-Golay Filter
ShmCov	Shimmer Covariance
ShpWdth	Shape Width
STBC	Shape and Temporal Based Clustering Algorithm
SVM	Support Vector Machine

	-T-
TA	Tiblias Anterior
Thk	MUP Thickness
Tr	Number of Turns
TrAmp	Turn Amplitude
TrAr	Turn Area
TrLn	Turn Length
	-V-
V	Volt
VM	Vastus Medialis
	-W-
WOE	Weight of Evidence
	-Z-
ZPC	Zero-shift Pseudo-correlation

Chapter 1

Introduction

1.1 Summary

This chapter presents the main objective of the research carried out for this thesis, namely improving the clinical utility of quantitative electromyographic (EMG) techniques. The chapter also lists the design constraints and goals underlying the development of the methods described in this thesis.

A brief review of the basics of muscle physiology, neuromuscular disorders, needle electromyography, and quantitative EMG techniques is presented. Understanding these basics allows a greater appreciation of and insight into the methods presented in the following chapters.

1.2 Objectives

Neuromuscular disorder (NMD) is a broad term used to refer to more than 40 different diseases that affect the muscles and/or their direct nervous system control [105]. Most of these diseases are rare, complex and incurable. Some of them, such as amyotrophic lateral sclerosis, are debilitating or even fatal [88].

While confirming a diagnosis of a NMD often involves physical evaluation, DNA analysis, muscle biopsy, and different electrodiagnostic tests, needle electromyography is the gold standard methodology for assessing NMDs. This can be attributed to the high temporal and spatial resolution of the information obtained, which are necessary for the detection of lesions, fibre depletion, and reinnervation [24].

The most widely accepted clinical practise for assessing needle-detected EMG signals relies on the auditory and visual capabilities of the examiner to detect disease-induced changes qualitatively. This qualitative assessment is highly dependent on the examiner's skill and experience, and has a limited or no ability for reporting and tracking longitudinal changes. Research has suggested that assessment based on quantitative techniques has the potential to be more specific and sensitive than qualitative assessment [84]. Moreover, important clinical information, such as neuromuscular junction stability and muscle fibre conduction velocities, can be only obtained using quantitative techniques.

The research presented in this thesis aims at improving the clinical utility of quantitative electromyographic (QEMG) techniques. To this end, this thesis describes the development of a system that allows electrodiagnostic clinicians to perform quantitative analysis of EMG signals for characterization of NMDs. For the system to be clinically viable, it needs to fulfil the following requirements:

- Informative: It should identify clinically relevant information from the EMG signal and present it through a set of visualizations that can be readily appreciated and validated by the examiner.

- Precise: It should be able to describe the identified information using a set of feature estimates that are not sensitive to noise and acquisition protocol and/or setup.

- Decisive: A muscle characterization should be induced based on the extracted quantitative features. These characterizations are to be used by the examiner as a basis of the diagnosis.

- Accurate: These characterizations should be consistent with an expert evaluation and conforming to the results obtained from other examinations.

- Transparent: Different system outputs, namely visualizations, quantitative features and muscle characterizations should be validated by the examiners. Examiners should also appreciate their clinical relevance and interpret their estimates based on their expectation of disease-induced changes on the muscle function and structure.

- Sensitive: The characterizations should be indicative of the disease involvement and discriminative across different NMDs.

- Fast: The system shall be capable of reaching results in a time span comparable to the time needed to complete a qualitative analysis.

The direct implication of these improvements is to increase the diagnostic power of QEMG techniques. The availability of visualizations, quantitative features, and muscle characterizations that can be automatically obtained will motivate further utilization of QEMG techniques for NMD assessment and other specialities such as senior care, rehabilitation, sport medicine, and pain management.

1.3   Background

A proper formulation of a diagnosis of a NMD through either qualitative or quantitative assessment of EMG signals should be based on interpreting extracted information using anatomical, physiological and pathological reasoning [30]. This section describes the processes underlying the generation of EMG signals and the effects of NMDs.

Unless otherwise mentioned, the term "EMG signal" will be used to refer to electromyographic signals as detected using a concentric needle electrode placed in the extracellular space of a muscle performing a low to moderate isometric contraction.

The contraction of a *muscle fibre* requires the propagation of transmembrane *muscle fibre action potential (MFAP)* along its axis. The properties of the MFAP mainly depend on fibre diameter and the velocity at which the MFAP propagates [83]. While, the properties of an extracellularly detected signal, referred to as *muscle fibre potential (MFP)*, in addition

depends on electrode geometry, the relative position of the muscle fibre to the detection surface of the electrode and the extracellular conducting medium.

The fibres comprising a given muscle are grouped into *motor units*. A motor unit is comprised of an alpha *motor neuron* and the muscle fibres that the motor neuron innervates. In a normal muscle, when a motor neuron fires, all the muscle fibres belonging to the motor unit are expected to contract. A group of motor units need to be recruited and they must fire repeatedly for a muscle to maintain a contraction.

The size principle explains which motor units are recruited at which contraction levels [55]. The principle states that smaller motor units, i.e., those spanning smaller cross sectional area, are recruited earlier. As the level of contraction increases, the recruited motor units fire more often (up to a certain limit) and larger motor units get recruited. The motor unit is therefore considered to be the functional output component of the neuromuscular system, since the relative amount of force generated by a muscle depends on how many motor units are recruited and their firing rates.

The motor unit potential (MUP) is defined as the extracellular signal detected by an electrode when a motor unit is activated. The MUP is the result of the summation of the MFPs produced by fibres of the motor unit. The sequence of MUPs generated by the repetitive activation of a given motor unit is called a *motor unit potential train (MUPT)*.

The morphology of MUPs of the same MUPT, i.e., MUPs created by the repetitive activations of the same motor unit, are expected to vary across different activations of the motor unit due to variability of the MFAP initiation times and conduction velocities, instrumentation noise and electrode movement.

NMDs result from different disease processes, such as inflammatory, metabolic and endocrine, affecting motor neurons, neuromuscular junctions, or muscle fibres. Still, NMDs can be broadly grouped as either *neurogenic* or *myopathic*.

- **Myopathic disorders** are a group of disorders linked to muscle fibre dysfunction. The most common EMG manifestations associated with myopathies can be summarized as:

  1. Smaller MUPs due to muscle fibre loss

2. Complex and dispersed MUPs due to the higher diameter variability of muscle fibres belonging to the same motor unit resulting from muscle fibre atrophy and hypertrophy

3. Earlier recruitment of motor units and elevated mean firing rates to compensate for motor unit weakness caused by muscle fibre loss.

- **Neurogenic disorders** are mainly caused by loss of motor neurons. Axonal sprouts of near surviving motor neurons often reinnervate some of the deinnervated muscle fibres. The most common EMG manifestations associated with neurogenic disorders can be summarized as:

  1. Large MUPs due to reinnervation

  2. Complex MUPs since the muscle fibres belonging to an affected motor unit will have a wider range of diameters compared to a normal motor unit

  3. Satellite MFPs due to delayed initiation of MFAPs in reinnervated muscle fibres

  4. Morphological instability due to inconsistency of the activation transmission across newly formed neuromuscular junctions

  5. Delayed recruitment of motor units and reduced mean firing rates as less motor units are required to attain the same contraction level, given that reinnervation leads to motor units having more muscle fibres which are therefore capable of producing more tension.

The grouping of NMDs as either neurogenic or myopathic provides a generic framework that is useful in predicting disease-induced changes in the neuromuscular structure and/or function from EMG manifestations. This grouping of NMDs is adopted in this research. This means that the collected EMG studies used in this work are not annotated by an experienced examiner to be affected with specific disorders but rather whether they are normal, myopathic or neurogenic.

Moreover, the utility of QEMG features or characterization will be equated to how indicative they are of a category of disorders rather than a specific disorder. However, it should be noted that some observed disorders can be associated with both myopathic and neurogenic processes.

1.4   System Overview

Figure 2.2 presents the information flow of the system presented in this thesis. The system can be decomposed functionally into three main steps: (1) Information extraction, (2) Information representation, and (3) Decision support.
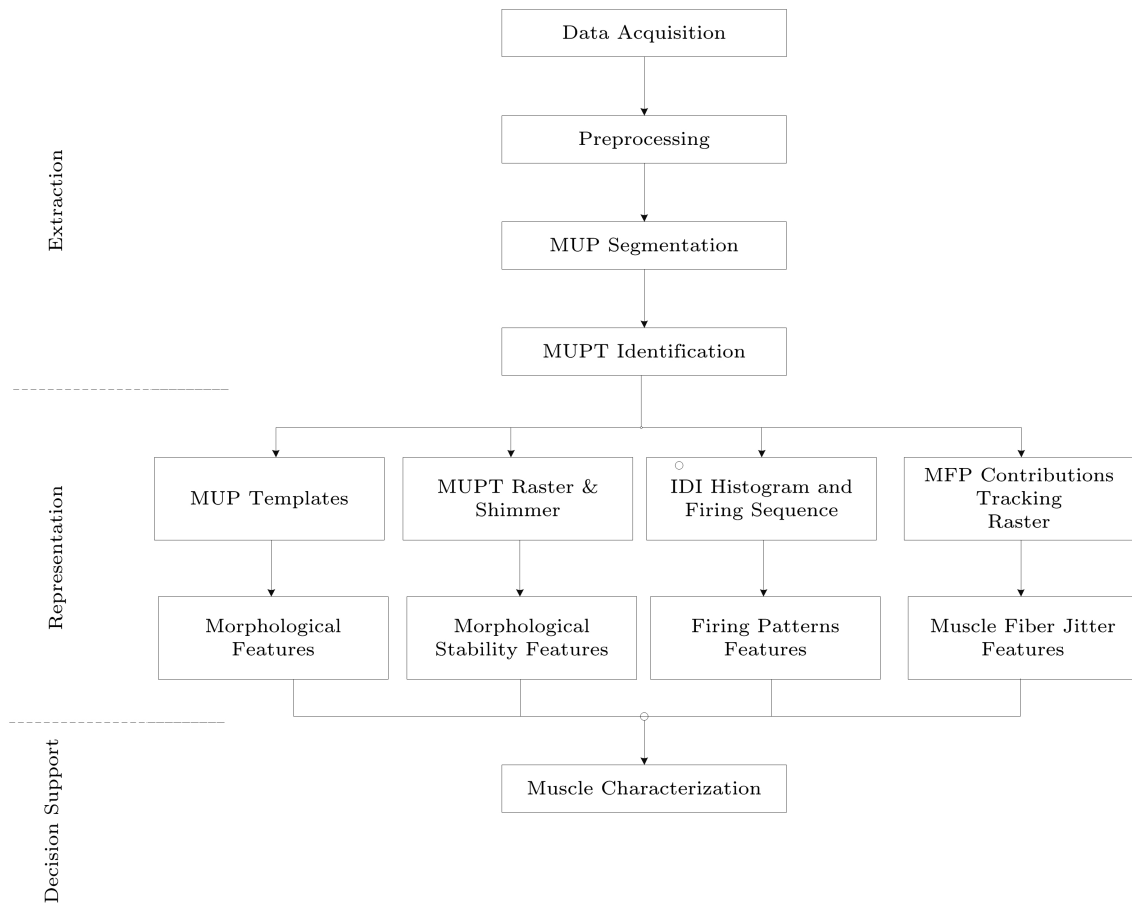
Figure 1.1: The information flow in a system capable of quantitatively analyzing an EMG signal for characterization of neuromuscular disorders

1.4.1 Extraction

Data Acquisition

The first stage of the system is the acquisition of intramuscular EMG signals using a concentric needle electrode during a voluntary, isometric, and low to moderate level contraction. It is important to emphasize here that the development of a system for quantitative analysis starts by defining an acquisition protocol.

The number of pulses per second is among the most important parameters to be specified in the protocol. In a proper acquisition setup, this parameter is correlated to the contraction level. This parameter also controls the trade-off between the information yield (i.e., the number of MUPTs to be identified from a single contraction) and the MUPTs' representativeness (i.e., the probability that the segmented MUPs are not superimposed by contributions from other motor units).

Another important parameter is the sharpness of the detected MUPs. Sharpness is mainly influenced by electrode focusing, i.e., the closeness of the electrode to the muscle fibres. Contributions from distant motor units are mainly comprised of low frequency components that obscure disease-induced morphological changes.

Preprocessing

The main objective of this stage is to accentuate the electrophysiological components of interest, i.e., to make MUPs as distinguishable as possible compared to instrumentation noise and/or contribution from other motor units. Other objective of this stage is to calculate rudimentary signal quality metrics to help the examiner asses the EMG signals utility and modify the electrode position accordingly.

Motor Unit Potential Segmentation

MUP morphology is expected to vary across different motor units depending on their muscle fibre compositions, levels of disease involvement and positions relative to the detection

7

surface of the electrode. In spite of this variability, some morphological characteristics, such as sharpness, duration and amplitude, are expected to maintain values within specific ranges distinguishable from noise and background activity. Many detection algorithms, such as the one discussed in [92], are based on calculating and thresholding these characteristics.

Other techniques, such as [70], are based on the observation that MUPs are temporally constrained, and have relatively high energy compared to the background activity. Such techniques attempt to adaptively estimate statistical characteristics capturing the background activity, and a MUP is detected whenever there is a statistically significant deviation.

Motor Unit Potential Train Identification

In this stage, a subset of detected MUPs are clustered into MUPTs, based on morphological similarity and firing pattern statistics. In this work, a partial rather than a complete decomposition is assumed. This means that there is no attempt to segment each MUP and assign it to a MUPT. Instead, partial decomposition attempts to extract MUPTs that can be identified with confidence, and are useful for characterization of NMDs. This streamlines MUP detection and MUPT identification eliminating the need to resolve superimposed MUPs or identify MUPTs that are not consistently active throughout the contraction.

1.4.2   Representation

Clinical Data Visualization

The aim of this sub-stage is to validate, summarize and present the information extracted from the MUP detection and MUPT identification stages. Various representations should be in formats that can be easily assessed both qualitatively and quantitatively.

For example, the typical morphology of the MUPs belonging to the same MUPT is captured through estimation of a template. The use of a template has the potential of decreasing noise and contributions from other motor units.

Another example is the MUPT raster, which is a display of a selected set of isolated MUPs of a given MUPT after being aligned and stacked. MUPT raster plots are useful for evaluating morphological instability across MUPs of the same MUPT. Another visualization is a histogram of inter discharge intervals (IDIs) to represent the temporal sequences of identified motor unit firings.

Quantitative Electromyographic Features

The output of this sub-stage is a set of quantitative features describing different visualization provided by the previous sub-stage such as features describing a MUP template, MUPT raster, or motor unit firings IDIs histogram. The author prefers to keep visualization and feature extraction as two different sub-stages, because the outputs of the clinical data visualization sub-stage might also be used for qualitative or semi-quantitative assessment.

1.4.3 Decision Support

The main objective of this stage is to use a subset of quantitative features calculated in the previous stage to estimate the likelihood of the muscle being affected by a specific category of NMD transparently, meaning that a set of transparency rules needs to be also induced to explain the likelihood estimates.

1.5 Thesis Organization

The thesis outline follows the basic structure of the information flow described in the previous section. The title of each chapter indicates whether it discusses information extraction, information representation, or decision support stages. Chapter 2 is primarily about the information extraction stage. Different digital signal processing and machine learning algorithms are presented which enable (1) preprocessing EMG signals, (2) segmenting MUPs, and (3) identifying MUPTs.

The information representation stage is studied and extended in the following three chapters. Chapter 3 focuses on quantitative features that describes MUP morphology and morphological stability across MUPs belonging to the same train. The chapter introduces new features that are shown to be discriminative across different disease categories. It also presents a grouping of features based on what aspect of the MUP morphology they describe. Each of these aspects can be linked to a different effect of neuromuscular disorder on muscle structure and function.

Chapter 4 proposes a new quantitative EMG feature called near fibre MUP Jitter. Similar to the conventional single fibre EMG based jitter, the feature aims at capturing disturbances in the neuromuscular junction function. The key difference between the newly proposed feature and the conventional jitter is that it is to be estimated from an automatically decomposed EMG signals. The signal acquisition and analysis involved in estimating near fibre MUP Jitter are significantly faster. The whole test can be completed in order of few seconds compared to tens of minutes necessary to complete the conventional single fibre EMG analysis. Also, the process does not demand expertise beyond that are necessary for completing a conventional clinical EMG test.

Chapter 5 investigates the possibility of detecting neurogenic disorders using quantitative features describing the firing patterns of a set of concurrently active motor units. The proposed features circumvent many limitations of the current clinical acquisition setup including incomplete decomposition and having the contraction level not measured nor controlled.

Contributions of the thesis to the decision support stage are discussed in Chapter 6. The problem of obtaining transparent muscle characterizations is remodelled using ten different binarization mappings. The aim of the chapter is to mitigate the decrease in categorization accuracy resulting from feature quantization and to obtain transparency rules that are more clinically relevant. In Chapter 7, the main results and contributions are summarized and discussed. Finally, the thesis concludes by discussing future directions of research efforts with respect to quantitative EMG techniques for characterization of neuromuscular disorders.

For ease of reference, each following chapter has its own literature review section. This

makes it easier for the reader to see how the newly proposed ideas in each chapter fit in and add to the current state of knowledge.

Chapter 2

Extraction: An Automated Decomposition Algorithm of Electromyographic Signals Tailored for Characterization of Neuromuscular Disorders

2.1 Summary

Objective: This chapter describes the development of methods capable of decomposing EMG signals recorded by a concentric needle electrode during a low to moderate isometric contraction. The system is specifically tailored for characterization of neuromuscular disorders. It focuses on identifying representative MUPTs that can capture disease induced changes.

Methods: The signals are smoothed using a Savitsky-Golay filter whose parameters are tuned based on the Durbin-Watson criterion. Segmenting MUPs from the composite signal starts by estimating the characteristics of the baseline activity. This is followed by finding peaks and evaluating the morphology of isolated MUPs.

Each of the potentially isolated segmented MUPs is set to be a node in a similarity graph. The edges in the graph are added based on morphological similarity as evaluated using dynamic time warping and firing times. A spectral analysis of the similarity graph is then utilized to perform clustering.

Results: The methods are validated and evaluated using simulated signals produced using electro-physiologically sound models. A set of performance measures are also presented to quantify different potential errors in the decomposition. The results show that a high yield of representative MUPTs can be identified accurately and automatically in times comparable to times required to complete qualitative clinical analysis.

2.2 Introduction

The term decomposition of EMG signals has been used in the literature to refer to a range of manual procedures and computational algorithms that resolve an EMG signal into its constituent MUPTs. This resolution allows researchers and clinicians to extract, from what seems to be a random signal, fine and essential details regarding muscle anatomy and electro-physiology. Decomposition is also the gateway to investigate the neurodynamics underlying muscle control.

Identification of MUPTs for characterization of neuromuscular disorders can be con-

sidered as an application tuned, special case of the EMG signal decomposition problem. In general, the results obtained from decomposing EMG signals can be potentially utilized for a wide variety of applications including investigation of neural mechanisms [26], control of prosthetic limbs [36], ergonomic studies [39], and many others.

Each of these applications imposes its own set of constraints and requirements on the design of the instrumentation, acquisition protocol, and analysis algorithms adopted in the decomposition process. The main objective of the presented work is to increase the clinical utility of decomposition-based EMG quantitative methods for characterization of neuromuscular disorders.

To this end, a method for MUPT identification for characterization of neuromuscular disorders was developed that possess the following characteristics:

- **Representative Sampling:** The identified MUPTs should include important aspects of MUP morphology and morphological stability that are useful for discrimination among different disease categories [6]. For example, MUPTs generated by motor units with fibres that are all distant from the detection surfaces of the electrode or from motor units that are active only briefly during acquisition should be excluded.

- **Fast:** The results should be obtained in times comparable to the times needed to complete a clinical qualitative characterization. This entails focusing only on extracting clinically relevant information, using computationally efficient algorithms, and producing results that need no or minimal manual editing.

- **Clinically Feasible:** The method should rely on acquisition instrumentation that are currently available in a conventional electro-diagnostic laboratory. The most commonly used electrodes are the standard concentric and monopolar electrodes [24]. Both of them are single channel intramuscular electrodes.

- **Unbiased Estimate:** The decomposition algorithms should not produce systematic errors resulting in a biased estimate of MUPT quantitative features. An example of such would be consistently not associating a satellite MFP with its MUP resulting in a lower estimate of morphological complexity.

14

- **High yield:** The decomposition algorithms should identify as many representative MUPTs as possible from each EMG signal recorded at each needle position.

- **Partial decomposition:** There is no need for a complete decomposition [119], i.e. attempting to identify every firing of each active motor unit with fibres close to the electrode detection surface. The level of contraction is not maintained nor measured in a conventional clinical electrodiagnostic examination. It is therefore not possible to attribute detailed aspects of motor unit firing patterns to pathology. In addition, methods such as [130] and [85] can robustly estimate firing pattern statistics from incomplete firing sequences with erroneously assigned firings. These statistics were shown to be useful in detecting neuropathy [4]. The main advantage of doing partial rather than complete decomposition is that it saves time and the uncertainty associated with resolving superimposed MUPs.

- **Invariant to disease induced changes:** MUPTs generated by normal motor units are often more homogeneous and regular in terms of MUP morphology and motor unit firing patterns, compared to those generated by motor units affected by myopathic or neurogenic disorders. A decomposition algorithm used for characterization of neuromuscular disorders should be equally capable of identifying MUPTs generated by normal or disease affected motor units.

2.3 Literature Review

In order to keep this review concise, only automated computer-aided decomposition methods that are designed for the characterization of neuromuscular disorders are considered. The discussion of methods relying on multiple recording sites that are shown to have clinical value [73] is avoided. These methods are very different from an algorithmic perspective. Their clinical feasibility is also questionable, because they need instrumentation that is not currently available in most clinical electrodiagnosic labs.

In the first phase of the system described by Gerber et al. [43], active segments based on an estimate of the total variation in a window surrounding each sample were extracted.

Each of the active segments was then described by a feature vector comprised of five features that mainly captured the morphology of the segment. The nearest neighbour method was then used for clustering. An average of the waveforms of MUPs belonging to each cluster was then used as a MUPT template for subsequent stages and to estimate the morphological features.

The second stage of the system focused on refining the estimated MUPT firing patterns by estimating the MUP firing times, identify the firing times of MUPs that slightly overlap with other MUPs, and resolving superimposed MUPs [131]. The authors tested their methods using a synthetic signal comprised of seven MUPTs (521 MUPs in total) and reported that 98.1% of the MUPs were correctly detected and assigned.

The first step in the ADEMG system described in [76] involved preprocessing the signal using a second order low-pass differentiator [134]. In the second step, the system detected every spike exceeding a given threshold. Each of the spikes then got aligned and interpolated by transforming it using a canonically registered discrete Fourier transform [77]. A matching was then done sequentially using the transformed spikes.

In the third step, ADEMG utilized the intervals between the spikes to (1) merge clusters that corresponded to the same train, (2) identify time locked clusters (expected to be spikes from multiphasic MUPs), and (3) validate MUPTs and the MUPs within the validated trains. ADEMG does not attempt to resolve superimposed MUPs. It was shown in [78] using simultaneous recordings of single fibre EMG signals for evaluation that ADEMG correctly identified between 33% and 98% of MUP firings.

The signal preprocessing and MUP detection in DQEMG [124] were similar to the methods described in ADEMG. The algorithm determined the number of the MUPTs using a modified k-means shape and temporal based clustering algorithm (STBC) [129]. The STBC algorithm was initialized by assuming that the number of number of motor units contributing representative MUPTs was the maximum number of MUPs occurring within any 30 ms of the signal, and used the MUPs occurring in this interval as initial cluster centres. The STBC then used the k-means algorithm to cluster the MUPs based on their morphology. In case, an inconsistency was observed in the firing patterns of the resulting clusters, a new cluster was created. Also during any of the K-means' iterations,

16

the STBC algorithm only kept MUPs that were found to be morphologically similar to the cluster centre.

In the final stage of the STBC algorithm, it iteratively refined the clusters by merging and splitting them. DQEMG then assigned each of the MUPs to one of the identified trains (or decided to exclude it from further processing) in a supervised manner by estimating a certainty measure evaluating its morphological similarity to the train template, whether it was likely to introduce inconsistency to the train firing patterns, and the relative similarity to the second closest MUPT. The algorithm was tested using 10 clinical EMG signals. The average error rate obtained was 2.5 % . 88.7 % of the detected MUPs were assigned to one of the trains.

In EMGTools [87], MUP segmentation relied on estimating the variance of a window surrounding each sample. The algorithm first attempted to find a sample surrounded with a window having a variance above a fairly high threshold to guarantee that it belonged to a MUP. Starting from this sample, it searched for the MUP onset and end using lower thresholds. All the thresholds were extracted adaptively from the signal.

A nearest-neighbour clustering algorithm based on a minimum spanning tree was used for clustering. The distance between a pair of MUPs was calculated as the variance of the difference between the two MUPs after performing a heuristic alignment by matching each of the samples sequentially. A successive iterative approach for resolving MUP superposition was used. The algorithm started by fitting the larger MUP templates to the superimposed segments first. The methods were validated using clinical EMG data by comparing the outputs to manual annotations and evaluating the residual signal after decomposition. The authors also evaluated the proposed methods using simultaneous recordings.

The system proposed by Pattichis et al. in [20] represented each of the candidate MUPs using a fixed length window centred around a peak with an amplitude above an adaptively calculated threshold. The clustering was performed using an artificial neural network. The training of the neural network was achieved in an unsupervised manner using a self-organizing feature map followed by learning vector quantization method [68]. An iterative procedure based on cross-correlation was then used to resolve superimposed MUPs. When

applied to clinical data collected from 40 subjects, the authors reported 97.6% accuracy in discriminating between normal, myopathic and neurogenic MUPs.

One of the main differences between the work described in this chapter and previous reported work in the literature is the use of spectral clustering algorithms. The main advantage of spectral clustering is that it optimizes for the connectivity between instances of a given cluster rather than optimizing for cluster compactness. MUPTs are expected to show both trending and random within-train morphological variability. Figure 2.1 shows every fifth MUP of MUPTs generated by two simulated motor units. In this example, the trending variability is assumed to be due to slow electrode movement. This is simulated by moving the electrode 2 μm in the horizontal direction after every motor unit discharge. The random morphological variations are modelled to be due to the variability in the times needed for the neural signal transduction across each of the muscle fibres' neuromuscular junctions. In this example, these times are assumed to be sampled from a zero mean Gaussian distribution with a standard deviation of 70 μS. Further details regarding the simulation model can be found in Chapter 5 on page 94. The figure shows the clusters obtained by spectral clustering and k-means algorithms. In this example, more miss-assignments are obtained using the k-means algorithm, which can be attributed to the fact that it optimizes for cluster compactness.

The design philosophy behind the methods described in this chapter and how they are evaluated are also different from those discussed in the literature in other aspects including:

- Focusing on extracting only representative MUPTs that can contribute clinically relevant information

- Accommodating for intra-train random morphological variations resulting from neuromuscular junction transmission variability by aligning segmented MUPs based on dynamic time warping (DTW)

- Tuning parameters of the preprocessing algorithm to accommodate for acquisition induced differences in signal characteristics.

- Developing techniques that aim at excluding superimposed MUPs
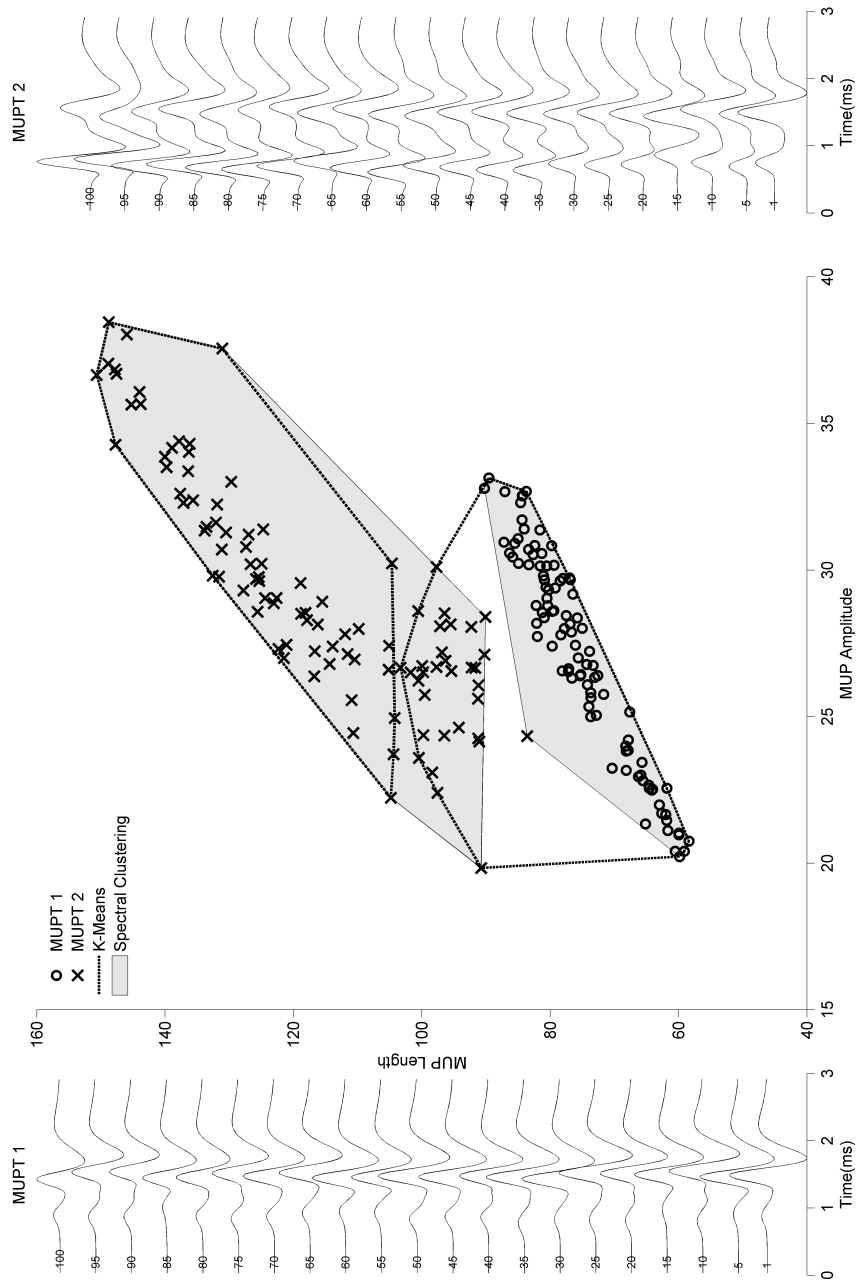
Figure 2.1: The diagram illustrates the advantages of clustering approaches that optimize for the connectivity between the instances of a given cluster rather than the cluster compactness for the MUPT identification problem. The text provides extra details.

- Optimizing for computational and space complexity

- Proposing new evaluation metrics that capture potential errors such as train splitting and merging.

2.4 Methods

Figure 2.2 shows the main steps of the proposed MUPT Identification methods. The steps can be divided into four main stages. The first stage is the data acquisition stage. The details of the recommended acquisition protocol are discussed in Section 3.4.1 on Page 55. For purposes of evaluation, synthetic EMG signals were produced using a physiologically and anatomically sound model. The model is described in greater details in Section 5.4 on Page 97.

The objective of the preprocessing stage is to reduce instrumentation noise and contamination from distant bio-electric sources while maintaining the morphological characteristics of contributions from the active motor units with fibres that are relatively close to the electrode detection surface. The output of the MUP segmentation stage is a set of EMG signals segments that are likely to include isolated MUPs. The last stage of the system is the MUPT identification stage. It aims at estimating the number of concurrently active motor units contributing representative MUPTs. It then assigns each of the segmented MUPs to one of the MUPTs or decides to exclude it.

2.4.1 Pre-processing

The smoothed EMG signal $\tilde{a}(t)$ and its first derivative $\tilde{a}^{(1)}(t)$ are estimated using the traditional Savitzky Golay (SG) filter, which was first proposed in [111]. For each sample at index t, the filter approximates $\tilde{a}(t)$ through fitting a polynomial of an order M_{SG} to L_{SG} equally spaced samples centered at t in a least-squares sense. It was shown in [111] that this local polynomial fitting can be achieved using a discrete convolution with a linear time invariant impulse response.
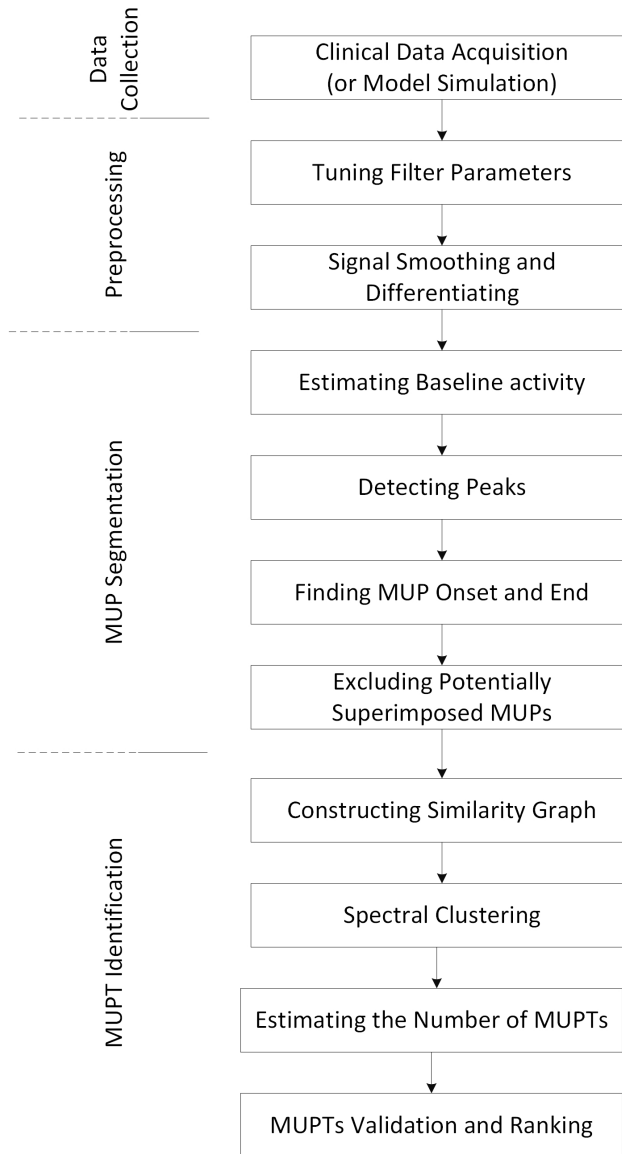
Figure 2.2: The main steps in the proposed MUPT identification method

From the perspective of the SG filter spectral characteristics [112], the choice of M_{SG} and L_{SG} affects the filter cut off frequency, its transition from the pass-band to the stop-band and the attenuation in the stop band. These filter characteristics should be ideally tuned

for each signal independently, as it is expected for EMG signals acquired from different muscles with different degrees of needle focusing and acquisition setups to have different characteristics for both the electro-physiological and noise components.

In this work, the tuning of the SG filter parameters M_{SG} and L_{SG} is performed in a fashion similar to the one described in [135]. The Durbin Watson (DW) criteria [31] is used as an estimate of the information content of $\tilde{x}(t)$ (the raw EMG signal) that is still maintained in $\tilde{a}(t)$.

$$\text{DW} = \frac{\sum_{2}^{t_f} \left(\tilde{\epsilon}(t) - \tilde{\epsilon}(t-1) \right)^2}{\sum_{1}^{t_f} \tilde{\epsilon}(t)}$$

$$\text{where } \tilde{\epsilon}(t) = \tilde{x}(t) - \tilde{a}(t) \text{ and } t_f \text{ is the length of the signal} \quad (2.1)$$

Defining $\rho_{\tilde{\epsilon}}$ as the least-squares estimate of the slope of a first-order linear fit of $\tilde{\epsilon}(t)$ to $\tilde{\epsilon}(t-1)$, The DW, as defined in Equation 2.1, can be shown to be approximately equal to $2(1 - \rho_{\tilde{\epsilon}})$ for long sequences. Therefore as DW approaches two, the consecutive residuals between the smoothed and the raw signal become less correlated. Ending with uncorrelated residuals suggests that the applied filtration removed only noise maintaining the physiological components, which are expected to be serially correlated.

To keep the tuning procedure computationally feasible, the order of the polynomial M_{SG} is fixed to six. The algorithm then searches for the fitting window length L_{SG} minimizing the serial correlation of the residuals. The search starts with $L_{\text{SG}} = M_{\text{SG}}+1$ (if $L_{\text{SG}} < M_{\text{SG}}$, no smoothing will be achieved [112]) and stops with L_{SG} corresponding to a window that is three ms in length. In each step, L_{SG} is incremented by two to make sure that L_{SG} stays odd.

The fixation of M_{SG} might result in not obtaining the best possible DW value. It is still not severely limiting knowing that the same cut-off frequency of the SG filter can be obtained with different combinations of L_{SG} and M_{SG} [112]. In order to make the computation even faster, the tuning is based on seven milliseconds window centred on the

22

highest peak found in the signal. The efficacy of the tuning procedure in maintaining the amplitude and width of MUP peaks is illustrated in Figure 2.3.

In Figure 2.3, the smoothed EMG signals (plotted in solid black) obtained by filtering the same simulated raw EMG signal (plotted in grey) using different L_{SG} values are stacked on the top of each other. Below each signal, a red trace shows the absolute difference between the simulated noise free EMG signal, which can be thought of as the electrophysiological component of the signal, and the smoothed signal.

The filter configuration selected by the tuning procedure resulted in the smoothing shown by the middle trace ($L_{\mathrm{SG}} = 37$), since it is the configuration that resulted in a DW value closest to two for this signal suggesting serially uncorrelated residuals. Compared to the smoothing obtained by $L_{\mathrm{SG}} = 15$, the selected smoothing provided a better reduction of noise. It is also obvious by investigating the difference between the noise free signal and the smoothed signal around the largest peak that the selected filter configuration better maintains the number of turns, amplitudes, and widths of the peaks.

The design process used in obtaining the impulse response of the SG filter readily gives the impulse responses of linear time invariant systems that can be used to estimate a discrete approximation of its derivative up to order $M_{\mathrm{SG}} - 1$ [111]. In this work, the first order and the second order differentiation of $\tilde{a}(t)$ are of particular interest.

2.4.2 Motor Unit Potential Segmentation

The proposed segmentation method operates on the signal in three main steps:

Estimating the characteristics of the baseline activity signal

Even when no motor unit, with fibres close to the detection surface of the electrode, is contributing to the detected signal, a baseline activity signal will be observed. The baseline activity is due to instrumentation noise, contributions from motor units belonging to the same muscle which do not have fibres close to the electrode detection surface and other electrophysiological sources.
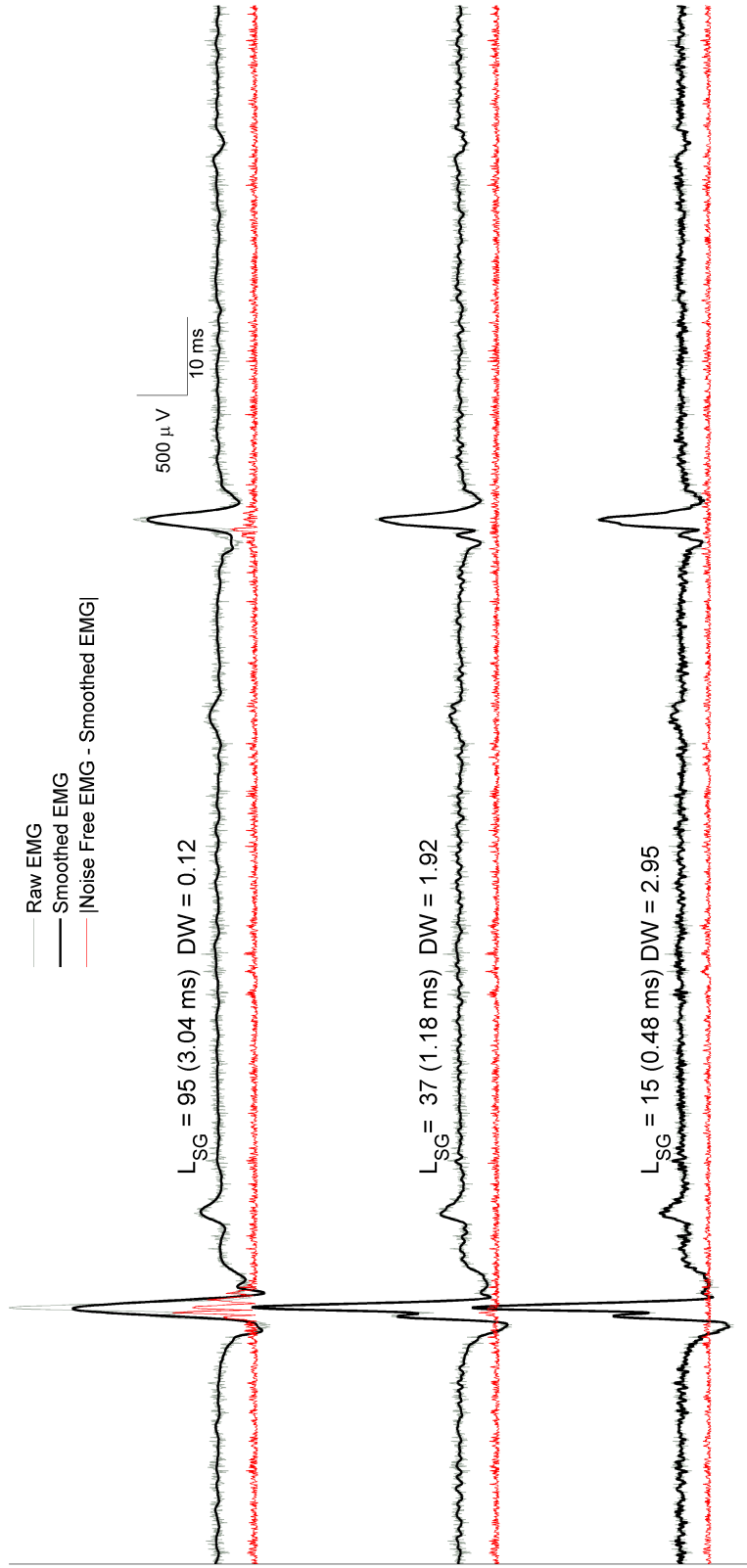
Figure 2.3: The diagram shows an example supporting the efficacy of the procedure used in tuning the SG filter based on the analyzed EMG signal characteristics. Refer to the text for further details.

For an EMG signal acquired using a well controlled setup during a brief (a few seconds) isometric contraction, the characteristics of the baseline activity can be assumed to be fairly constant throughout the duration of the signal. Given this assumption, the characteristics of the baseline activity signal can be estimated by searching for periods within the EMG signal that have no MUPs.

For each sample of an index t, the signal $\tilde{u}(t)$ is estimated by calculating the standard deviation of a window spanning from $t-\tau_A$ to t. τ_A is the analysis window length in samples, and, unless otherwise mentioned, τ_A is chosen so that the window length corresponds to ten milliseconds worth of the signal. The standard deviation of the baseline activity of the raw signal σ_x was estimated to be the mean value of the lowest ten values of $\tilde{u}(t)$. Applying the same procedure to the smoothed signal, the standard deviation of the baseline activity of the smoothed signal σ_a is also estimated.

Detecting Peaks

The algorithm starts by finding all local maxima and minima in the pre-processed signal by searching for a change in the sign in its first derivative signal $\tilde{a}^{(1)}(t)$. A peak is then detected at a sample of index t, if a local maximum is found at t with the following characteristics:

1. $\tilde{a}(t)$ has an amplitude of at least $\lambda_A \sigma_x (\mu V)$. λ_A is the peak amplitude threshold factor. Note that σ_x, and not σ_a, is used for peak detection threshold, even when the threshold is applied to the pre-processed signal. This is to make sure that the detected peak is significantly higher than the actual background activity signal as observed in the raw data, irrespective to the level of smoothing that may be applied during the pre-processing stage.

2. $\tilde{a}(t)$ is at least $\lambda_S \sigma_x$ (μV) higher in amplitude than all surrounding local minima. λ_S is the peak separation threshold factor. A surrounding local minimum to a local maximum is defined as a local minimum that either precedes or follows the local maximum with no other local maxima in between with an amplitude above $\lambda_A \sigma_x$.

The default value for both λ_A and λ_S is three.

Finding the MUP onset and end

The algorithm then proceeds by attempting to detect inactive periods within the signal. A window of a length τ_I samples is assumed to be in-active, when a Δ_I percentage of the number of the samples of the smoothed signal $\tilde{a}(t)$ within the window are found to have an amplitude below $\lambda_I \sigma_a$. Δ_I is the inactivity window length ratio, while λ_I is the inactivity amplitude limit factor. The values for Δ_I and λ_I used in this chapter are 90% and two respectively. τ_I is set to be the same length as τ_A.

It is important to detect the onset and end of a MUP carefully to make sure that the estimates of the quantitative features such as MUP duration, length and area are not systematically biased. Therefore for each sample of an index t, a binary left inactivity indicator $I_{Le}(t)$ signals whether a window from $t - \tau_I$ to t is found to be inactive or not. A transition of $I_{Le}(t)$ from 0 (active) to 1 (inactive) suggests a candidate MUP onset.

In a similar manner, a binary right inactivity indicator $I_{Ri}(t)$ is defined over a window ranging from t to $t + \tau$. In this case, a transition from 0 (active) to 1 (inactive) suggests a candidate MUP end. A MUP is assumed to be detected between a candidate MUP onset and an immediately following candidate MUP end, if one or more peaks are found in between them.

Excluding Potentially Superimposed MUPs

The objective of this sub-stage is to exclude potentially superimposed MUPs. The morphology of superimposed MUPs often, but not necessarily always, is different compared to the morphology of isolated MUPs. An example of such differences is the existence of two peaks within a single MUP (not separated by inactivity) that are separated widely.

The algorithm proceeds by calculating the inter peak intervals between every two consecutive peaks within a segmented MUP. If any of the intervals is found to be above a threshold Λ, the algorithm assumes that the two peaks are contributed by two different motor units. The resulting MUP is then labelled as potentially superimposed. As will be explained later, the MUPT identification algorithm does not assign potentially superimposed MUPs during the identification stage.

Note that the algorithm at this stage does not have any prior information regarding the morphology of the MUPs in the examined signal. Therefore the rules applied at this stage are capturing domain knowledge for the limits of what can be considered as an isolated MUP morphology. This stage can be extended by applying rules limiting the amplitude, duration, or number of turns that can be accepted. An example showing the application of the MUP segmentation algorithm to a simulated signal is illustrated in Figure 2.4. The algorithm starts by estimating the characteristics of the baseline activity and uses these estimates to set thresholds necessary for peak detection ($\lambda_A * \sigma_x$ plotted as a blue dashed line in the upper panel) and finding the MUP onset and end ($\lambda_I * \sigma_a$ plotted as a red dashed line in the upper panel).

Around the 25 ms mark, the algorithm segments a MUP (shaded in green) by detecting a peak in between a candidate MUP onset and end. The candidate onset is assumed due to a transition of the left activity indicator I_{Le} (plotted in the lower panel) from inactive to active. While, the candidate MUP end is assumed due to a transition of the right activity indicator I_{Ri} from active to inactive. A similar scenario occurs around the 75 ms mark. However in this case, the algorithm decides that this is a potentially superimposed MUP because the MUP has an inter peak interval that is above Λ, which is set to have a default value of three microseconds.

The last sub-stage in the MUP segmentation is to represent the potentially isolated segmented MUPs in a format that can be processed by later stages. This includes an initial alignment and zero padding of the MUPs. A matrix $\tilde{Y}$ of size $N_{\mathrm{IMUP}} \times L_{\mathrm{IMUP}}$ is constructed. N_{IMUP} is the number of the MUPs segmented and assumed to be isolated, while L_{IMUP} is the preset maximum length of each MUP (15 ms in this work).

Each row of the matrix $\tilde{Y}$ represents a different segmented MUP. The peak of each MUP is aligned to $L_{\mathrm{IMUP}}/2$. This results in the segmented MUPs being initially aligned by their peaks. As will be further explained in the following section, this initial alignment is necessary to make constrained DTW alignment more effective. In case the MUP length is less than L_{IMUP}, the row is padded by zeros at both ends.
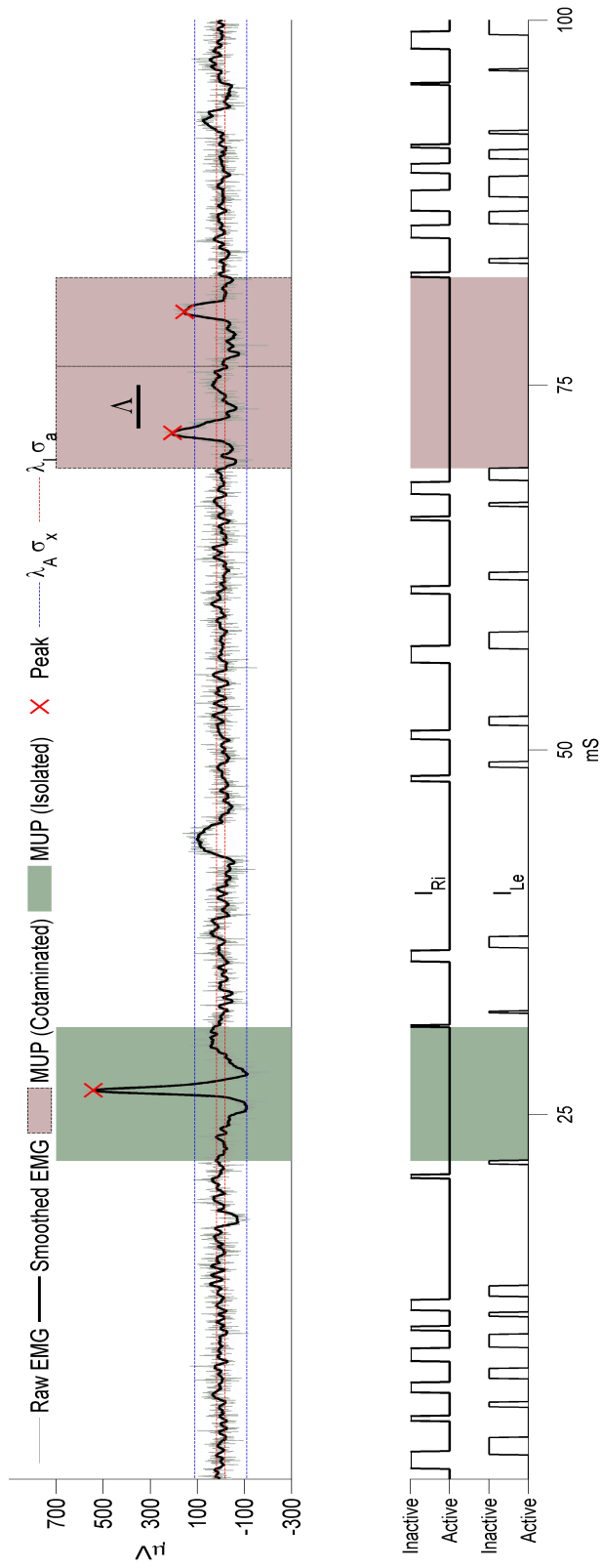
Figure 2.4: This figure illustrates the results of applying the proposed MUP segmentation procedure to a 100 ms wide EMG signal segment. Please refer to the text for detailed explanation.

2.4.3   Motor Unit Potential Train Identification

The objective of this stage is to assign segmented MUPs into groups, where each group represents a distinct MUPT. The problem is posed as a clustering task. The input to this stage is $\tilde{Y}$, which is a matrix with each row representing a potentially isolated segmented MUP. The outputs of the identification stage are (1) the number of identified MUPTs N_{MUPT} and (2) a set of labels assigning each of the MUPs to one of the identified trains or setting it as unidentified.

Spectral Clustering

A family of effective clustering algorithms widely known as spectral clustering are based on the spectral graph theory [21]. These algorithms cluster the data using eigenvectors of matrices associated to a graph, which capture the similarities between the data points.

Let a graph $G = (V_G, E_G)$ be a graph with node set V_G and edge set E_G. In the context of MUPT identification problem, each vertex represents one of the potentially isolated MUPs. The presence of an edge between two vertexes indicates that they are found to be neighbours. To consider two MUPs to be neighbours, they need to be morphologically similar (relative to other segmented MUPs) and the interval between their firings to be large enough.

The graph can be represented using an affinity matrix A_G of size $|V_G| \times |V_G|$, where $|V_G|$ represents the number of nodes in the graph. If the nodes $V_G(k)$ and $V_G(l)$ are connected by an edge, $A_G(k,l)$ will be set to one. Otherwise, $A_G(k,l)$ will be set to zero. The main difference between spectral clustering alternatives [28, 113, 86] is in whether they use the eigenvectors of the affinity matrix or some normalized form of the affinity matrix. A more detailed review of spectral clustering methods can be found in [136].

The methods for spectral clustering used in this study mainly follow the work described in [86]. For completeness and to facilitate further discussion of the methods, a pseudo code is given in Algorithm 1.

Algorithm 1 Spectral Clustering Algorithm

1: **function** SPECTRAL-CLUSTERING(A_G,$N_\mathcal{C}$) $\triangleright\ N_\mathcal{C}$: Number of clusters

2:     Calculate the degree matrix D_G. It is a diagonal matrix with $D_G(i,i) = \sum\limits_{j=1}^{j=|V_G|} A_G(i,j)$

3:     Calculate the normalized symmetric graph Laplacian matrix $L_G = D_G^{\frac{-1}{2}} A_G D_G^{\frac{-1}{2}}$

4:     Calculate the eigenvectors corresponding to the largest $N_\mathcal{C}$ eigenvalues of Matrix L_G

5:     Construct the spectral embedding matrix E_G by stacking each of the eigenvectors as a different column resulting in a matrix of size $|V_G| \times N_\mathcal{C}$

6:     Normalize each row of E_G such that $E_G(i,j) = \dfrac{E_G(i,j)}{\sqrt{\sum\limits_{j=1}^{j=|V_G|} E_G(i,j)^2}}$

7:     $\triangleright$ Each row of E_G can be seen as a non-linear embedding of a vertex in V_G [10]. The i$^{\text{th}}$ row of E_G will be further notated as $\hat{V}_G(i)$

8:     Use k-means to assign each of the mapped data points $\hat{V}_G$ to one of the $N_\mathcal{C}$ clusters

9:     Assign each of the nodes in V_G to the cluster assigned to the corresponding embedded point
       return $\mathcal{C}_G$

10:    $\triangleright$ $\mathcal{C}_G$: A vector assigning each of the nodes in V_G to a cluster

---

Choosing The Number of Clusters

The silhouettes coefficient was first proposed in [104] as a measure to evaluate how well clusters represent a data set. In this case, the dataset is the nonlinear embedding of the vertexes ($\hat{V}_G$). The coefficient measures the similarity of the data point to other data points of the same cluster compared with data points belonging to the next closest cluster.

For each data point $\hat{V}_G(i)$, two metrics are calculated:

- $a_{\text{sil}}(i)$: The average distance of the point $\hat{V}_G(i)$ to all the points assigned to the same cluster

- $b_{\text{sil}}(i)$: The computation of this measure starts by calculating the average distance of $\hat{V}_G(i)$ to each of the clusters that $\hat{V}_G(i)$ is not assigned to. $b_{\text{sil}}(i)$ is then set to the minimum average distance. Therefore, $b_{\text{sil}}(i)$ captures the closeness of $\hat{V}_G(i)$ to the closest cluster.

The silhouette coefficient for the data point $\hat{V}_G(i)$ is then estimated

$$\text{Sil}(i) = \frac{b_{\text{sil}}(i) - a_{\text{sil}}(i)}{max(a_{\text{sil}}(i), b_{\text{sil}}(i))} \tag{2.2}$$

The pseudocode outlined in Algorithm 1 is repeated for $N_{\mathcal{C}} = 2, 3, ..., 15$. For each value of $N_{\mathcal{C}}$, the average of the silhouette coefficients of all points is calculated. The largest $N_{\mathcal{C}}$ with an average silhouette coefficient within a given tolerance γ_{sil} (default value $= 0.1$) to the largest attained average silhouette coefficient is selected.

Similarity Graph Construction

This subsection describes the methods used for construction of the graph G. This entails deciding which potentially isolated MUPs will be considered in the graph's set of nodes (V_G). It also involves finding the set of the graph edges E_G by finding the neighbours to each MUP, i.e., the MUPs that are more likely to belong to the same MUPT as this MUP. The construction of the graph can be broken down into the following three stages:

1. **Finding the nearest neighbours:** The morphological similarity is estimated using a distance based on DTW alignment. As shown in Figure 2.5, the use of dynamic time warping results in distances that are, to a great extent, less influenced by within-train morphological variations. These variations are mainly due to neuromuscular transmission variability. An ideal distance should be indifferent to these variations, and therefore changes the least due to such changes in MUP morphology.
   The algorithm finds the $\mathcal{K}_G$ nearest neighbours to each MUP. The default value used for $\mathcal{K}_G$ is 15. A link is added to E_G if the two MUPs are mutual nearest neighbours. This means that each of them is among the $\mathcal{K}_G$ nearest neighbours to the other MUP.

2. **Validating the edges:** The fact that a MUP is found to be among the nearest neighbours of another MUP only indicates that two MUPs are morphologically similar compared to the other potentially isolated MUPs. Superimposed MUPs that do not get filtered out in the segmentation stage or MUPs with onsets and ends not accurately detected might be erroneously linked to each other. Even though, their

31

morphology might be remarkably different. Examples of these erroneous links include large MUPs resulting from constructive superposition.

Another scenario that needs to be accounted for is when the MUPs from two MUPTs are morphologically very similar. In this case, the use of their firing times is necessary. The time intervals between motor unit firings in an isometric well controlled contraction are expected to be regular (but still having some variability). This was found to be the case in normal and affected muscles [40].

Therefore, a link is excluded when the DTW accumulated distance (L2-norm based distance) is higher than a Γ_G (default value = .5) fraction of the smaller of the areas of the two MUPs linked by the edge. For the definition of the MUP area, please refer to Table 3.2. Also an edge is excluded if the interval between the firing times of the MUPs linked by the edge is less than τ_G. The default value of τ_G is set to 25 ms allowing mean firing rates up to 40 discharges/s.

3. **Pruning the nodes:** The number of edges connected to each node might vary. This is because edges are only connected between mutual nearest neighbour MUPs. Spurious nodes resulting from inaccuracies in the segmentation stage are expected to be linked to fewer edges compared to correctly segmented isolated MUPs. The algorithm therefore prune nodes, and consequently the edges linked to them, that are found to have less than λ_G links. λ_G is set by default to one fifth of K_G. The idea of pruning graphs before performing the spectral clustering was previously investigated in [58].

Dynamic Time Warping

Let the alignment between two arbitrary samples of two waveforms each representing a different MUP, say $\tilde{y}_k(t_{m_j})$ and $\tilde{y}_l(t_{n_j})$, be denoted as $\langle m_j, n_j \rangle$ and the distance associated with this alignment be the Euclidean distance between the two samples $\mathfrak{d}(\langle m_j, n_j \rangle)$.

DTW searches for a path (i.e., a sequence of alignments between pairs of samples $\mathcal{P} = \langle \mathcal{P}(1) = \langle m_1, n_1 \rangle, ..., \mathcal{P}(j) = \langle m_j, n_j \rangle .... \mathcal{P}(|\mathcal{P}|) = \langle m_{|\mathcal{P}|}, n_{|\mathcal{P}|} \rangle \rangle)$, that minimizes the

accumulated distance defined as:

$$\grave{d}(\langle m_{|\mathcal{P}|}, n_{|\mathcal{P}|}\rangle) = \sum_{j=1}^{|\mathcal{P}|} \mathfrak{d}(\langle m_j, n_j\rangle) \tag{2.3}$$

where $||$ represents the length of the sequence.

The path is subject to the following conditions:

- Boundary: $\mathcal{P}(1) = \langle 1, 1\rangle$ and $\mathcal{P}(|\mathcal{P}|) = \langle |\tilde{y}_k|, |\tilde{y}_l|\rangle$.

- Monotonicity: If $\mathcal{P}(j) = \langle m_j, n_j\rangle$ and $\mathcal{P}(j+1) = \langle m_{j+1}, n_{j+1}\rangle$, then $m_{j+1} \geq n_j$ and $n_{j+1} \geq n_j$ $\forall j$.

- Step size: If $\mathcal{P}(j) = \langle m_j, n_j\rangle$ and $\mathcal{P}(j+1) = \langle m_{j+1}, n_{j+1}\rangle$, then $m_{j+1} - m_j \leq 1$ and $n_{j+1} - n_j \leq 1$ $\forall j$.

The search for the path $\mathcal{P}$ can be obtained using dynamic programming. Let $\mathcal{P}_{\langle m_j, n_j\rangle}$ be the optimal path between $\langle \tilde{y}_k(:,1)...\tilde{y}_k(t_{m_j})\rangle$ and $\langle \tilde{y}_l(:,1)...\tilde{y}_l(t_{n_j})\rangle$ that minimizes the accumulated distance $\grave{d}(\langle m_j, n_j\rangle)$. The path can be obtained using the following recursive formula:

$$\begin{aligned} \grave{d}(\langle m_j, n_j\rangle) = {} & \mathfrak{d}\langle m_j, n_j\rangle + \\ & min(\grave{d}(\langle m_j - 1, n_j - 1\rangle), \grave{d}(\langle m_j, n_j - 1\rangle), \grave{d}(\langle m_j - 1, n_j\rangle)) \end{aligned} \tag{2.4}$$

In this work, the distance between $\tilde{y}_k$ and $\tilde{y}_l$ is defined as the accumulated distance $\mathcal{D}(\tilde{y}_k, \tilde{y}_l) = \grave{d}(\langle |\tilde{y}_k|, |\tilde{y}_l|\rangle)$.

Constraining the alignment path

Minimizing the accumulated distance $\mathcal{D}$ does not guarantee that the alignment accommodates for changes in the morphology resulting from variability in the time needed for transduction across the neuromuscular junctions. This variability ranges between 15 μS to 100 μS [67]. Given an initial alignment based on the peaks of segmented MUPs, any

33

1) DTW 1.45 Euclidean 83.80   2) DTW 1.30 Euclidean 21.18

3) DTW 1.46 Euclidean 7.68   4) DTW 0.94 Euclidean 16.83

500 μ V

2 ms
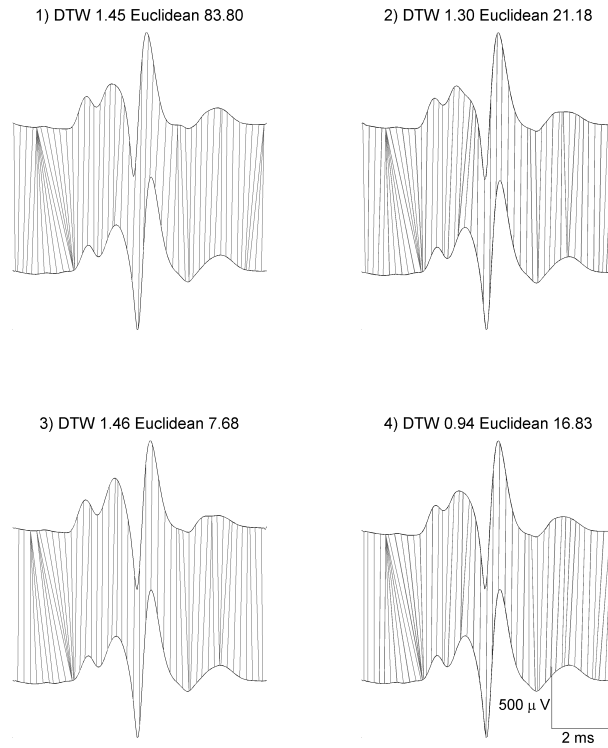
Figure 2.5: The figure illustrates that the distance based on DTW alignment is less sensitive to random within-train morphological variability in MUP morphology compared to the Euclidean distance. The DTW alignments and distances computed between an examined MUP (shown as the lower trace in the four panels) and four other MUPs produced from the same motor unit are shown in the figure. The grey lines represent every 10th alignment from one time instance of a MUP to a time instance in the other MUP. To simulate the changes in MUP morphology due to neuromuscular transmission variability, the initiation time of the MFPs are randomly picked from a zero mean Gaussian distribution with a standard deviation of 70 μs. As shown in the figure, the distances obtained based on DTW alignments are not only smaller but also less variable.

34

alignment between two samples from two different MUPs separated by more than $\lambda_{\mathcal{P}} = 300$ microseconds is probably erroneous, in a sense that it is not accommodating for an electrophysiological phenomenon.

A Sakoe-Chiba band [107] limits the possible alignments of a sample t_m from one MUP to the samples $\{t_{m-\lambda_{\mathcal{P}}}, \ldots, t_m, \ldots, t_{m+\lambda_{\mathcal{P}}}\}$ in the other matched MUP. This results in the time and space complexities of the DTW procedure to be reduced from $\mathcal{O}(L_{\mathrm{IMUP}}^2)$ to $\mathcal{O}(L_{\mathrm{IMUP}} \times 2\lambda_{\mathcal{P}})$. L_{IMUP} is the preset length of the MUP. This is a significant improvement, knowing that DTW is by far the most computationally expensive stage in the system.

Speeding Up Finding Nearest Neighbours with Lower Bounding

The intuition behind the lower bounding idea is to use a less computationally expensive technique to compute a distance between two MUPs. This lower-bound distance should be guaranteed to be lower than or equal to the DTW-based distance $\mathcal{D}$. If the lower-bound distance between the examined MUP and a query MUP is found to be larger than the maximum of the $\mathcal{K}_G$ smallest DTW-based distances that are already computed. The computation of the DTW-based distance between the examined MUP and this particular query MUP can be skipped.

An important property of the lower bound distance is its tightness, i.e., how close its value is to the actual DTW-based distance. For instance, a trivial lower bounding technique that always returns zero will result in no skipping of the computation of the DTW based distance. As expected, increasing the tightness often results in increased computational and space complexities of the lower bounding technique. Therefore, the choice of a lower-bound distance for a particular problem entails a trade-off between the lower bounding technique complexity and the probability of skipping the computations of the original distance (the DTW based distance in this context).

Among various methods for DTW lower bounding discussed in the data mining literature [143, 66], the lower-bound distance proposed in [64] was shown to be tighter and with comparable complexity. This distance will be referred to further in this thesis as the LB-Keogh distance. For clarity, the idea behind LB-Keogh distance is illustrated in Figure 2.6.
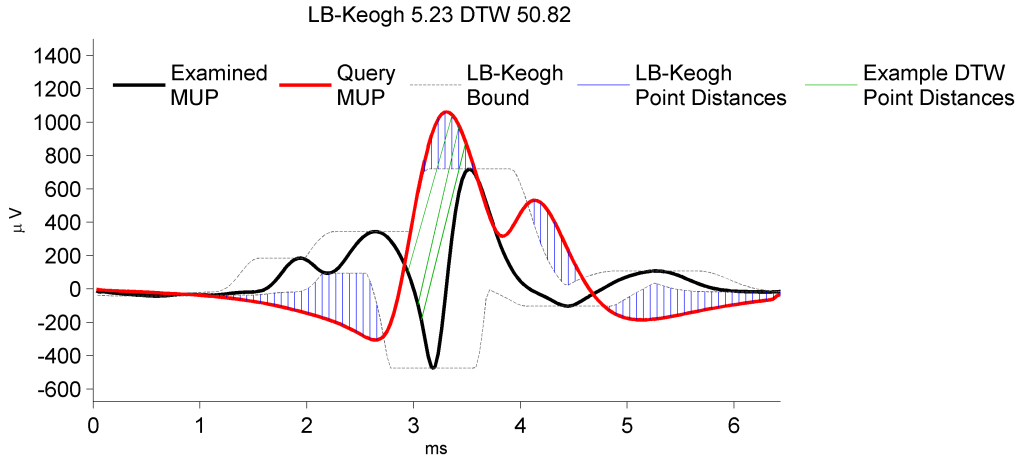
Figure 2.6: The figure illustrates the computation and intuition behind the LB-keogh distance.

Figure 2.6 shows two MUPs: (1) the examined MUP (the MUP that the algorithm is trying to find its $\mathcal{K}_G$ nearest neighbours) and (2) the query MUP (the algorithm is investigating whether it is one of the $\mathcal{K}_G$ nearest neighbours of the reference MUP or not). For each sample in the examined MUP, an upper bound is computed by finding the maximum of the reference in a window of length $2\lambda_{\mathcal{P}}$ (the Sakoe-Chiba band width) centred at this sample.

A lower bound is computed in a similar fashion. To compute the contribution of a particular sample in the query to the LB-Keogh distance (sample distance), a vertical one-to-one alignment is assumed. The sample distance is computed relative to the upper bound in the case that the amplitude of the query at this particular sample is higher than the amplitude of the reference. It is computed relative to the lower bound in the case that the query amplitude at this sample is lower than the amplitude of the reference.

For three samples, the figure shows the sample distances resulting from DTW alignments. It can be seen that the minimum contribution to the DTW distance can only happen if (1) there are one-to-one alignments to each of these query samples and (2) the sample distances are equal to the sample distance computed by the LB-Keogh distance.

36

2.5 Evaluation

In order to evaluate the performance of the proposed methods, it is necessary to obtain a reference composition of the analysed EMG signal. Ideally, this composition should define the neuro-dynamical, anatomical, and electrophysiological characteristics of the active motor units which are contributing significantly to the detected signal. This reference composition should also capture the characteristics of the conducting medium and the acquisition system; and reflect the temporal evolution and non-stationarity of such characteristics.

Such detailed reference composition would not only allow comparison of different proposed methods for MUPT Identification, but also could be used to identify the empirical confidence limits for the obtained information. For instance, how close should the detection surface be to a muscle fibre before it can be detected reliably. This motivated the reliance of the presented experiments in this section on a physiologically based simulation of intramuscular EMG signals. This simulation is discussed in more details in Chapter 3 on Page 51.

There have been other methods reported in the literature that aim at generating a reference labelling for a decomposition rather than a reference composition of an EMG signal. These labelling methods include:

1. synthetic signals simulated using real MUPs and a model of their motor units' firing patterns [35, 34]

2. evidence extracted from an EMG signal itself assuming that a correct decomposition will extract MUPTs having regular firing patterns and high within-train morphological similarity [79]

3. the concensus among independent decomposition results of simultaneously acquired signals using multiple detection surfaces [74]

4. expert annotation

2.5.1 Tuning Motor Unit Potential Segmentation

The main objective of this experiment is to estimate an empirical lower limit for MUP amplitude to noise ratio (ANR) at which MUPs can be accurately and consistently segmented. The ANR is defined as the ratio of the maximum MUP amplitude (with either negative or positive polarity) to the standard deviation of the simulated noise.

In order to evaluate the performance of the MUP detection algorithm at different MUP ANRs, it is necessary first to establish a correspondence between the simulated firing instances and the detection instances extracted by the segmentation algorithm. They are not expected to align because of many reasons including the inability to sense motor neuron firings, group delay due to signal filtration, and MUP superposition. A heuristic is therefore needed to establish this correspondence. In this work, a detection instance is defined as the instance at which the segmented MUP has a maximal amplitude.

On the other hand, a simulated firing is defined using both (1) a firing instance and (2) an observation range. The range attempts to capture the duration in time at which the firing can be effectively observed in the EMG signal, and therefore is dependent on the noise level. The observation range is estimated from the MUP simulation buffer (with no added noise) using a 200 microseconds wide moving window to scan for the start and end of the MUP. Both the start and end of the MUP are assumed to occur, when the amplitude of the MUP stays above one standard deviation of the simulated noise throughout the window width.

Superimposed MUPs are ignored to simplify the analysis in this experiment. A superposition is assumed to occur when two or more observation ranges of MUPs with amplitude above twice the noise standard deviation overlap. A true positive detection TP_D corresponds to the algorithm reporting a detection instance during an observation range. A false positive detection FP_D corresponds to the algorithm reporting a detection instance within no MUP observation range. Finally, a false negative detection FN_D corresponds to the algorithm reporting no detection instances during an observation range, regardless whether this range is superimposed or not. The MUP segmentation algorithm is evaluated using both precision ($Pr_D = \frac{TP_D}{TP_D+FP_D}$) and recall ($Re_D = \frac{TP_D}{TP_D+FN_D}$).

In this experiment, 50 muscles were simulated, with each muscle assumed to be com-

posed of 200 motor units. The diameter of motor unit territories (i.e., an assumed circular area enclosing all the muscle fibres belonging to the motor unit) ranged from 2 to 8 mm with a density of 10 motor unit fibres/mm^2. The excitatory input to the motor neuron pool was increased until 40 to 80 MUPs per second were observed. The variability in the times needed for the neural signal transduction across each of the muscle fibres' neuromuscular junctions were modelled to be sampled from a zero mean Gaussian distribution with a standard deviation of $70\mu S$. Finally, a normally distributed white noise with a standard deviation of 40 μV was added to the signals. All the signals were simulated to be ten seconds long. This resulted in each of the simulated EMG signals having from 5 to 13 observable MUPTs, which were defined as MUPTs having any of their MUPs with an amplitude above twice the simulated noise standard deviation. The detection recall Re_D was only calculated for MUPTs with more than ten non-superimposed ranges.

Figure 2.7 shows the averages and ranges of the detection recall for different intervals of MUP ANR values. The detection recall Re_D is calculated for each MUPT independently. It is clear that MUPs with amplitude above three times the noise standard deviation (40 μV) can be detected reliably with minimal detection recall more than 0.8. Most of the FN_D at higher ANR ranges were due to the segmentation algorithm mistakenly merging two or more temporally close non-superimposed MUPs together. It is therefore safe to assume that MUPs with ANR above three can be consistently segmented. The following section reports on investigations into the lower bound of the MUP ANR in terms of its effect on the accuracy of the MUPT identification. It is worth mentioning that having a MUPT consistently identified does not necessarily mean that it will be useful for characterization of neuromuscular disorders, however, this question is not in the scope of this study.

The average precision across different simulated signals was 0.924 ± 0.072. The relatively low detection precision can be mainly attributed to using a low peak amplitude threshold factor $\lambda_a = 2$. The use of low λ_a made it more likely to have false detections due to superposition of more than one non-observable MUPs resulting in a peak with an amplitude above λ_a. When λ_a was set to 2.5, the precision increased to 0.966 ± 0.035. This led to no significant change in the average detection recall values for MUPTs with MUPs having three ANRs or higher.
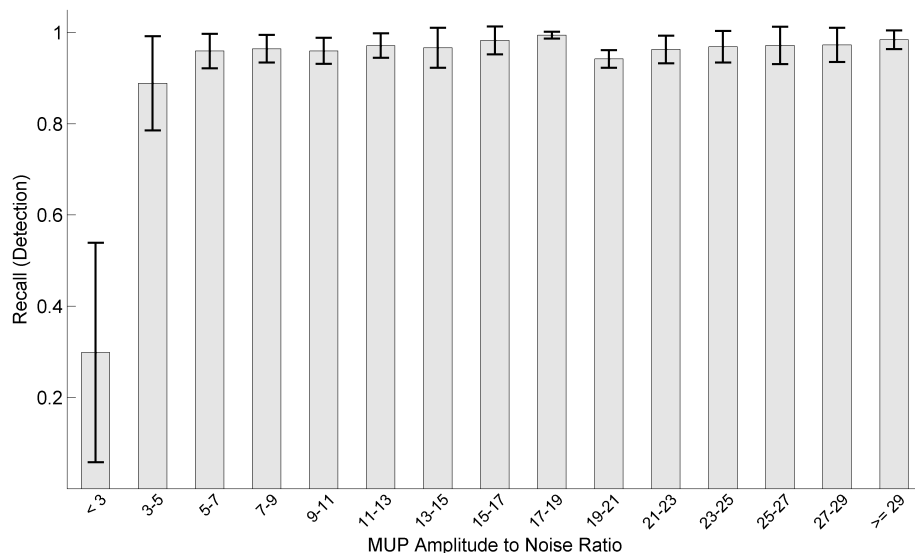
Figure 2.7: Evaluating MUP Segmentation: Each bar represents the average of recalls calculated for MUPTs belonging to a particular interval (right-open and left-closed) of MUP ANRs. Each stick denotes one standard deviation around the obtained average value.

2.5.2 Evaluating Motor Unit Potential Train Identification

The experiments reported in this section focus on evaluating the results of cascading the segmentation and identification stages. In order to evaluate the MUPT Identification stage, it is necessary first to establish an association between the simulated (gold standard) and identified MUPTs. This is not straightforward, due to ambiguity resulting from many sources including train merging and train splitting.

In this context, train merging refers to an identified train includes *most of* the MUPs are from more than one simulated train, while train splitting refers to having more than one identified train with *most of* their MUPs belonging to the same simulated train. Ambiguity even goes to the MUP assignment level, as it is not clear how to assign a reference label for a detection instance within a superimposed observation range.

40

To resolve this ambiguity and develop appropriate indexes of performance, a definition for an ideal MUPT identification should be first conceptualized. The indexes of performance can be then developed to capture potential deviations from the ideal case. Intuitively, an ideal decomposition will result in the number of identified MUPTs being equal to the number of simulated MUPTs with each of the identified MUPTs containing only the isolated MUPs of a unique simulated MUPT. This is however an unrealistic definition, because it ignores the possibility of MUP superposition which is expected to happen in almost all EMG signals.

A more realistic definition for an ideal MUPT identification should take into consideration the superposition phenomena. In this case, each of the identified MUPTs should contain none but (1) all the isolated MUPs belonging to one of the simulated MUPTs, and (2) the associated superimposed ranges where the morphology of the range is influenced more by the MUP of this particular simulated train than by other superimposed MUPs. The degree of the morphological influence of a particular MUPT to a superimposed range is approximated by the ratio of the energy of the train's MUP contributing to the range to the total energy in the range.

The evaluation procedure starts by assigning each of the identified MUPTs to the simulated MUPT to which most of the detection instances (isolated MUPs and associated superimposed ranges) are associated with. Once this assignment between the identified and simulated trains is established, three performance indexes can be calculated to evaluate the identified trains

1. **Splitting** This performance index can be only calculated for each of the represented MUPTs (i.e., a simulated MUPT to which one or more identified trains are assigned). Splitting is defined as the number of the identified trains assigned to this train.

2. **Purity** The ratio of correctly assigned MUPs to the total number of assigned MUPs in each of the identified trains. This metric is adopted from the work described in [71].

3. **Merging** The ratio of the number of MUPs mistakenly assigned to the train that belong to the second most abundant MUPT in the identified train to the number of

41

MUPs that are correctly assigned.

The performance indexes shown in Figure 2.8 constitute the identified MUPT view evaluation. They do not reflect how much information is extracted from the signal. Instead, these performance indexes focus on evaluating the quality of the identified trains. On the other hand, Figure 2.9 presents the simulated train view evaluation. This view primarily focuses on the completeness of the decomposition reporting the percentage of the detected MUPTs. This view also reports the completeness within each train using precision and recall calculated in the same way as in the previous section. Superimposed MUPs are set to be associated to a train, if a MUP from this train contributes more than 60 % of the energy of the observation range of the superimposed MUP.

2.5.3 Evaluating the Representativeness of the Identified Motor Unit Potential Trains

In this section, the representativeness of an identified train is equated to how accurately can the quantitative EMG morphology and morphological stability features be estimated from it? This, in essence, is an end-to-end evaluation of the methods described in this chapter. This is because feature values can be either under or over estimated due to errors or inaccuracies in any of the sub-stages. This includes inaccurately estimating the onsets and ends of MUPs, assigning MUPs to a wrong MUPT, excluding MUPs that could have otherwise contributed to elevated morphological instability values, and failing to exclude significantly superimposed MUPs.

The true values of the features are estimated from the simulated MUPTs. Simulated MUPTs include all of the MUPs in the train with no added noise or superposition from other MUPs. Four features are chosen for this experiment: area, length, number of phases and jiggle. These features are chosen based on the analysis performed in Chapter 3 on Page 51. Only MUPTs having an ANR above three are included in this study. The results are shown in Figure 2.10.

In the case of evaluating the representativeness of MUPTs in terms of their ability to estimate Jiggle (a feature estimating morphological variability across the MUPs belonging

Figure 2.8: Identified MUPT view Evaluation: The idea here is to evaluate the quality of the identified trains. Each bar in the top panel represents the average purity for MUPTs belonging to a particular interval of MUP ANRs. For the same ANR intervals, the middle panel shows the average merging and the bottom panel shows the average splitting. Each stick denotes one standard deviation obtained around the average value.

43
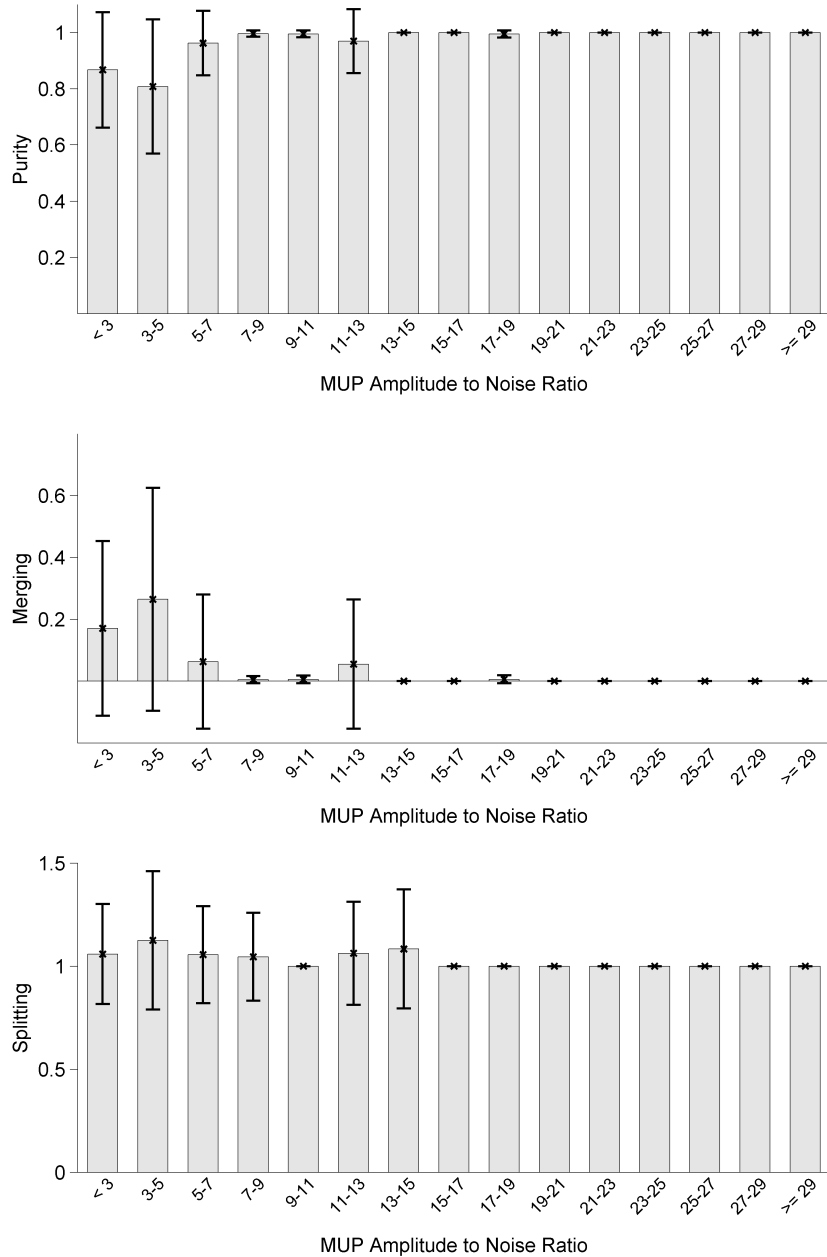
Figure 2.9: Simulated MUPT view Evaluation: The idea here is to evaluate how much information is extracted from an EMG signal. Each bar in the top panel represents the percent of simulated MUPTs that were identified belonging to a particular interval of MUP ANRs. For the same ANR intervals, the middle panel shows the average precision and the bottom panel shows the average recall. Each stick denotes one standard deviation obtained around the average value.
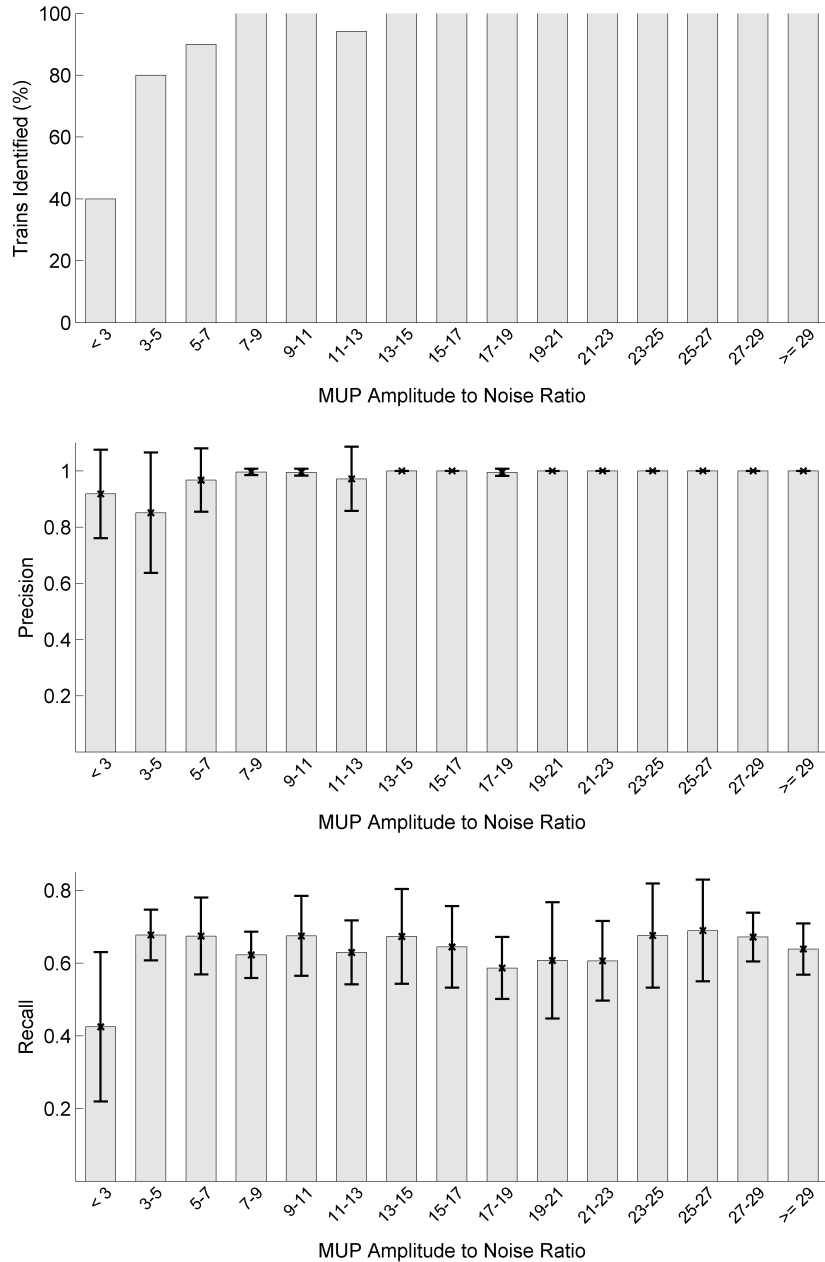
to the same train), noise is added to the simulated MUPTs. This is necessary to get comparable estimates by having similar baseline fluctuations [16] (in a statistical sense) for both the simulated and identified MUPTs. The morphological features (area, length and phases) are estimated from a MUP template calculated using the following procedure:

1. **Choose a reference MUP:** For identified MUPTs, it is selected to be the MUP with the smallest average of distances to its mutual nearest neighbours in Graph G. Any MUP from the simulated MUPT can be selected as a reference MUP.

2. **DTW Alignment:** Using the procedure for DTW alignment described on Page 32, the alignment path $\mathcal{P}$ is evaluated between the reference MUP and each of the MUPs in the train. MUPs aligned based on their peaks (rows of $\tilde{Y}$) are used as an input to this stage. The same procedure is applied for both identified and simulated MUPTs.

3. **Find the minimal alignment:** Each of the samples in the reference MUP can be aligned to one or more samples when matched to another MUP. In case of multiple alignments, the alignment that has the smallest Euclidean distance $\mathfrak{d}$ among all alignments is kept in the set of alignments associated with this particular sample. A trimmed averaging (excluding the top and bottom 5%) is used to to estimate the template sample value.

Alternative methods for estimating morphological MUP templates can be found in [123, 60].

2.6 Discussion

The key advantages of using spectral clustering for the MUPT identification problem are:

- Unlike other clustering algorithms such as k-means, there is no need to represent each MUP using a fixed length vector of morphological features or MUP samples. This estimation of these features requires a precise alignment of the MUPs belonging to the same train. Precise alignment is not feasible, since there is no way to obtain
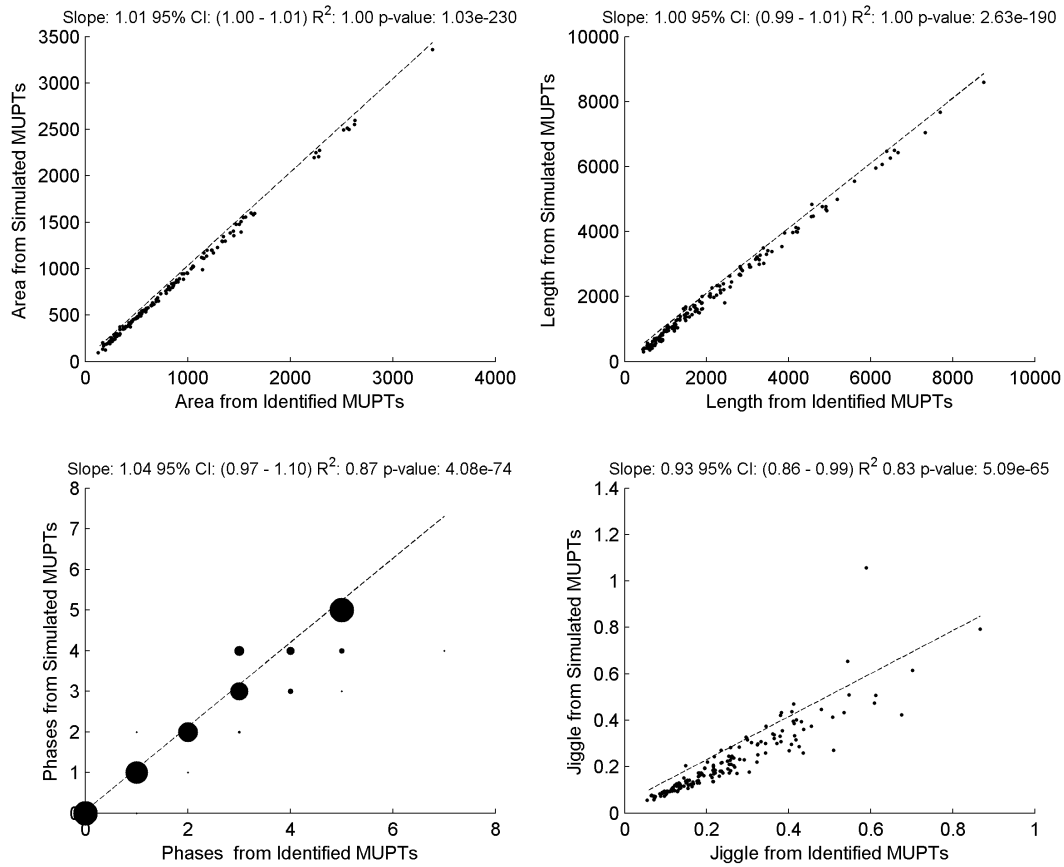
Figure 2.10: Each of the subplots is a bivariate graph. It shows the relation between the feature values as estimated from the simulated trains (assumed to be the true values) and when estimated from the identified MUPTs using the methods proposed in this chapter. Dashed line represents regression line. The slope of the regression line, its 95% confidence interval (CI), R^2 statistic, and the p-value (rejecting the null hypothesis that the linear model coefficients are equal to zero) are shown in the title of each subplot. The size of the dot in the lower left subplot is proportional to the number of MUPTs. Please refer to Chapter 3 on Page 51 for feature definitions and units.

an accurate measurement of the motor neuron firing instance. The use of a single morphological landmark (such as the peak with largest amplitude) as a reference point can be misleading for highly unstable MUPTs. In contrast, the input to the spectral clustering algorithm is a similarity graph constructed by evaluating pairwise distances.

- The use of the k-nearest neighbour graph allows finding clusters with different similarity densities. This can account for the non-uniformity of disease involvement across motor units of the same muscle; which leads to detected MUPTs from concurrently active motor units having different degrees of morphological variability across their MUPs.

- The use of the k-nearest neighbour graph also allows efficient use of lower bounding techniques.

- It is a graph based clustering approach finding clusters optimizing the connectivity criteria rather than compactness. This means that the cluster is a set of points that are connected to one another. The points belonging to the same cluster are not necessarily assumed to form a dense region, as in the case of mixture models. This can help in tracking MUPTs with slowly varying characteristics due to slow electrode movement.

- The calculation of the Laplacian matrix and its spectral decomposition can be implemented efficiently using optimized matrix operations. Also, the evaluation of the adjacency matrix can be performed in parallel.

DTW-based distance is significantly more computationally expensive when compared to the Euclidean distance. The computational complexity of DTW alignment is reduced using early termination and lower bound distances. Early termination means stopping the computation once the accumulated distance up to a certain sample index (either for the DTW-based or the LB-Keogh distances) is above the maximum of the $\mathcal{K}_G$ smallest DTW-based distances that are already computed. The initial alignment of the MUPs allows constraining the alignment path. This also contributes effectively to reducing computational cost.

The main reasoning behind using DTW alignment is to calculate a distance that is least affected by within-train morphological variability resulting from the instability in neuromuscular transmission. DTW alignment can also accommodate to a great extent inaccuracies in finding MUP onsets and ends by *deleting* activities mistakenly added to the MUP. Moreover, the use of the DTW-based distance eliminates the need for representing a MUP using a set of morphological features (e.g., duration, amplitude and area) to perform clustering.

SG filtering is used instead of a simple digital filtering schema due to its ability to preserve the amplitude and width of signal peaks and valleys. This can be attributed to the SG filter's flat frequency response in the pass-band, linear phase response, and modest attenuation in the stop-band. It is worth mentioning that the same desirable filter characteristics (if not better) can be reached using other filter design methodologies [112].

The author still prefers to use an SG filter, because it provides a more intuitive and convenient design process. The filters desirable characteristics can be maintained for different degrees of smoothing by changing either or both of the polynomial order and the fitting window length. This is particularly useful for the applied tuning process, where the degree of the applied smoothing is chosen based on the analyzed signal characteristics. The SG design method also readily provides the impulse responses of linear time invariant systems that can be used to obtain discrete approximations of differentiations up to an order one below the set filter polynomial order. In this case, the first and second order differentiation are useful in later analysis stages.

The main advantage of using a segmentation method that segments variable length MUPs, rather than assuming that all MUPs have the same length, is that it potentially decreases the chance of including contributions from other motor units. These erroneously included contributions degrade the accuracy with which the quantitative features can be calculated.

The described methods are mainly implemented using Matlab™except for the DTW and LB-Keogh distance functions which are written in C. The methods were evaluated on a computer having an i7-3820 processor and 32 GB of RAM. The implementation made use of the four cores of the processor to realize a parallel execution for some methods including SG

filter tuning, similarity graph construction, and spectral clustering. The average processing time for a ten seconds long EMG signal is 4.7 ± 0.38 seconds. Nowadays, the extra cost to purchase a computer powered by a multi-core processor (up to 16 cores) only represents a small fraction of the cost of the acquisition hardware and the disposables.

The results of the identified MUPT view evaluation, shown in Figure 2.8, illustrate the representativeness of the identified MUPTs. Those with an ANR that is five or above are mostly comprised of MUPs whose morphology are mainly contributed by the same motor unit (Purity: 0.99 ± 0.058). There is also a slight chance of train merging or splitting (Merging: 0.016 ± 0.11 Splitting: 1.03 ± 0.17). On the other hand, the simulated train evaluation view addresses the completeness of the extracted information. It is shown in Figure 2.9 that 97.84 % of the simulated trains with an ANR that is five or above are correctly identified with high precision (Precision: 0.99 ± 0.06). The obtained recall for those trains is 0.65 ± 0.1. This low recall is partly by design, since the algorithm focuses on excluding superimposed and inaccurately segmented MUPs.

As shown in Figure 2.10, the correlations between the quantitative EMG feature values as estimated from the simulated MUPTs and when identified using the proposed methods are highly significant. The estimated linear regression slopes are found to be statistically significant and close to 1. The estimated linear model explains the variability in the data around its mean (R^2 statistic ranges between .83 and 1). This suggests that the identified MUPTs can be used to accurately estimate features capturing different aspects of MUPT typical MUP morphology and MUP stability. The same aspects are shown to be indicative of neuromuscular disorders in Chapters 3 and 6.

The main advantage of evaluating the proposed methods using EMG signals obtained from an electrophysiologically based model rather than a phenomenological model [35] is that it prevents unjustified simplifications or complications of the MUPT identification problem. An example of such simplifications in [35] is simulating contributions from distant motor units as part of the added noise. It is true that MUPs from such motor units are characterized with low amplitude. However, the fact that these MUPs are bandwidth limited and observed with statistically consistent firing intervals and morphology poses challenges to the segmentation and identification stages.

On the other hand, the main advantage of using a phenomenological model to generate EMG signals is that it allows a convenient direct association between the obtained performance indexes and signal characteristics. For example, the performance indexes can be obtained for trains with increased degrees of morphological variability. In comparison to our approach, simulating increased morphological variability can be realized by increasing the variability in neuromuscular junction transmission. There is no guarantee, however, that this will lead to a monotonic increase in morphological variability.

The presented experimentation could have benefited from using reference labelling obtained from multiple detection surfaces [74]. Such reference labelling could have been used to confirm the obtained completeness of the decomposition results. It is worth emphasizing that this approach of evaluation does not suffice by itself, since the characteristics of the labelled MUPTs (signal to noise ratio, morphological variability, etc.) would have been unknown, which would preclude analyzing the algorithm sensitivity with respect to different physical properties and signal characteristics or evaluating the capability of the algorithm to extract descriptive quantitative features reliably. Decomposition completeness is of a secondary importance to the MUPT identification problem as explained earlier.

Chapter 3

Representation: Feature Selection For Motor Unit Potential Train Description

3.1 Summary

Objective: Ten new features of motor unit potential morphology and stability are proposed. These new features, along with eight traditional features, are grouped into five aspects: size, shape, global complexity, local complexity, and stability.

Methods: Sequential forward and backward search strategies were used to select subsets of these 18 features to discriminate accurately between muscles whose motor unit potentials are predominantly neurogenic, myopathic, or normal.

Results and Conclusions: Results based on 8102 motor unit potential trains extracted from four different limb muscles (336 total muscles) demonstrate the usefulness of

these newly introduced features and support an aspect-based grouping of the motor unit potential train features.

3.2   Introduction

An important part of the current practise of electrodiagnostic medicine entails acquisition and qualitative, or semi-quantitative analysis of needle-detected EMG signals. Qualitative or semi-quantitative analysis involves auditory and visual assessment of spontaneous EMG signals (recorded from resting muscle or after very small abrupt needle movements) and of EMG signals recorded during slight voluntary muscle contraction. When signals are assessed during slight voluntary muscle contraction, analysis is based on recognition and semi-quantification of pathological changes in the morphology and/or stability of MUPs as well as in recruitment levels and firing rates of the active motor units whose fibres are close to the needle electrode. MUPs and their patterns of occurrence are assessed to determine the likelihood they reflect normal or diseased motor units. After sampling a suitable number of motor units, MUP characterizations are aggregated to obtain an overall muscle characterization leading to a muscle categorization as normal or diseased [24].

Only a minority practitioners chose to perform quantitative analysis. This analysis uses MUPTs extracted from signals recorded during low level voluntary contractions using amplitude level or window triggering or signal decomposition algorithms. A more detailed discussion of methods used in extracting MUPTs is provided in Chapter 2.

Each extracted MUPT is represented by an estimated MUP template and its ensemble of MUPs. This allows assessment of MUP shape stability across multiple motor unit firings as well as motor unit activation. Aspects of MUPTs related to MUP template morphology, the consistency of their individual MUP morphologies, or motor unit recruitment and firing pattern can be characterized using the values of various features.

As with qualitative analysis, MUPTs can therefore be characterized to determine whether a disorder of nerve or muscle is likely and, if so, whether it is mild or severe. MUPT feature values can be compared to reference normal and diseased values [37] to estimate the likelihood that an extracted MUPT was detected in a normal or a diseased

muscle. These individual MUPT characterizations can then be aggregated to create an overall muscle characterization that can be used to categorize an examined muscle as being normal or abnormal.

Varying subsets of newly proposed and existing features were compared. The utility of a feature subset was judged in terms of its accuracy in classifying muscles as myopathic, normal or neurogenic. Higher accuracy was equated with higher utility. Although this study focuses on features evaluated using quantitative analysis, the findings are also applicable to qualitative and semi-quantitative analysis, in that the same questions are addressed:

1. What aspects of MUPTs are most relevant to accurate muscle categorization?

2. Which features most reliably convey each MUPT aspect?

3. Which aspects are most useful in distinguishing myopathic versus neurogenic, myopathic versus normal or neurogenic versus normal muscle?

4. Can feature subsets be generalized across different muscle types?

5. Can features sensitive to acquisition settings and/or operator skill be replaced by other features which do not have these limitations without compromising accuracy?

3.3   Literature Review

MUPs from neurogenic muscles are often larger than those in myopathic or normal muscles, and MUP size can be represented by duration and amplitude. MUPs from neurogenic or myopathic muscles are often more complex than those from normal muscles, and the number of phases and turns can characterize MUP complexity. As such, a feature set comprised of duration, amplitude, number of phases, and number of turns can be used to distinguish between normal muscles and those affected by myopathic or neurogenic disorders [12, 15]. However, the influence of electrode type, sampling position, amplification, and filter settings on the reproducibility of statistical estimates of these four conventional features must also be considered [14, 13].

Therefore, better ways of extracting motor unit information from MUPs have been investigated. MUP thickness [81], the ratio of MUP area to amplitude, mitigates electrode positioning effects and can discriminate between muscles affected by neurogenic and myopathic disorders better than conventional MUP features [15]. MUP size index, a function of area and amplitude developed using discriminant analysis, is effective for differentiating normal muscles from those affected by a neurogenic process [115], but it is difficult to interpret visually, because it is based on logarithmic scaling.

The MUP irregularity coefficient and the relative irregularity coefficient (RIR) are measures of MUP complexity and represent details of MUP shape rather than simply its global features [144, 106]. MUPT jiggle and MUPT consecutive discharge cross-correlation coefficient measure morphological variability across MUPs of the same MUPT [121, 17]. Elevated jiggle and cross-correlation coefficient values correspond with increased muscle fibre jitter.

Features representing motor unit activation patterns and MUP features estimated using spectral and time-scale representations [92, 137] have also been investigated. Activation pattern features are discussed in further details in Chapter 5. Spectral and time-scale based features were not considered, because they are difficult to conceptualize or visualize and their inferred characterizations are not explained easily.

In this work, size, shape, global complexity, and local complexity were considered as four different aspects of MUP morphology. The fifth aspect studied relates to the stability of MUP morphology of all the MUPs comprising an MUPT. The utility of different sets of quantitative features was investigated using two different feature selection methods [47].

The relationships between different QEMG features were investigated previously. A comprehensive review can be found in [120]. These studies mainly focused on statistical relationships between pairs of features, for example the dependence of area and amplitude, or the optimal way of combining feature values to obtain features with better statistical characteristics. Also, feature subset selection methods have been applied previously to QEMG data [95, 96]. In this work, a larger group of feature subsets using more exhaustive search strategies and more computationally intensive classification methods were studied to answer more general questions about MUPs.

3.4 Methods

3.4.1 Data Acquisition

In the course of EMG laboratory evaluation of clinical patients referred for diagnostic EMG studies, individuals were offered participation in the institutional review board approved protocol.

A variety of subjects were enrolled and some declined enrolment. Recordings were made without respect for diagnosis as enrolment took place prior to the EMG examination. Subjects were selected for whom EMG evaluation was likely to require assessment of both upper and lower limb muscles. The patients studied ended up having a wide variety of conditions.

Subjects with neurogenic disorders had such diagnoses as polyneuropathy, polyradiculopathy, or motor neuron disease. Individuals eventually diagnosed with myopathy most commonly had inflammatory myopathies or dystrophies such as facioscapulohumeral muscular dystrophy or oculopharyngeal muscular dystrophy. Most of the subjects had symptoms for a number of weeks to many months.

Routine clinical needle EMG was collected with a Viking EMG machine using a 10 to 10 kHz bandwidth and a 48 kHz sampling rate in the first dorsal interosseous (FDI), deltoid (DLT), tibialis anterior (TA), and vastus medialis (VM) muscles. Following needle positioning to detect suitably "sharp" MUPs (with rise times < 0.5 ms) during low level muscle contraction, a manual semiquantitative assessment of the detected signal was completed. The level of contraction was then increased until 40 to 60 MUPs per second were detected and 15 sec of needle detected signal was acquired. This was repeated at multiple distinct needle positions. Muscles were annotated by an experienced clinical neurophysiologist as myopathic, normal, or neurogenic based on manual semiquantitative assessments of MUP signals detected during the low level muscle contractions across all sampled needle positions.

For each needle position, MUPTs were extracted from the EMG signal detected during the increased level of muscle contraction using a standard DQEMG algorithm [124]. Table

Type	Normal		Neurogenic		Myopathic	
	Muscles	MUPTs	Muscles	MUPTs	Muscles	MUPTs
TA	48	868	31	429	24	548
FDI	59	1008	26	446	8	86
VM	55	830	19	330	9	112
DLT	40	690	13	246	10	171

Table 3.1: Number of muscles examined and the corresponding number of extracted MUPTs for each muscle type

3.1 lists the number of muscles examined in this study and the corresponding number of extracted MUPTs for each muscle type. All data was acquired under IRB approval and sanitized of personal identifying information.

After extracting MUPTs that contributed significantly to a detected EMG signal, a MUP template was estimated for each train. See [124] for a more complete description. Morphological features of the MUP template were then measured as well as measures of MUP stability across the MUPs comprising the MUPT.

3.4.2 Feature Definitions

All MUPT features included in this study and their definitions or formulae are listed in Table 3.2.

Morphological Features		
Size Aspect		
Duration (Dur)	ms	The time difference between onset and end point of an MUP template.
Amplitude (Amp)	μV	The difference in voltage from the maximal negative to the maximal positive peak of an MUP template.
Area (Ar)	$ms\mu$V	Summation of the absolute values of samples of the MUP template over its duration.

Shape Aspect		
Thickness (Thk)		$\frac{\text{Area}}{\text{Amplitude}}$
Global Complexity Aspect(G.Cmpl)		
Number of Phases (Ph)		Phase is the part of an MUP template that falls between baseline crossings
Number of Turns (Tr)		Turn is a local peak, either negative or positive in an MUP template.
Length Index (LnInd)		MUP Length (Ln) is the summation of the absolute amplitude differences for every two consecutive samples within the duration of the MUP template. Length index is obtained through normalizing the MUP length using the following formula: $\frac{\text{Length}-2\times\text{Amplitude}}{2\times\text{Amplitude}}$
Shape Width (ShpWdth)	ms	$\frac{\text{Area}}{\text{Length}}$
Fibre Count (FbrCnt)		The number of turns estimated from the second derivative of the MUP templates.
Local Complexity Aspect(L.Cmpl)		
Phase Area (PhAr)	$ms\mu$V	$\frac{\text{Area}}{\text{Number of Phases}}$
Phase Complexity (PhCmpl)		$\frac{\text{Number of Turns}}{\text{Number of Phases}}$
Turn Length (TrLn)	μV	$\frac{\text{Length}}{\text{Number of Turns}}$
Turn Amplitude (TrAmp)	μV	$\frac{\text{Amplitude}}{\text{Number of Turns}}$

Turn Area (TrAr)	msV	$\dfrac{\text{Area}}{\text{Number of Turns}}$
Turn Width (TrWdth)	ms	$\dfrac{\text{Shape Width}}{\text{Number of Turns}}$
Ensemble Features		
Jiggle(Jig)		A measure of the average variation between motor unit discharges of the individual voltage samples used to represent an MUP, normalized by the energy of the MUP.
B Jiggle(BJig)		Similar to Jiggle but calculated using the second derivative.
Shimmer Covariance (ShmCov)		Average Euclidean distance of the ensemble of MUPs to the estimated MUPT template normalized by the area of the template.

Table 3.2: Features included in this study. All features were calculated automatically. Only duration was assessed and modified accordingly by Daniel Stashuk.

These MUPT features can be broadly classified into 2 main categories:

- **Morphological Features:** These features quantify the shape of the MUP template. The MUP template is calculated to estimate a typical MUP within the MUPT. MUP templates have the advantage of reducing noise from contaminating MUPs from other MUs but they also represent a smeared estimate of a typical MUP due to MUP shape instability across the MUPT.

- **Ensemble Features:** These features describe how much MUP morphology varies across the MUPs in an MUPT. Assuming negligible instrumentation noise and no MUP superposition, MUP instability is attributed mainly to the variable times of arrival of constituent muscle fibre action potentials at the electrode detection surface

across consecutive motor unit discharges, which is due to variation in neuromuscular transmission and in muscle fibre action potential conduction velocity.

Morphological features can be further classified into three different categories based on which aspects of MUP morphology they best represent:

- **Size:** Size features, such as amplitude, duration, and area, are related to the number and sizes of fibres in a given motor unit. Simulation studies [82], however, have suggested that each of these features is affected by not only the number and sizes of fibres that comprise a motor unit but also by the range of distances between muscle fibres and the electrode detection surface, such that the closest fibres have the greatest impact on the value of these features. In this regard, duration is less affected than amplitude by individual fibre distance, but it is highly dependent on placement of onset and end markers. Area is less dependent on individual fibre location than amplitude and depends less on marker location than does duration.

- **Shape:** Shape features describe the overall shape of an MUP template. In this study, thickness (area to amplitude ratio) is the only shape feature considered. Thickness measured in milliseconds conveys information that can be thought of as the effective width of an MUP. In myopathic muscles, MUPs can have amplitudes comparable to those found in normal muscles, because amplitude is highly dependent on the size of the closest fibre. Myopathic MUPs are, however, often thinner because of muscle fibre loss. On the other hand, neurogenic MUPs are often thicker, as more muscle fibres comprise the motor unit due to reinnervation.

- **Complexity:** MUP morphology is influenced by many factors, including the number of muscle fibres, range of fibre diameters, spatial arrangement of fibres with respect to the electrode detection surface, the variability of neuromuscular transmission, and muscle fibre action potential conduction velocities.

  Fibres in normal motor units are expected to exhibit more homogeneity and less temporal dispersion, leading to simpler and more uniform MUPs. On the other hand, diseased motor units tend to have more variation in all factors listed above and therefore yield more complex MUPs. The features studied here attempt to

59

represent MUP complexity at both global and local levels. The most obvious global complexity features are number of phases and turns. Fibre count is different from number of turns in that only positive turns detected in the second derivative of an MUP template are counted. This gives more confidence that each of the counted peaks is produced by a separate muscle fibre or a small group of fibres [125]. Another way of expressing MUP irregularity uses MUP length, which can be thought of as the length of the stretched out MUP contour. Length index and shape width feature values are calculated by normalizing and standardizing MUP length with respect to amplitude and area, respectively.

Local complexity features focus on representing the finer morphological details of phases and turns. These features attempt to differentiate between neurogenic and myopathic complexity. On average myopathic MUPs often have smaller phases and turns compared with neurogenic MUPs.

3.4.3   MUPT Characterization

An MUPT characterization can be thought of as a set of conditional probabilities, one for each category of muscle considered. Each element of an MUPT characterization represents the conditional probability of the examined muscle falling into a specific category given the feature values of the MUPT [i.e., $P(y_l \mid x)$], where y_l is the muscle category and x is a feature vector used to describe the MUPT. For example, to discriminate between normal and neurogenic muscles, $y_l \in \{normal, neurogenic\}$ and an MUPT characterization would have two conditional probability values. The conditional probabilities were estimated assuming a multivariate Gaussian probabilistic model such that:

$$P(x \mid y_l) = \mathcal{N}(x \mid \mu_l, \Psi) \tag{3.1}$$

Using various sets of training data, maximum likelihood was used to estimate the mean feature vector μ_l for each category. The averaged covariance matrix was estimated using:

$$\Psi = \sum_l \Psi_l P(y_l) \tag{3.2}$$

where $P(y_l)$ represents the probability of having a muscle assigned to category l, and all categories are assumed to be equally likely.

3.4.4 Muscle Characterization and Categorization

A muscle characterization is a set of conditional probabilities, one for each of the three categories of muscle considered. Each element of a muscle characterization represents the conditional probability of the examined muscle belonging to a specific category given the set of MUPTs sampled from the examined muscle $[P(y_l \mid x_1, \cdots, x_n)]$. A muscle characterization was calculated as the mean of the MUPT characterizations of all MUPTs sampled from the examined muscle.

Assuming n MUPTs were sampled from an examined muscle, its muscle characterization is estimated as:

$$P(y_l \mid x_1, \cdots, x_n) = \frac{\sum_{i=1}^{n} P(y_l \mid x_i)}{n} \tag{3.3}$$

A muscle is categorized as belonging to the category which has the highest muscle characterization value. Muscle and MUPT characterization are explained more formally and in further details in Section 6.4 on Page 117.

3.4.5 Validation and performance metrics

Leave-one-out cross-validation (LOOCV) was used. In each iteration, the feature vectors of the MUPTs of a given muscle were used for testing, and feature vectors of the remaining MUPTs were used as training data for estimating the parameters of the assumed Gaussian model. For each category, category error was calculated as the ratio of the number of misclassified muscles to the total number of muscles belonging to that category. The overall classification error was then estimated as the mean value of individual category errors.

3.4.6 Backward Feature Selection Algorithm (BFS)

The BFS algorithm starts by using a feature set containing all studied features. In each subsequent iteration, all possible sets of features with one less feature than the previous iteration are evaluated by calculating its respective classification error using LOOCV. A feature is discarded if it does not belong to one of the best feature set combinations, in which case it is redundant and/or irrelevant. If during an iteration no feature is discarded, the algorithm evaluates all possible sets of features with two fewer features during the subsequent iteration.

3.4.7 Statistical Forward Feature Selection Algorithm (SFS)

To improve the resolution with which muscle categorization accuracy might be measured, muscle examinations were simulated using the MUPT data extracted from the actual muscles examined. For each muscle category (i.e., myopathic, normal, and neurogenic) all of the MUPTs extracted from muscles of each category were combined into one set (i.e. pooled sets of myopathic, normal, and neurogenic MUPTs were created). For each muscle category, 1000 sets of 20 MUPTs, randomly selected from its respective pooled set, were created to simulate 1000 examinations of muscles pertaining to that category (i.e. 3000 sets of 20 MUPTs, representing 3000 simulated muscle examinations were created in total). These 3000 sets of MUPTs were divided equally into ten groups of 300 simulated muscle examinations for testing purposes.

The SFS algorithm starts with a single feature. In subsequent iterations larger feature sets, created by adding one feature to each feature set selected during the previous iteration, are evaluated by calculating the classification error for each group of simulated muscle examinations using LOOCV. The best performing feature set, (i.e. the one having the minimum average error across all groups of testing sets), and all statistically equivalent sets (based on student t-tests) are selected. The algorithm terminates when none of the selected feature sets brings a statistically significant improvement in classification accuracy compared to the sets constituting the previous iteration. The algorithm is summarized in Figures 3.1 and 3.2.

62
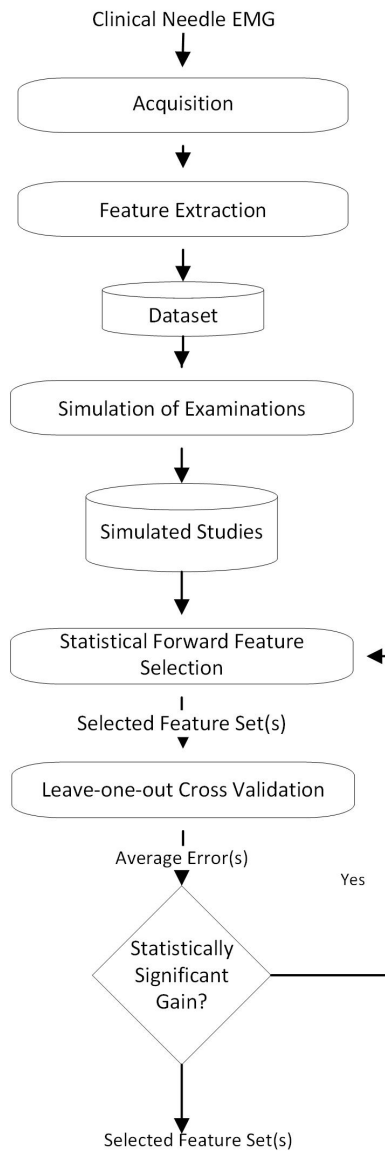
Figure 3.1: Summary of the SFS algorithm. Boxes represent steps of the algorithm. Conditions are shown as diamonds and datasets as cylinders.

3.5 Results

The muscle characterization was applied in a one-to-one schema. Three multivariate Gaussian models were used to discriminate between neurogenic and normal muscles, between
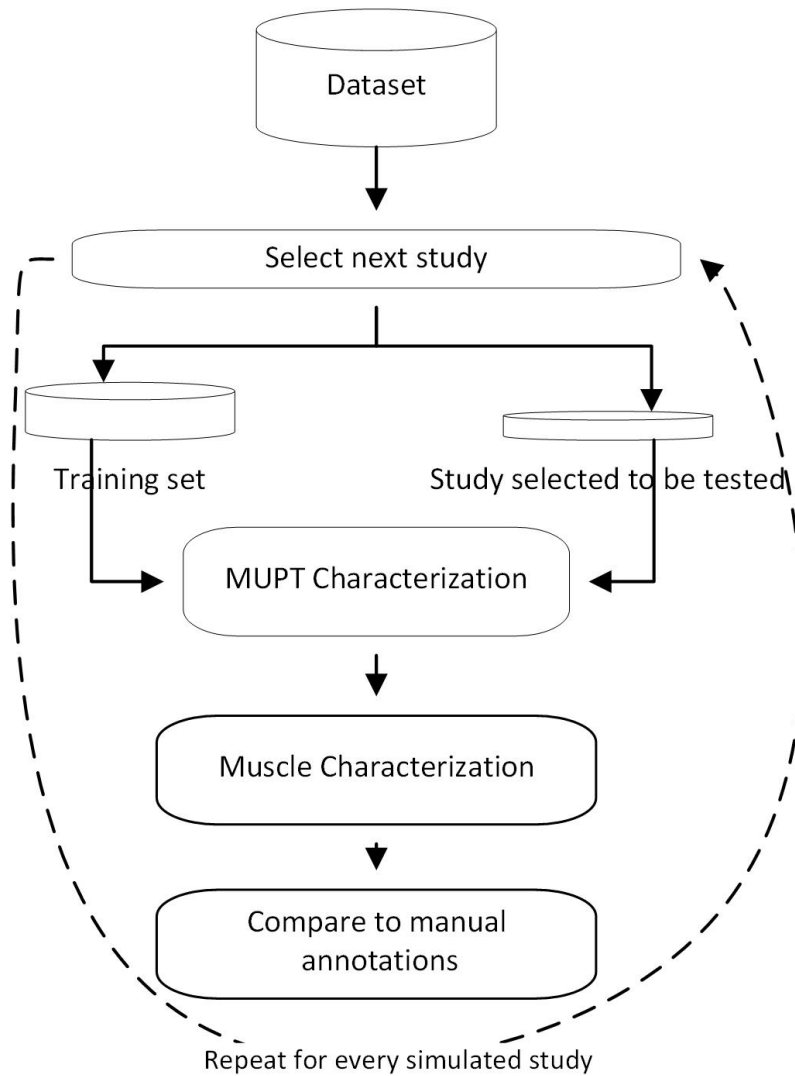
Figure 3.2: Summary of leave-one-out cross validation. Boxes represent steps of the algorithm. Iterations are shown as dashed lines, while datasets as cylinders.

myopathic and normal muscles, and between neurogenic and myopathic muscles. The findings using the BFS algorithm and those from the SFS algorithm are summarized in Table 3.3. The SFS algorithm was designed in such a way that all feature sets having equivalent performance to the feature set(s) achieving the minimal mean classification error were pro-

Muscle	BFS Error	SFS Avg. Error	SFS No. of Sets
Discrimination between neurogenic and normal muscles			
FDI	14.92	3.6	20
DLT	16.67	5.15	89
VM	22.13	2.75	45
TA	4.37	2.5	47
Discrimination between myopathic and normal muscles			
FDI	18.96	2.1	334
DLT	16.25	7.3	17
VM	10.56	0.3	36
TA	23.54	5.25	171
Discrimination between neurogenic and myopathic muscles			
FDI	7.69	0.15	154
DLT	13.33	2.55	14
VM	10.53	0	140
TA	3.33	0.7	43

Table 3.3: Summary of feature selection algorithm findings: The first column lists the smallest classification error obtained by the BFS algorithm, the second lists the smallest mean classification error obtained by the SFS algorithm using simulated studies, and the final column notes the number of set(s) selected by the SFS algorithm which are equivalent statistically to the set(s) which achieve minimal mean classification error (based on student t-tests with alpha set to 0.05).

moted to the following iteration. This resulted into tens or even hundreds of equivalently performing feature sets being selected for a particular decision level and muscle type as shown in the last column of Table 3.3.

The relative importance of an aspect is proportional to the number of times a feature representing that aspect was selected and at which iteration, since a feature selected at an earlier iteration is more relevant to making a correct category assignment. A rank score

for each aspect was therefore calculated to denote its relative importance. The rank score of the contribution of each selected feature in each equivalently performing feature set selected by the SFS algorithm was incremented by a weighting factor. The value of the weighting factor was determined by the iteration number during which that feature was selected. The weighting factor for a feature selected during the first iteration was equal to the number of features included in its feature set. The weighting factors of the features selected during subsequent iterations were then decreased correspondingly, such that the weighting factor of the feature selected during the last iteration was 1.0. In cases where more than one feature from the same aspect was selected in the same feature set, only the earliest selected feature was considered. This is important to account for the fact that different aspects have different numbers of features representing them.

The accumulated ranking scores of the different aspects were then normalized, such that the highest was made equal to 100. These results are summarized in Table 3.4. The features that were selected most often to represent a specific aspect for the various decisions made, and those contributing to the various muscle type categorizations studied are also shown in Table 3.4.

Muscle		1st Aspect	2nd Aspect	3rd Aspect	4th Aspect	5th Aspect	Err.	Sim Err.
Discrimination between neurogenic and normal muscles								
FDI	**Aspects**	Size	Stability	L.Cmpl	G.Cmpl	Shape		
	Ranking	100	65	11.67	10	6.67		
	Features	Ar	Jig	TrWdth	ShpWdth	Thk	22.4	3.9
DLT	**Aspects**	L.Cmpl	Size	G.Cmpl	Stability	Shape		
	Ranking	100	99.34	78.95	26.32	18.42		
	Features	PhAr	Ar	Tr	ShmCov	Thk	19.2	4.9
VM	**Aspects**	Size	Stability	L.Cmpl	G.Cmpl	Shape		
	Ranking	100	66.67	11.11	11.85	2.96		
	Features	Ar	Jig	TrLn	Tr	Thk	25.7	1.9
TA	**Aspects**	Size	Stability	L.Cmpl	G.Cmpl	Shape		
	Ranking	100	71.30	33.04	19.13	10.43		
	Features	Ar	ShmCov	PhAr	ShpWdth	Thk	11.5	2.1

66

	Discrimination between myopathic and normal muscles							
FDI	**Aspects**	G.Cmpl	L.Cmpl	Stability	Size	Shape		
	Ranking	100	54.71	45.54	35.36	9.26		
	Features	ShpWdth	PhAr	Jig	Ar	Thk	22.3	1.5
DLT	**Aspects**	G.Cmpl	L.Cmpl	Size	Stability	Shape		
	Ranking	100	17.62	8.82	8.82	2.94		
	Features	ShpWdth	PhCmpl	Dur	Jig	Thk	22.5	6.4
VM	**Aspects**	G.Cmpl	Size	L.Cmpl	Stability	Shape		
	Ranking	100	62.04	18.52	5.56	1.85		
	Features	ShpWdth	Ar	Trln	Jig	Thk	16.5	0.4
TA	**Aspects**	L.Cmpl	Stability	G.Cmpl	Size	Shape		
	Ranking	100	76.14	50.53	36.73	1.17		
	Features	TrAr	Jig	FbrCnt	Ar	Thk	30	5.1
	Discrimination between neurogenic and myopathic muscles							
FDI	**Aspects**	G.Cmpl	Size	L.Cmpl	Stability	Shape		
	Ranking	100	89.79	73.94	22.89	19.72		
	Features	ShpWdth	Ar	TrAr	Jig	Thk	13.9	0.1
DLT	**Aspects**	Size	L.Cmpl	G.Cmpl	Stability	Shape		
	Ranking	100	17.86	14.29	7.14	3.57		
	Features	Dur	TrLn	ShpWdth	Jig	Thk	17.5	2.7
VM	**Aspects**	Size	L.Cmpl	G.Cmpl	Shape	Stability		
	Ranking	100	34.29	24.29	15	9.05		
	Features	Ar	TrWdth	ShpWdth	Thk	Jig	15.5	0
TA	**Aspects**	Size	Stability	L.Cmpl	G.Cmpl	Shape		
	Ranking	100	61.46	47.92	40.63	3.13		
	Features	Ar	Jig	PhAr	FbrCnt	Thk	8.3	0.2

Table 3.4: For a particular muscle and decision, aspects are sorted based on their estimated ranking factors, i.e. their utility. A set is also constructed by selecting the most frequently selected feature for each aspect. The performance based on simulated studies is equivalent statistically based on student t-tests with alpha set to 0.05 to the set(s) selected by the SFS algorithm. The errors obtained for these sets using actual data are within $\pm 8\%$ of the minimal errors for the feature sets selected by the BFS algorithm.

3.6   Discussion

Using a global set of 18 MUPT features comprised of traditional and newly defined features and representing different MUPT aspects, feature subset selection methods were used to select discriminating QEMG feature sets. The selected feature subsets were selected by considering the following properties:

1. **Discriminative:** Characterization based on selected features should be accurate and consistent with an expert electromyographers assessments.

2. **Simple:** A lower number of features is preferable, eliminating irrelevant information and simplifying the basis on which a characterization is based, and increasing the confidence that results can be generalized.

3. **Least redundant:** It is preferable to have a feature set in which every relevant aspect is represented using the most relevant feature, yielding a more structured decision process.

4. **Interpretable:** The numerical estimates of features should be appreciated readily and able to be understood based on visual inspection.

5. **Informative:** Selected features should promote the use of electrophysiological and anatomical knowledge to infer the muscle condition or readily explain decisions inferred though statistical modeling.

6. **Acquisition Independent:** The measured feature values should be as insensitive as possible to needle positioning and instrumentation settings

7. **Easily estimated:** Some features can be more consistently and accurately estimated using automated methods, thereby avoiding time-consuming marker editing.

8. **Generalizable:** It is preferable to end up with a feature set that can be in all muscle types: large and small, proximal and distal, and limb, axial, and cranial muscles.

The best feature subsets were found to be comprised of a reduced number of features, which together can be used to distinguish accurately between neurogenic, myopathic, and normal muscles. The main advantage of methods which consider feature subsets, as opposed to methods which investigate each feature independently, is the consideration of inter-feature dependencies or correlations. This is especially important for QEMG features, because the same MUPT aspect often contributes to more than one feature. For example, duration, amplitude, and area all represent the size of an MUP template. Even though each of them can be used to discriminate between neurogenic and normal muscles, they are unlikely to be selected in the same subset due to their interdependence. Moreover, some of these features convey redundant information, in that they are calculated using other feature values.

A multivariate classification method was used rather than more traditional multiple univariate methods, because multivariate methods use covariance or correlation matrices to estimate and utilize the interrelatedness of the features within a selected set of features to find linear combinations of the features to maximize discrimination among different classes. On the other hand, multiple univariate analyses accumulate evidence from each feature by assuming independence among the features or by employing heuristics [97].

The most comprehensive way to select a feature subset would be exhaustive search, which means measuring the discriminatory power of all possible feature subsets. However, because across the 18 features investigated in this study more than 250,000 subsets can

be constructed, sequential search methods were used instead. Both forward and backward search strategies were used to assure convergence to feature sets with the smallest numbers of features that provide maximal discrimination. The discriminatory power of a selected feature subset can be estimated using a filter or wrapper method. Filter methods rely on general properties of the estimated distributions of feature data. These properties include class separability, relevance, independence, and others. Wrapper methods measure the classification accuracy of a specific feature subset using a chosen classification algorithm [47]. The author used a wrapper method based on probabilistic muscle characterizations.

Simulated muscle studies were used for the following reasons:

- To provide more uniform evaluation across disease categories, even with imbalances among different categories as shown in Table 3.1.

- To increase the resolution with which discrimination accuracy could be determined to avoid drastic changes in search results caused by small numbers of misclassifications.

- To smear (reduce the effect of) muscle categorization inaccuracies, because MUPTs from inaccurately categorized studies are to be distributed across many simulated studies and their characterizations (the probability that a given MUPT was detected in a muscle of a specific disease category) will be averaged with other MUPTs during the aggregation stage in order to reach an accurate muscle categorization.

The resulting simulated studies may contain MUPTs belonging to muscles affected by different levels or stages of disease involvement. BFS was therefore conducted using actual muscle studies. The errors of feature sets selected by SFS were re-evaluated using actual muscle studies, resulting in errors within ±8% of the minimal errors for the feature sets selected by the BFS algorithm.

The large number of feature subsets selected by the SFS algorithm that have statistically equivalent performance is not surprising given the large number of tested feature subsets, as well as considering the redundancy and interdependence among investigated features and the small size of the data set used for statistical validation. It is clear that features belonging to the same selected set mostly represent different MUPT aspects, while alternative selected feature sets are more often formed by replacing one feature by another,

70

reflecting the same aspect. These two observations support the proposed aspect-based grouping of features, as they validate the independence among the proposed aspects (i.e. that each aspect conveys some degree of unique information). It also demonstrates that features belonging to the same aspect convey very similar information.

Another clear observation is that feature aspects that allow discrimination between myopathic muscles and normal muscles are often different from feature sets that provide discrimination between neurogenic and normal muscles even for the same muscle type. Still, there appears to be clear consistency among aspect rankings for a given decision across different muscle types. For instance, stability and size were selected as the most relevant aspects for discrimination between neurogenic and myopathic muscles for all muscles types studied except the deltoid. These two aspects correlate with reinnervation and abnormally variable neuromuscular transmission. On the other hand, global and local complexity features were found to be among the top three ranked aspects for discrimination between myopathic and normal muscles. MUPs detected in myopathic muscles often have increased complexity due to fibre loss, fibre atrophy, and fibre hypertrophy leading to increased variability of muscle fibre diameters belonging to a given motor unit, which in turn leads to higher variability in fibre conduction velocities.

Amplitude was selected rarely to represent MUP size. This is consistent with findings of simulation studies [82], which have verified that amplitude is mainly influenced by proximity of the electrode to the nearest muscle fibre, whereas both area and duration are more acquisition independent. Area was selected more often than duration to represent MUP size, which can be attributed to the fact that area is less influenced by onset and end marker positioning.

For discrimination between myopathic and normal muscles, shape width was selected more often than any other feature representing global complexity. MUPs in each row of Figure 3.3 have almost the same thickness and area. MUPs in the right column are extracted from myopathic muscles with clear morphological complexity. This complexity is captured successfully using shape width, which is significantly smaller for the MUPs extracted from myopathic muscles. Another advantage of using shape width to characterize global complexity rather than turns is that shape width estimates are less sensitive to baseline fluctuations and noise. Shape width was selected more often than length index,

71

because shape width is normalized using area instead of amplitude.
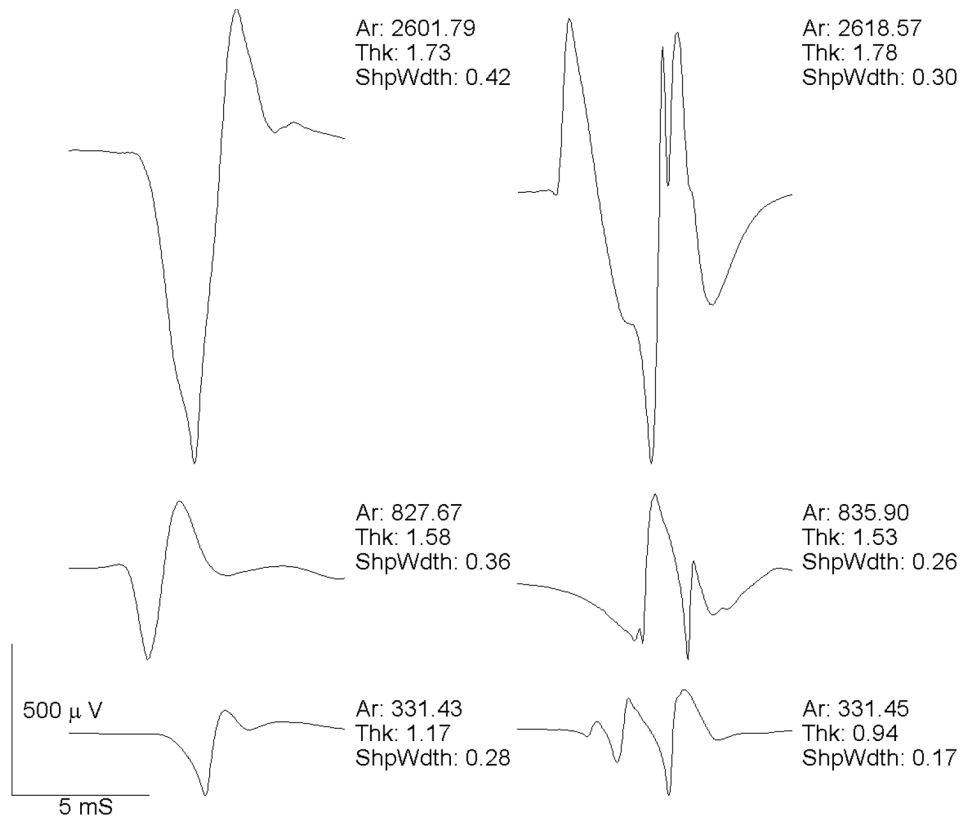
Figure 3.3: The left column shows MUP templates extracted from normal muscles, and the right column shows MUP templates extracted from myopathic muscles. In each row, the two MUP templates have nearly the same size (area) and shape (thickness), while MUP templates extracted from myopathic muscles show significantly lower shape width.

Local complexity features related to phase characteristics such as phase area, are intended to augment discrimination between neurogenic and normal muscles. Figure 3.4 shows an increase in phase area for MUP templates estimated from MUPTs recorded in neurogenic muscles compared to those of MUPTs recorded in normal muscles. This can be attributed to re-innervation. On the other hand, local complexity features related to turns such as turn area augment discrimination between myopathic and normal muscles. A clear decrease in turn area for MUP templates estimated from MUPTs recorded in my-

72
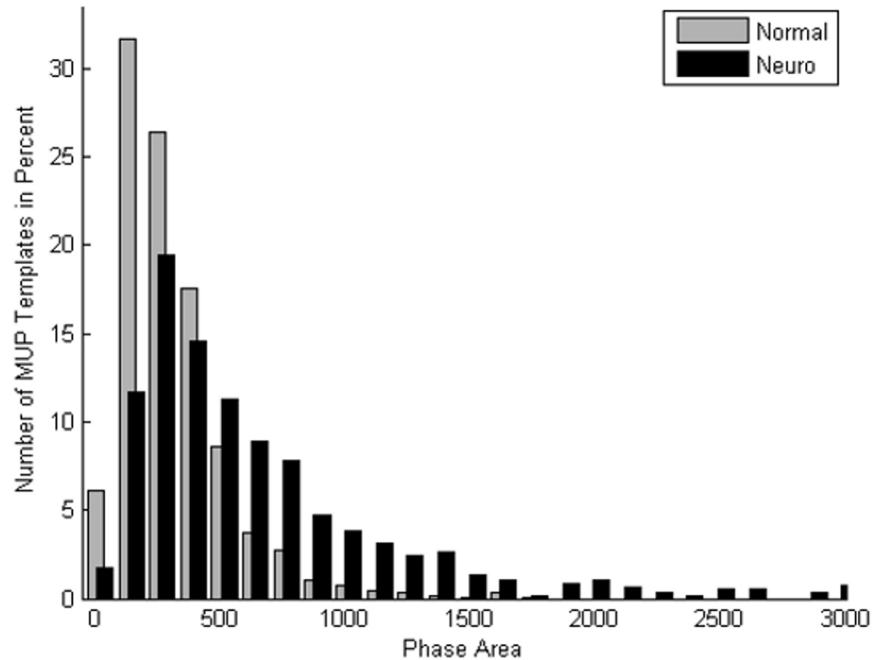
Figure 3.4: Black bins represent phase area measurements from MUP templates extracted from neurogenic muscles, while grey bins represent measurements from MUP templates extracted from normal muscles.

opathic muscles compared to those of MUPTs recorded in normal muscles can be seen in Figure 3.5 , which is expected due to muscle fibre depletion. It is important to note that MUPT labelling was based on muscle characterization (i.e., at the muscle level and not at the motor unit level). Therefore, normal MUPTs are expected to be detected in both neurogenic and myopathic muscles, with a probability dependent on the degree to which the muscle has been affected by disease.

Each row in Figure 3.6 shows MUP templates having almost the same size (area). The MUP template on the right in each row was extracted from a neurogenic muscle and has a higher turn area, while the MUP on the left was extracted from a myopathic muscle. This demonstrates how local complexity features can augment the discrimination between myopathic and neurogenic morphological complexity in equivocal cases.

73
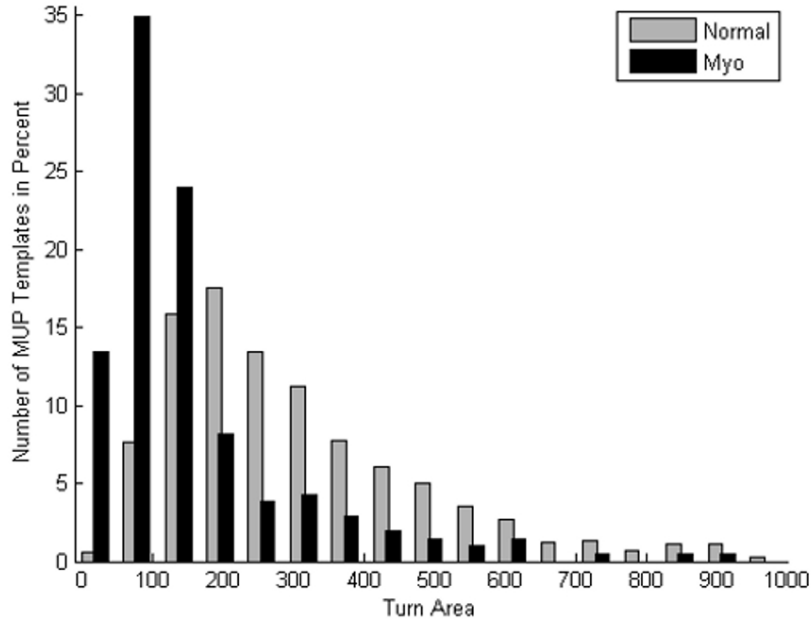
Figure 3.5: Black bins represent turn area measurements from MUP templates extracted from myopathic muscles, while grey bins represent measurements from MUP templates extracted from normal muscles.

It is possible to obtain smaller average error rates when discriminating between neurogenic and myopathic muscle than the average errors obtained for the other two decisions, because for most QEMG morphological features, normal MUPT values tend to lie between the neurogenic and myopathic values, and therefore the neurogenic and myopathic categories are well separated.

The results obtained from this study are preliminary. Perhaps more convincing findings could be obtained by studying EMG signals collected by a group of electrodiagnostic experts contributing to a larger data set. Investigating additional features and employing improved strategies for estimating the features studied here may eventually lead to a set of features accepted by broad census which provide greater power to discriminate between neurogenic, myopathic and normal muscles.

Figure 3.6: The left column shows MUP templates extracted from myopathic muscles, and the right column shows MUP templates extracted from neurogenic muscles. In each row, the two MUP templates have nearly the same size (area) but with clear differences in turn area.

Chapter 4

Representation: Near Fibre MUP Jitter: A New Quantitative Electromyographic Feature For Characterizing Neuromuscular Junction Transmission

4.1 Summary

Objective: The main objective of this chapter is to address technical difficulties associated with estimating jitter using single fibre EMG signals. The chapter proposes a variant of

---

Portions of the methods described in this chapter previously appeared in T. Chen, M. Abdelmaseeh, and D. Stashuk. Affine and regional dynamic time warpng. *arXiv preprint arXiv:1505.06531*, 2015.

the jitter feature, called near fibre MUP jitter, that can be estimated quickly from an automatically decomposed EMG signal. A signal that can be acquired using a conventional clinical protocol and equipment that have been shown to be useful for evaluating MUP morphology and morphological stability.

Methods: At the core of the proposed method is a classifier capable of detecting single fibre MUP segments, i.e., parts of the MUP where the contribution from a single muscle fibre is not highly contaminated by contributions from other fibres. For a set of MUPs created by the same motor unit, single fibre MUP segments may have varying occurrence times within the MUPs but will have consistent morphology across the MUPs. Aligning single fibre MUP segments and evaluating their morphological consistency are achieved using regional dynamic time warping.

Results: Results based on 680 simulated MUPTs show that near fibre MUP jitter can be estimated with an average error rate as low as 8.9%. Also, one or more single fibre MUP segments can be detected in more than 85.3% of the studied MUPTs. The analysis for a single MUPT can be completed in 3.6 seconds on average using a conventional personal computer.

4.2 Introduction

Myasthenia gravis is a chronic autoimmune NMD caused by antibodies binding to receptors for acetylcholine in the neuromuscular junction. This results in altering and/or blocking of the transduction of the motor neuron impulses at the neuromuscular junction [56]. Other NMDs can also disrupt neuromuscular transmission, especially disorders that involve denervation and reinnervation of muscle fibres [140].

In the mid sixties, Stålberg and Ekstedt developed an electro-physiological test known as single fibre electromyography (SFEMG) [116, 32]. As the name of the test suggests, they utilized a spatially selective electrode to record EMG activity created by a single muscle fibre. The major contribution of SFEMG to characterization of NMDs is the definition of a new quantitative EMG feature, called jitter. The authors defined jitter in [118] as "the variability in time interval at consecutive discharges between two action potentials from

two muscle fibres belonging to the same motor unit". The MFPs can be produced as a result of either low voluntary contraction or repetitive stimulation.

Jitter was shown to be sensitive to disturbances in neuromuscular transmission. In [108], jitter was shown to have a sensitivity of up to 99 % in detecting deficiencies in neuromuscular transmission due to generalized myasthenia gravis. The same study also showed that jitter is suitable for tracking longitudinal changes. In recent years, there have been many attempts [33, 11, 110] to use less spatially selective electrodes, such as concentric and monopolar electrodes, for jitter estimation. One compelling argument for replacing single fibre electrodes is that they are not disposable. The use of reusable clinical electrodes is restricted in many countries [117]. Compared to single fibre electrodes, needle electrodes are usable for other electrodiagnostic tests, and they are cheaper. On the other hand, the fact that these electrodes are less spatially selective makes it more likely that detected MFPs are contaminated by contributions from other distant fibres belonging to the same motor unit or other motor units.

Therefore, the use of conventional less spatially selective clinical electrodes, such as a concentric needle electrode, is normally accompanied by high pass filtering to attenuate contributions from distant fibres and manual editing to exclude highly contaminated MUPs from the analysis. Regardless the type of the electrode used for jitter analysis, the clinical procedure used in estimating jitter has been constantly described by a majority of neurologists and electromyographers to be challenging. The authors of the textbook "EMG pearls" [44] described the analysis to impose *substantial* technical demands for both the patient and the practitioner. A mini-monograph published by the American association of neuromuscular and electrodiagnostic medicine (coauthored by Stålberg [109]) mentioned that it is a *must* for a practitioner to have *considerable* experience to be able to perform the analysis. These difficulties were also reported in other clinical studies [52, 91, 19].

This study aims at elevating these difficulties by estimating a new quantitative EMG feature that the author refers to as near fibre MUP jitter (NF-MUP-Jitter). Similar to the conventional SFEMG based jitter, the feature aims at capturing disturbances in neuromuscular transmission. The key difference between NF-MUP-Jitter and conventional jitter is that NF-MUP-Jitter is to be estimated from an automatically decomposed EMG signal. Please refer to Chapter 2 for further discussion on automated decomposition of EMG sig-

nals. These signals are to be collected using a conventional clinical acquisition protocol that is used for evaluating MUP morphology and morphological stability. An example of such an acquisition protocol is discussed in Chapter 3 on Page 51. Given the nature of the utilized signal and how it is processed and decomposed, the newly proposed feature (NF-MUP-Jitter) deviates from the original definition of jitter in that:

- The NF-MUP-Jitter analysis does not attempt to find isolated MFPs. Instead, it focuses on finding segments in the MUPs assigned to a given identified train that are observed to have consistent morphology and hence the name of the new feature contains the term MUP. These segments are hypothesized to be *mainly* created by a single fibre and not significantly contaminated by contributions from other fibres.

- The MUPs used for NF-MUP-Jitter analysis are not necessarily assumed to be consecutive. This assumption is not realizable for signals acquired during a low to medium contraction level. Such EMG signals are normally comprised of multiple MUPTs, which increases the chance of MUP superposition.

- The MUPs used for NF-MUP-Jitter analysis are low-pass double differentiated [134] to eliminate contributions from muscle fibres that are distant from the electrode detection surface without accentuating the high frequency components of the noise.

The signal acquisition and analysis steps involved in estimating NF-MUP-Jitter are significantly faster compared to the SFEMG based analysis. The whole test can be completed in the order of a few seconds compared to the tens of minutes necessary to complete conventional SFEMG analysis. Also, the process does not demand expertise beyond that necessary for completing a conventional clinical EMG test, which is found in almost every electrodiagnostic lab.

4.3 Literature Review

This review only focuses on a subset of the jitter analysis literature that addresses characterization of disturbances in neuromuscular transmission based on clinical EMG signals

acquired using conventional needle electrodes. In the late seventies, Payan showed in a short technical note [94] that increasing the cut-off frequency of the high-pass filtering applied to EMG signal from the standard 500 Hz to as high as 3000 Hz reduces contributions from muscle fibres that are distant from the electrode detection surface. These contributions are mainly comprised of low frequency components. Therefore, they obscure disease-induced MUP complexity.

Payan used the analogy of looking under blanket to demonstrate the effect of high-pass filtering on revealing MUP complexity. An investigation of the utility of features describing the complexity and size aspects of high-pass filtered MUPs in discriminating between normal, myopathic and neurogenic muscles is presented in Appendix A. It was not until 1998 that Stashuk presented a comprehensive study of the possibility of detecting contributions from muscle fibres [126] from MUPs acquired using a concentric needle electrode. The detection of MFPs was performed by searching for peaks in band-pass filtered (or low-pass double differentiated) MUPs. For these peaks to qualify as contributions from muscle fibres, they needed to have an amplitude and rise time above preset thresholds.

The evaluation in this study mainly relied on computational models to produce MUPs with known MFP composition. Results based on 720 simulated MUPTs showed that up to 84 % of significant MFPs were detected in the case of using an amplitude threshold of 2.5 KV/ s^2. A simulated MFP was considered to be significant (i.e., detectable) only if it exceeded the same amplitude threshold. This direction of investigation was further extended by Stashuk and his collaborators.

In [72], it was shown that the acceleration filter (low-pass double differentiation) was better for detection of MFPs compared to using a Butterworth band-pass filter. The work also presented methods for jitter measurement by identifying and tracking detected MFPs along the MUPs of a given train. Results based on simulated MUPTs showed that jitter can be measured with an average error of 8.37%. This work was further extended in [138, 54] by refining MUP filtration techniques and introducing an algorithm, based on minimum spanning tree clustering [46], for classifying MUPs within a given train as either isolated or superimposed. This resulted in reducing the average error for measuring jitter to 7.3%.

The main differences between the work presented in this chapter and the previous work

performed by Stashuk et al. is that this work does not detect MFPs by investigating the morphology of the MUPs (i.e., searching for peaks) but through analyzing morphological consistency across the MUPT. This work instead focuses of detecting single fibre MUP segments, which is defined as a part of a MUP created by a single muscle fibre and not significantly contaminated by contributions from other muscle fibres. Therefore, for a particular MUPT, these segments may have varying occurrence times within the MUPs because of the variable time required for neuromuscular transmission. However across the MUPs of a MUPT, a single fibre MUP segment is expected to have a consistent morphology in most MUPs of a given MUPT when compared to the segments of the MUPs resulting from overlapping muscle fibre contributions. Given this definition, a peak in a NF-MUP, even when significant and not bifuricating, might or might not be a single fibre MUP segment. Figure 4.1 provides an example of single fibre MUP segment.

Other technical differences between this work and previous work completed by Stashuk et al. are:

- Using regional dynamic time warping (RDTW) for tracking single fibre MUP segments and estimating NF-MUP-Jitter.

- Utilizing learning algorithms trained using simulated MUPTs for detection of single fibre MUP segments rather than a set of fixed criteria such as minimal amplitude or slope.

4.4 Methods

The proposed system operates in two phases: training and estimation. The output of the training phase is a classifier that can segment single fibre MUP segments from unseen MUPTs. The input to the training phase is a set of simulated MUPTs with known MFP composition and jitter values. Up to the author's knowledge, there is no laboratory method capable of revealing the MFP composition of a MUP nor the variability in neuromuscular transmission. The training algorithm learns a model using a set of feature vectors that are assumed to be probabilistically independent. Each of the vectors describes a group of

81
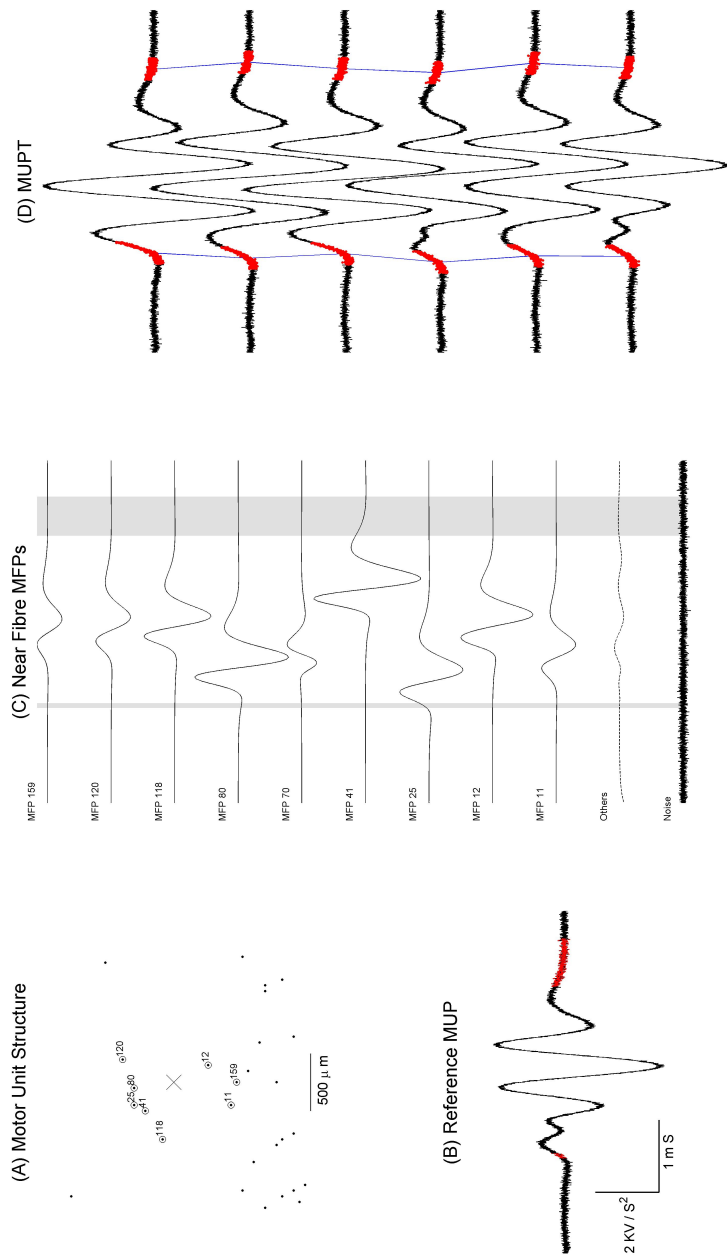
Figure 4.1: Figure (A) shows the spatial distribution of muscle fibre centres in the cross section of a simulated motor unit. The centre of each muscle fibre is depicted using a dot '.'. The electrode, represented as 'x', is assumed to be at the centre. Figure (B) shows one of the resulting MUPs. Figure (C) shows a stacking of the potentials resulting from the fibres that have a contribution above 0.5 KV / s^2, while the two bottom traces show the summation of other potentials and the simulated noise. Single fibre MUP segments detected by the proposed algorithm are highlighted in red in Figure (B) and shaded by grey in Figure (C). Figure (D) shows a raster of five simulated MUPs generated by the motor unit and the tracking of two regions belonging to two single fibre MUP segments.

aligned regions using a constrained DTW procedure, where each region belongs to one of the MUPs in a MUPT. The feature vector captures the aligned regions' alignment properties. A label is assigned to each feature vector based on how accurately the NF-MUP-Jitter can be estimated based on this region. That is to say, a single fibre MUP segment is equated to a region, which can be used to accurately calculate NF-MUP-Jitter.

The inputs to the estimation phase are MUPTs identified from a clinical EMG signal and a trained classifier. The MUPs belonging to each MUPT are aligned using the same procedure applied in the training phase. Also, the resulting aligned regions are described using the same feature vector definition. These feature vectors are classified to either represent a single fibre MUP segment or not. The alignments between regions found to represent single fibre MUP segments can be then used for NF-MUP-Jitter estimation. The difference between the NF-MUP-Jitter estimation method in the estimation stage compared to the training stage is that it demands using a pair of single fibre MUP segments created by two different muscle fibres. This is because there is no direct way to estimate the motor neuron firing times and therefore neuromuscular junction transmission variability can be only estimated indirectly through investigating the variability in the intervals between two MFPs. The information flow of the system is depicted in Figure 4.2. The same nomenclature used in Chapter 2 is adopted here.

4.4.1 Alignment

The alignment procedure operates on a single MUPT at a time. The MUPs belonging to the MUP are first low-pass double differentiated. A reference MUP, say $\ddot{y}$, which can best capture the typical morphology of the MUPs belonging to the train is then selected. Therefore, the morphology of the reference MUP is expected to be the least affected by superposition from other MUPs, MFP blocking, and other factors including electrode movement. This problem was previously dealt with in Section 2.5.3 on Page 42 for the purpose of estimating a typical morphology template to be used for estimating quantitative EMG features. The idea behind the proposed solution is to find the MUP which is on average closest (based on some similarity measure) to the other MUPs belonging to the train. The assumption was that the changes in morphology due to superposition are
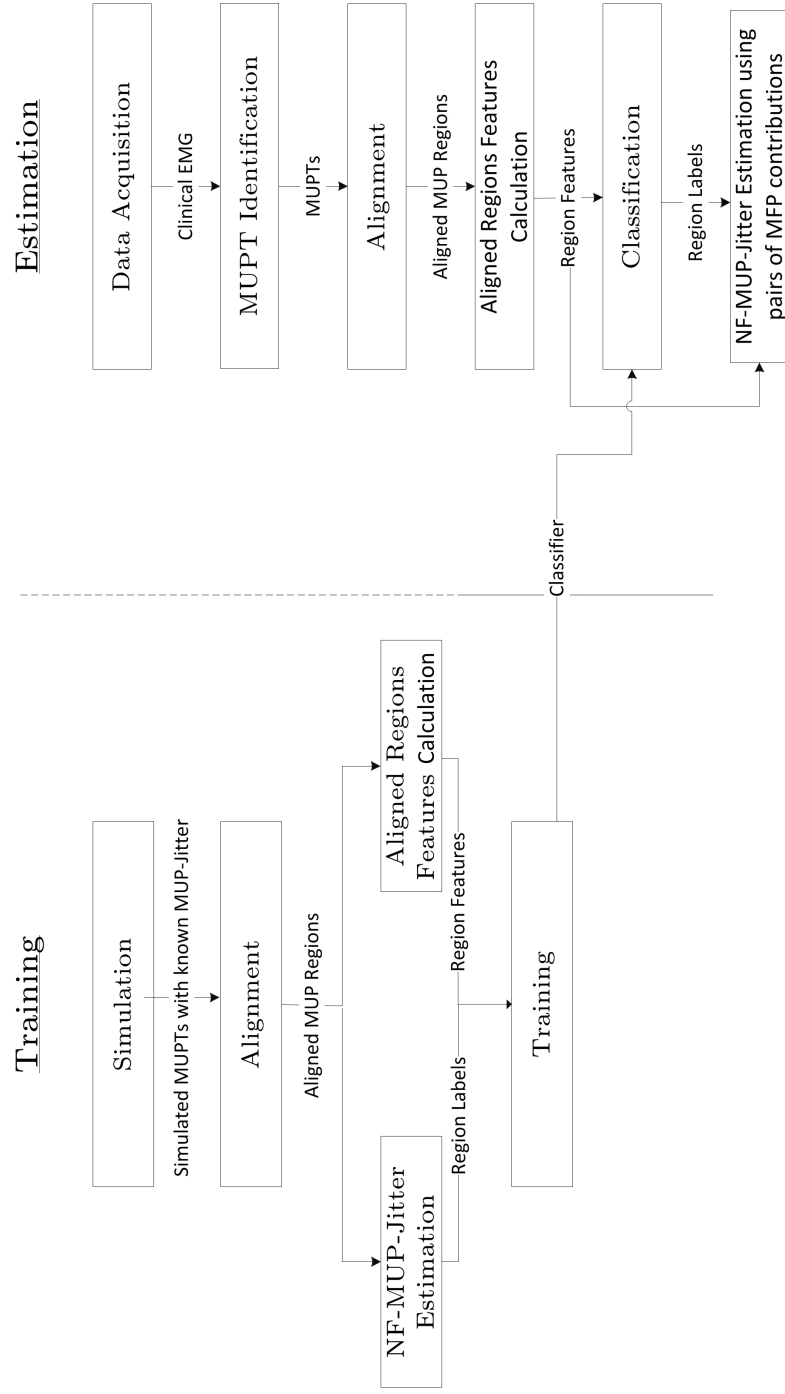
Figure 4.2: The information flow in NF-MUP-Jitter analysis

expected to produce random changes that were different from one MUP to another.

The simulated MUPTs used for training are modelled to be isolated. Therefore, any MUP in the MUPT can be selected as the reference MUP. Each MUP in the MUPT, except the reference MUP, is then aligned to the reference MUP using RDTW. RDTW uses the same dynamic programming optimization explained in Section 2.4.3 on Page 32. The major difference is that a zero-shift pseudo-correlation (ZPC) distance [38] is used instead of the Euclidean distance. ZPC can be calculated for an alignment between two arbitrary samples, say $\tilde{y}_k(t_n)$ from the kth MUP in the train and $\ddot{y}(t_m)$ from the reference MUP as:

$$ZPC(t_m, t_n) =$$

$$\frac{\sum\limits_{j=-L_{\mathrm{RDTW}}}^{j=L_{\mathrm{RDTW}}} (\tilde{y}_k(t_n + j)\ddot{y}(t_m + j) - |\tilde{y}_k(t_n + j) - \ddot{y}(t_m + j)|\max\{|\tilde{y}_k(t_n + j)|, |\ddot{y}(t_m + j)|\})}{\sum\limits_{j=-L_{\mathrm{RDTW}}}^{j=L_{\mathrm{RDTW}}} (\max\{|\tilde{y}_k(t_n + j)|, |\ddot{y}(t_m + j)|\})^2}$$

$$\mathfrak{d}(t_m, t_n) = 1 - ZPC(t_m, t_n)$$

where L_{RDTW} is the half region width. It is set to 50 μS, unless otherwise is mentioned. $||$ indicates taking the absolute value of the sample. The alignment path is constrained in the same way as described in Section 2.4.3 on Page 32. The half length of the Sakoe-Chiba band [107] is set to 300 μS, because it is expected that the standard deviation of the neuromuscular transmission times to be less than 150 μS. In order to speed up the computation time of the ZPC for different alignments, the sums in the denominator and the nominator of $ZPC(t_m + 1, t_n + 1)$ are computed in an incremental manner from $ZPC(t_m, t_n)$, i.e. removing the elements for $(t_m - L_{\mathrm{RDTW}}, t_n - L_{\mathrm{RDTW}})$ and including an element for $(t_m + L_{\mathrm{RDTW}} + 1, t_n + L_{\mathrm{RDTW}} + 1)$.

The evaluation of disturbances in neuromuscular transmission demands estimating jitter with a resolution as low as few microseconds. Therefore, it is necessary to sample the EMG signal with a resolution of 1 MHz or preferably higher. Most of the clinically available systems use much lower sampling rates (below 50 KHz). This is because MUP morphology can be well reproduced when sampled at this rate. Also, the equipment used

in these systems are based on legacy designs that were constrained by computational power and storage capacity. To circumvent these limitations, the MUPs are interpolated using linear interpolation to have a sampling rate of 1 MHz.

4.4.2 Aligned Regions Features Calculation

For each sample in the reference MUP, say t_m, two sets are constructed: the aligned indexes set $AI^{(t_m)}$ and the aligned distances set $AD^{(t_m)}$. Each of these two sets has a number of elements that is one less than the number of MUPs in the MUPT. The kth element in the $AI^{(t_m)}$ set is the index of the sample to which $\ddot{y}(t_m)$ is matched to, when the reference MUP is aligned to the kth MUP of the train. When $\ddot{y}(t_m)$ is aligned to more than one sample, the index of the sample that has the least distance $\eth$ is kept. The corresponding alignment distance is kept in $AD^{(t_m)}$. A feature vector $x_{\text{NFJ}}^{(t_m)}$ is constructed defining six statistics over $AD^{(t_m)}$: (1) mean, (2) standard deviation, (3) range, (4) minimum, (5) maximum and (6) median. It is worth reemphasizing here that both alignment and feature calculation are applied in the same way during both training and estimation phases of the analysis.

4.4.3 NF-MUP-Jitter Estimation

NF-MUP-Jitter ($NFJ(t_m)$) is estimated for every sample in the reference MUP during the training phase. It is set to the standard deviation of $AI^{(t_m)}$. For all MFPs belonging to a particular simulated muscle, the neuromuscular transmission times are modelled to be sampled from normal distributions having the same standard deviation. This means the expected NF-MUP-Jitter values for any of the single fibre MUP segments are the same.

NF-MUP-Jitter is estimated differently, when using non-simulated data during the estimation phase. In this case, the estimation starts by choosing a sample in the reference MUP to act as a synchronizing sample t_{Sync}. $NFJ(t_m)$ is then estimated as the standard deviation of the synchronized aligned indexes set $AI_{\text{Sync}}^{(t_m)}$, such that $AI_{\text{Sync}}^{(t_m)}(k) = |AI^{(t_{\text{Sync}})}(k) - AI^{(t_m)}(k)|$. k is the index of the MUP aligned to the reference MUP.

4.4.4 Classification

A binary label is assigned to each feature vector $x_{\mathrm{NFJ}}^{(t_m)}$. A positive label ($z_{\mathrm{NFJ}}^{(t_m)} = +1$) is assigned when the absolute difference between $NFJ(t_m)$ and the simulated NF-MUP-jitter value is below or equal to λ_{NFJ}. Conversely, a negative label ($z_{\mathrm{NFJ}}^{(t_m)} = -1$) is assigned to $x_{\mathrm{NFJ}}^{(t_m)}$, when this difference is above λ_{NFJ}. A training dataset is then constructed by pooling examples (feature vector and label pairs) from all simulated MUPTs. The dataset is then sub-sampled to only include 15,000 positive examples and 15,000 negative examples, resulting in $D_{\mathrm{NFJ}} = \{x_{\mathrm{NFJ}}(i), z_{\mathrm{NFJ}}(i)\}_{i=1}^{N_{\mathrm{NFJ}}}$. N_{NFJ} is the number of samples in the training dataset after sub-sampling (30,000). The index t_m is dropped to emphasize that all examples are considered to be identical and probabilistically independent.

To further ensure that the positive examples are not due to a random chance, the sub-sampling only selects examples from samples that are preceded and followed with a 150 μS worth of samples with absolute error less than or equal to λ_{NFJ}. The sub-sampling is necessary to make training the classifier more computationally feasible. The size of a training set constructed from a few hundred simulated MUPTs is in the order of a few million samples. This is because, the dataset has a feature vector for every sample in the reference MUPs sampled at a one MHz rate. Moreover, there will be a significant imbalance between the number of positive and negative examples.

The training dataset is then used to build a support vector machine (SVM) model. The use of support vectors for the supervised binary classification task was first introduced by Cortes and Vapnik in [23]. The weights $\{\alpha_{\mathrm{SVM}}(i)\}_{i=1}^{N_{\mathrm{NFJ}}}$ defining an SVM classifier are

obtained by solving the following quadratic optimization problem:

$$\max_{\{\alpha_{\mathrm{SVM}}(i)\}_{i=1}^{N_{\mathrm{NFJ}}}} \Big(\sum_{i=1}^{N_{\mathrm{NFJ}}} \alpha_{\mathrm{SVM}}(i)$$

$$- \frac{1}{2} \sum_{i=1}^{N_{\mathrm{NFJ}}} \sum_{k=1}^{N_{\mathrm{NFJ}}} \alpha_{\mathrm{SVM}}(i)\alpha_{\mathrm{SVM}}(k)z_{\mathrm{NFJ}}(i)z_{\mathrm{NFJ}}(k)\phi_{\mathrm{SVM}}^{T}\big(x_{\mathrm{NFJ}}(i)\big)\phi_{\mathrm{SVM}}\big(x_{\mathrm{NFJ}}(k)\big) \Big)$$

$$\mathrm{s.t.} \sum_{i=1}^{N_{\mathrm{NFJ}}} \alpha_{\mathrm{SVM}}(i)z_{\mathrm{NFJ}}(i) = 0$$

$$0 \le \alpha_{\mathrm{SVM}}(i) \le C_{\mathrm{SVM}}, i = 1, ..., N_{\mathrm{NFJ}}$$

C_{SVM} is a regularization factor controlling the trade-off between the model complexity and empirical risk. ϕ_{SVM} is a nonlinear mapping of the feature vector to a higher (possibly infinite) dimensional space, where the positive and negative examples can be classified linearly. Training vectors with a corresponding $\alpha_{\mathrm{SVM}}(i)$ that is not equal to zero are referred to as support vectors. The objective of the above optimization problem is to find a linear separation surface with a maximum distance to the two margins (one for the positive class and the other for the negative class) along which the support vectors lie. The mapping ϕ_{SVM} does not need to be explicitly evaluated. Only an estimation of its dot product $K_{\mathrm{SVM}}(x_{\mathrm{NFJ}}(i), x_{\mathrm{NFJ}}(j)) = \phi_{\mathrm{SVM}}^{T}\big(x_{\mathrm{NFJ}}(i)\big)\phi_{\mathrm{SVM}}\big(x_{\mathrm{NFJ}}(k)\big)$ is needed for either SVM training (the above optimization problem) or evaluation, where K_{SVM} is known as the kernel function. It is not even necessary to know ϕ_{SVM} to design a valid Kernel function, as long the kernel function satisfies Mercer's conditions. The radial basis function (RBF) kernel was used in this work:

$$K_{\mathrm{SVM}}(x_{\mathrm{NFJ}}(i), x_{\mathrm{NFJ}}(k)) = exp\Big(- \frac{\big(x_{\mathrm{NFJ}}(i) - x_{\mathrm{NFJ}}(k)\big)^{T}\big(x_{\mathrm{NFJ}}(i) - x_{\mathrm{NFJ}}(k)\big)}{2\gamma_{\mathrm{RBF}}} \Big)$$

γ_{RBF} controls the width of the kernel

During the evaluation phase, the label for a new sample, say $h_{\mathrm{SVM}}(x_{\mathrm{NFJ}})$, can be obtained using:

$$h_{\mathrm{SVM}}(x_{\mathrm{NFJ}}) = \begin{cases} +1, \mathrm{if} \sum_{i=1}^{N_{\mathrm{NFJ}}} \alpha_{\mathrm{SVM}}(i)z_{\mathrm{NFJ}}(i)K_{\mathrm{SVM}}(x_{\mathrm{NFJ}}(i), x_{\mathrm{NFJ}}) \ge 0 \\ -1 \mathrm{if} \sum_{i=1}^{N_{\mathrm{NFJ}}} \alpha_{\mathrm{SVM}}(i)z_{\mathrm{NFJ}}(i)K_{\mathrm{SVM}}(x_{\mathrm{NFJ}}(i), x_{\mathrm{NFJ}}) \le 0 \end{cases}$$

4.5　Evaluation

Eleven, randomly selected, simulated muscles from the dataset described in Chapter 2 on Page 12 were used for evaluation. The details of the model used for simulation are further discussed in Chapter 5 on Page 94. Each of the muscles was modelled to have 200 motor units with varying motor unit territory diameters (ranging between 1.52 to 8.53 mm), number of muscle fibres (ranging from 31 to 434 muscle fibres) and muscle fibre diameters (the mean muscle fibre diameter of a single motor unit ranges between 44.97 and 64.54 μm). All of the motor units were assumed to be recruited. Only motor units with any of its MUPs having a peak to peak acceleration amplitude above 2 KV/S^2 were used for evaluation. This resulted in 680 MUPTs. Each of the trains was assumed to have 50 MUPs.

The variability in neuromuscular transmission times was modelled to be sampled from a zero-mean Gaussian distribution. All the muscle fibres belonging to the same muscle were sampled from distributions with the same standard deviation. The standard deviation for the first muscle was simulated to be 14.12 μS. In case of evaluating NF-MUP-Jitter using a pair of single fibre MUP segments, the resulting expected jitter was equal to 20 μS. The standard deviation for each of the following muscles was incremented by 7.07 μS.

Ten folds cross validation was used for calculation of performance metrics. In each fold, two metrics were calculated:

- **Error Percent:** It is the absolute difference between the simulated and estimated NF-MUP-Jitter values normalized by the simulated value.

- **Yield Percent:** It is the percent of the number of MUPTs that have one or more single fibre MUP segments to the total number of MUPTs.

The upper panel in Figure 4.3 shows the average performance metrics over a coarse grid search for different combinations of γ_{SVM} and λ_{NFJ}. The lower panel shows the break down of the results for different simulated NF-MUP-Jitter values for $\gamma_{\mathrm{SVM}} = 10^6$ and $\lambda_{\mathrm{NFJ}} = 3$. This point is selected, since it represents an acceptable trade-off between the average error

percent 8.9% and yield percent of 85.3%. The average time for analyzing one MUPT is 3.6 seconds.

4.6 Discussion

The main justification for using regional DTW rather than conventional DTW is that the objective of the proposed methods is to segment regions that clinicians can track and validate the consistency of their morphologies across different MUPs belonging to the same train. Therefore, the purpose of the alignment procedure is to evaluate the consistency of regions. Moreover, it is highly likely to mistakenly find, by random, a set of consistent alignments for a single sample in the reference MUP.

The Euclidean distance was replaced with a pseudocorrelation based distance. The main reason is that Euclidean distances will be low, i.e., indicating consistent alignments, for regions in the reference MUP that have energies close to energies of the baseline regions. On the other hand, ZPC will approach zero (therefore, the alignment distance will be close to one) when the two regions have low energy. This is because the instrumentation noises contaminating different regions of the EMG signal are not expected to be correlated.

The idea behind using double differentiation is to accentuate contributions from fibres close to the detection surface of the electrode by relatively suppressing low frequency contributions from distant muscle fibres. This, in turn, increases the chance of having segments in the MUP with morphologies that are mainly influenced by a single muscle fibre. Therefore, a higher probability of finding and tracking single fibre MUP segments.

In most real-life problems, the choice of the classification technique is mostly determined by empirical and experimental evaluation. This is not different for the problem of segmenting single fibre MUP segments. The decision to use SVM was made after pilot experiments with other classifiers and regression methods, including Gaussian mixture models, logistic regression, artificial neural networks and multiple linear regressions. Review of these techniques can be found in multiple foundational machine learning text books including [9]. The results for these experiments are omitted for the sake of brevity. SVMs
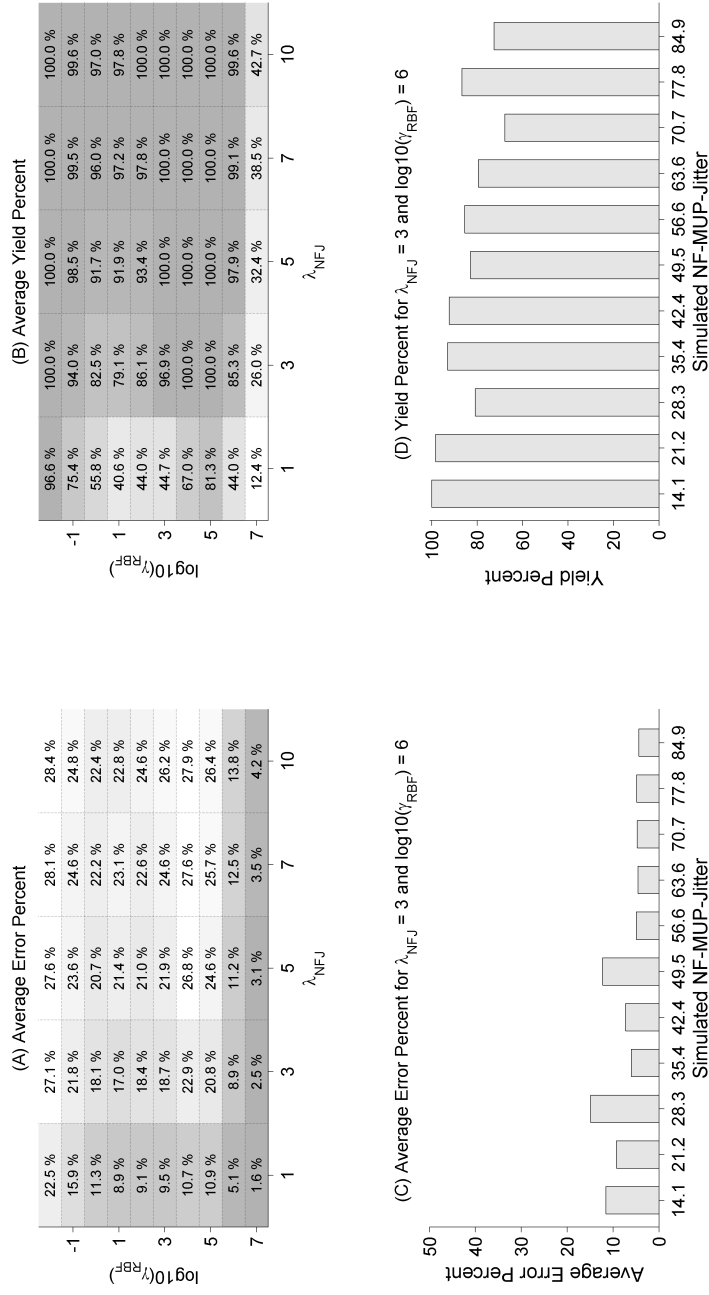
Figure 4.3: Each of the colour-coded cells in Figure (A) represents the average error percent obtained for different combinations of γ_{SVM} and λ_{NFJ}. Figure (B) shows the corresponding average yield percents for the same combinations. Figures (C) and (D) show the break-down of the results for $\gamma_{\text{SVM}} = 10^6$ and $\lambda_{\text{NFJ}} = 3$. Each bar in the two graphs represents the obtained results for a particular simulated NF-Jitter value.

outperformed the other techniques, which can be attributed to the following characteristics of an SVM classifier:

- SVM training is based on a convex optimization problem that can be solved efficiently, and has no local minima.

- The use of kernels, though not unique to SVM, allows estimation of a nonlinear separation surface (compared to logistic regression and Gaussian mixture models).

- It has fewer parameters, so it is easier and faster to tune (compared to artificial neural networks).

- Its model size (the number of support vectors) scales linearly with the number of the training examples.

- The sparsity of the solution allows efficient evaluation of the SVM decision for new samples.

It is clear from the results shown in Figure 4.3 that a trade-off exists between yield and error. For a particular γ_{RBF}, increasing λ_{NFJ} increases the yield at the cost of higher error. This is expected, because increasing λ_{NFJ} is equivalent to having a looser definition for what can be considered as a positive example for training in a sense of allowing higher error. A better performance (lower error and higher yield) is expected to be obtained by (1) tuning parameters using finer search, (2) tuning more parameters (SVM regularization parameter, RDTW half region width, and others), (3) performing feature selection similar to the one performed in Section 3.4.6 on Page 62, and (4) using more MUPs from each MUPT .

A further investigation is necessary to specify what settings are optimal for a clinical setup. The author believes that performing the analysis with an average error percent of 8.9% and a yield percent of 85.3% (i.e., setting γ_{SVM} to 10^6 and λ_{NFJ} to 3) is sufficient for the proposed analysis to be useful for discrimination between normal muscles and muscles affected by a NMD disturbing neuromuscular transmission. The effect of error in estimating jitter on discrimination accuracy will be limited due to the fact that the proposed methods allow performing the analysis on multiple MUPTs acquired from a single contraction.

The training and testing data for the work presented in this chapter can be considered to be drawn from two different joint distributions of alignment features. The training data is based on simulated MUPTs, while the testing data (in a clinical setup) will be extracted from MUPTs identified from clinical EMG studies. This will be probably always the case regardless how realistic the utilized models are. Even within the testing dataset, it is likely that there are differences between the distributions of features calculated from different muscle types or even from the same muscle type at different levels of contraction. The problem is known in the machine learning community as transfer learning [89]. More specifically, this problem will fall under the category of transductive transfer learning as there are no labels available for the testing data. Further testing is necessary to evaluate the usefulness of these techniques.

This study could have also benefited from simultaneous recording of single fibre and concentric needle EMG signals. By registering the two signals, the estimated values for jitter can be validated. This is only applicable when the MFPs detected by the single fibre are registered to single fibre MUP segments in one of the MUPTs identified from the EMG signals acquired by the concentric electrode. It is worth mentioning that this evaluation can not replace the use of simulated MUPTs for evaluation. This is because there is no straightforward experimental method to decide whether the MFPs detected by the single fibre electrode are superimposed or not by the activity of other muscle fibres contributing to the MUP detected by the concentric electrode.

Chapter 5

Representation: Detecting Neuropathy Using Measures of Motor Unit Activation

5.1 Summary

Objective: Motor unit loss associated with neuropathic disorders affects motor unit activation. Quantitative electromyographic features of motor unit activation estimated from the sequences of motor unit potentials created by concurrently active motor units can support the detection of neuropathic disorders.

Interpretation of most motor unit activation feature values are, however, confounded by uncertainty regarding the level of muscle activation during EMG signal detection. A set

---

Portions of this chapter previously appeared in M. AbdelMaseeh, B. Smith, and D. Stashuk. Detecting neuropathy using measures of motor unit activation extracted from standard concentric needle electromyographic signals. In *Engineering in Medicine and Biology Society (EMBC), 2014 36th Annual International Conference of the IEEE*, pages 4066–4070. IEEE, 2014

of new features circumventing these limitations are proposed, and their utility in detecting neuropathy is investigated using simulated and clinical EMG signals.

Methods: The firing sequence of a motor neuron was simulated using a compartmentalized Hodgkin-Huxley based model. A pool of motor neurons was modelled such that each motor neuron was subjected to a common level of activation. The detection of the firing sequence of a motor neuron using a clinically detected EMG signal was simulated using a model of muscle anatomy combined with a model representing muscle fibre electrophysiology and the voltage detection properties of a concentric needle electrode.

Results and Conclusion: Findings are based on simulated EMG data representing 30 normal and 30 neuropathic muscles as well as clinical EMG data collected from the tibialis anterior muscle of 48 control subjects and 30 subjects with neuropathic disorders. These results demonstrate the possibility of detecting neuropathy using motor unit recruitment and mean firing rate feature values estimated from standard concentric needle detected EMG signals.

5.2   Introduction

The amount of force produced by a muscle is controlled by activating or deactivating motor units and by modulating the firing rates of active motor units [25]. Neuropathic processes can change the number, territory, and contractile properties of motor units. These pathological changes are in turn expected to induce changes in motor unit activation patterns [45]. Therefore, QEMG features estimated from the sequences of firing times of MUPs created by concurrently active motor units are likely to be useful for detecting neuropathy.

This work attempts to answer questions that, from a clinical perspective, are practical:

- Can we extract discriminating QEMG motor unit recruitment and firing rate features from EMG signals detected using a conventional clinical concentric needle electrode?

- Can this be achieved using a clinically practical signal acquisition protocol that is also suitable for extraction of morphological features?

- Can these QEMG features be extracted automatically, quickly, accurately and using a procedure the output of which can be evaluated and validated by a physician?

These questions have been addressed through the analysis of simulated and clinical EMG studies. Analyzing simulated data is useful because it overcomes many inherent limitations of clinical data such as labelling inaccuracies, non-uniformity of disease involvement, acquisition dependence (such as needle focusing and instrumentation noise) and incompleteness of extracted MUPTs. Simulation can also provide clearer insight by excluding irrelevant phenomena and factors, such as MUP instability caused by neuromuscular junction jitter, and by modelling other relevant parameters that are very difficult to measure experimentally, namely excitatory input to a motor neuron pool.

5.3 Literature Review

Earlier studies have evaluated the discriminability of motor unit mean interdischarge intervals (IDIs) and their standard deviation using MUPTs extracted from EMG signals detected using a single fibre needle electrode [40, 48]. A single fibre needle electrode was used because the selectivity of this electrode allows the signals detected to be more reliably decomposed into their constituent MUPTs.

Results from both of these studies demonstrated that neuropathic muscles had decreased mean IDI and higher IDI variability. Similar results were obtained in [29] using a standard concentric needle electrode. In all these studies, the level of contraction was measured and controlled.

Several models related to different aspects of low level isometric skeletal muscle contraction have been developed with different inputs, outputs, and level of detail to serve different objectives. For instance, a detailed model of a motor neuron pool was built to answer neurophysiological questions such as the schema of input distribution in [132, 133]. While, a model was constructed in [59] to investigate quantification of motor neuron firing synchrony and common drive. Nandedkar [83, 82] devised a model focusing on electrode properties and MFPs to contrast the spatial selectivity of different electrodes and the relationship between muscle fibre anatomy and detected EMG signal features.

Models in [122, 50] proposed a detailed muscle layout to investigate EMG signal decomposition and analysis in a structured manner. In this work, these models of Traub, Nandedkar and Hamilton-Wright and Stashuk are combined to simulate the detection of motor neuron firings using concentric needle-detected EMG signals.

The remainder of this chapter is structured as follows: Section 5.4 discusses the motor unit pool model. Section 5.5 summarize the acquisition and analysis of the clinical EMG data. Results are presented and discussed in section 5.6.

5.4   Composite Model Construction

5.4.1   Modularized Architecture

To simulate the use of concentric-needle-detected EMG signals to quantify motor neuron activity, the parts of the human neuromuscular system that control motor neuron activation and the parts of the acquisition and analysis systems that influence the estimation of the corresponding motor unit activation features were independently modelled and subsequently combined into a composite model composed of modularized functional component models.

This means that each component model processes a specific set of inputs and produces a defined set of outputs. As long as the interfaces (outputs and inputs) are maintained compatible between the different component models, a different realization of any component model can be utilized. The functional descriptions of the five component models are summarized in Tables 5.1 and 5.2, while the specific component model realizations adopted for this study are presented in subsequent subsections.

5.4.2   Motor Neuron Model

To provide a basis for the accurate study of the quantification of the firing sequence of a motor neuron, a rigorous and detailed motor neuron model based on previous work completed by [27] and [133] was developed. The key advantage of this relatively detailed

Component	Description
Motor Neuron: $s_{\mathrm{Nr}}(j) = f_{\mathrm{Nr}}(a_{\mathrm{Nr}}(j), \overline{g}_{ex})$	$s_{\mathrm{Nr}}(j)$ is the firing sequence of the jth motor neuron. $s_{\mathrm{Nr}}(j)$ is a function of the soma-dendritic equivalent cylinder diameter $a_{\mathrm{Nr}}(j)$ of the motor neuron and the steady excitatory inputs to the different dendritic compartments $\overline{g}_{ex}$.
Muscle Fiber Potential: $P_{\mathrm{MF}}(i) =$ $f_{\mathrm{MF}}(d_{\mathrm{MF}}(i), \overline{c_{\mathrm{MF}}}(i),$ $n_{\mathrm{MF}}(i), \overline{e_{\mathrm{CN}}})$	$P_{\mathrm{MF}}(i)$ is the MFP of the ith muscle fiber as detected by a concentric needle electrode placed at $\overline{e_{\mathrm{CN}}}$. $P_{\mathrm{MF}}(i)$ is a function of muscle fiber diameter $d_{\mathrm{MF}}(i)$, center location $\overline{c_{\mathrm{MF}}}(i)$, and neuro-muscular junction location $n_{\mathrm{MF}}(i)$.

Table 5.1: Functional description of the dynamic component models. Note that insignificant parameters and those assumed to be fixed are excluded from the lists of input parameters. Scalars are notated as lower case variables, vectors as lower case variables with an overline, while matrices are notated as uppercase variables with an overline

model is its ability to model motor neurons having different sizes and input resistances. This model can therefore be used as a building block in a motor unit pool model.

The main aspects of the developed model are:

- Motor neuron morphology and membrane heterogeneity are represented by five compartments comprised of three dendritic compartments (proximal, middle, and distal), the soma, and the initial segment.

- The dendritic tree is converted into an equivalent cylinder using the method of Rall [102].

- The membrane of a dendrite is passive, while the time and voltage dependence of potassium and sodium conductance of the active membrane compartments (the soma and the initial segment) are modelled using Hodgkin-Huxley like equations modified to match voltage clamp data.

Component	Description
Muscle Layout: $[\overline{d_{\mathrm{MF}}}, \overline{c_{\mathrm{MF}}}, \overline{n_{\mathrm{MF}}}, \overline{W_{\mathrm{Mus}}}] = f_{\mathrm{layout}}(N_{\mathrm{MU}}, \overline{e_{\mathrm{CN}}})$	Muscle layout is defined by the muscle fibre diameters $\overline{d_{\mathrm{MF}}}$, centre locations $\overline{c_{\mathrm{MF}}}$, neuromuscular junction locations $\overline{n_{\mathrm{MF}}}$ and the muscle fibre assignments to the N_{MU} motor units. The specific muscle fibre to motor unit assignments are represented using matrix $\overline{W_{\mathrm{Mus}}}$. The needle location $\overline{e_{\mathrm{CN}}}$ is an input parameter because needle insertion causes nearby fibers to be pushed aside.
Neuropathy: $\overline{W'} = f_{\mathrm{neuro}}($ $\overline{d_{\mathrm{MG}}}, \overline{c_{\mathrm{MF}}}, \overline{W_{\mathrm{Mus}}}, \gamma_{\mathrm{Mus}}, \delta_{\mathrm{Mus}})$	Neuropathy causes a loss of a γ_{Mus} fraction of the motor neurons and muscle fiber reinnervation, i.e. reassignment of the muscle fibres from the lost motor neurons to surviving motor neurons, represented by matrix $(\overline{W'_{\mathrm{Mus}}})$, such that a surviving motor neuron can innervate up to δ_{Mus} percent more fibres.
Motor Neuron Pool: $\overline{a_{\mathrm{MU}}} = f_{\mathrm{pool}}(\overline{t})$	The motor unit territory radii of the corresponding motor units $\overline{a_{\mathrm{MU}}}$ belonging to the pool are modelled as a function of the muscle force $\overline{t_{\mathrm{Mus}}}$ at which the motor neurons are recruited.

Table 5.2: Functional description of the structural component models.

- The after hyper-polarization following an action potential in a motor neuron is realized using a slow potassium conductance.

- Membrane specific properties, such as membrane capacitance and leakage resistivity, are assumed to be independent of the motor neuron size.

- The inputs to the model are restricted to excitatory synaptic conductance values $\overline{g}_{ex}$ associated with the three dendritic compartments.

The radii of the soma equivalent cylinder and the dendritic equivalent cylinder are set equal. It was shown that this radius a_{Nr} can be estimated from a set of preset values (membrane resitivity R_m, internal resistivity R_i, equivalent length of the soma-dendritic

length L_{Nr}, and characteristic length λ_{Nr}) and the input resistance R_{input} using the following formula:

$$a_{\text{Nr}} = \left[\frac{R_m R_i}{2} \right]^{1/3} \times \left[\frac{coth(L_{\text{Nr}}/\lambda_{\text{Nr}})}{\pi R_{\text{input}}} \right]^{2/3} \tag{5.1}$$

The resulting system of 15 coupled differential equations is solved using the Runge-Kutta method with a variable time step. Figure 5.1 shows that the model creates repetitive motor neuron firings with an appropriate time course. Figure 5.2 shows that the firing rate vs. excitatory input curve has primary and secondary ranges with steeper slopes for larger motor neurons.
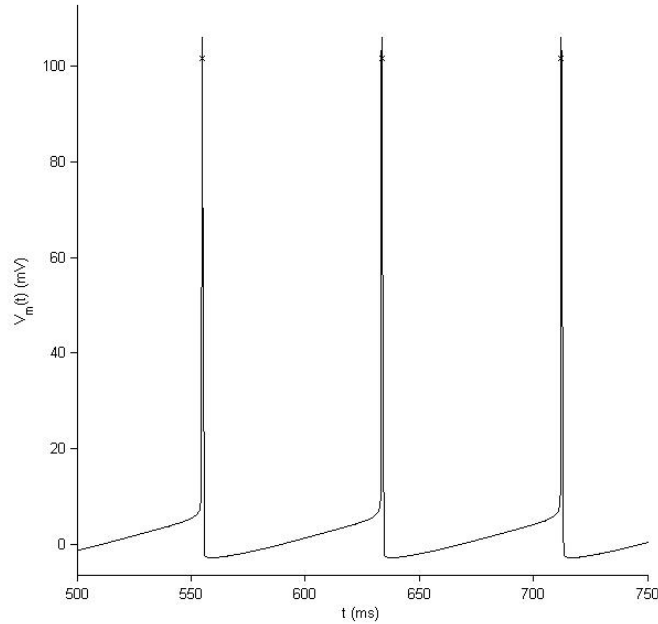
Figure 5.1: (a) Transmembrane potential across the initial segment of a motor neuron having $R_{\text{input}} = 1.5\text{M}\Omega$. Remaining parameters and rate functions are from [133].

5.4.3 Motor Neuron Pool Model

In [132], it was shown that the threshold force of activation (h_{Nr}) in grams, i.e., the force at which a motor neuron is recruited, can be modelled as a function of the recruitment order j of the motor neuron using:

$$h_{\mathrm{Nr}} = 1000 - 469 \times \log(j) \tag{5.2}$$

R_{input} in MΩ is then estimated using:

$$R_{\mathrm{input}} = 2.5 - \frac{h_{\mathrm{Nr}}}{600} \tag{5.3}$$

and the potassium slow conductance time constant in ms as:

$$\frac{1}{\beta_q} = 13.3 + 6.7 \times R_{\mathrm{input}} \tag{5.4}$$

Figure 5.2 shows that the model realizes ordered recruitment.

5.4.4 Muscle Model

Motor neurons via their axonal projections and neuromuscular junction are connected to groups of muscle fibres and together comprise motor units. Activation of a motor neuron in turn activates each of its connected muscle fibres, i.e., its entire motor unit. The activity of a motor neuron can therefore be determined by detecting MUPs produced by its muscle fibres. Therefore, if the MUPs associated with the activity of a motor neuron can be consistently detected in an acquired needle-detected EMG signal, the extracted MUPT is defined as decomposable and can be used to estimate statistics related to the firing sequence of the motor neuron. With respect to simulated data, it is assumed that a MUP can be consistently detected and therefore its MUPT considered decomposable, when the second derivative of any of its composite MFPs have a value higher than 1 kV/s^2.

The simulation of a MFP P_{MF} as detected by a needle electrode requires determining the diameter of the muscle fibre and the location of the muscle fibre and its neuromuscular junction relative to the electrode detection surface. Therefore, the muscle layout model
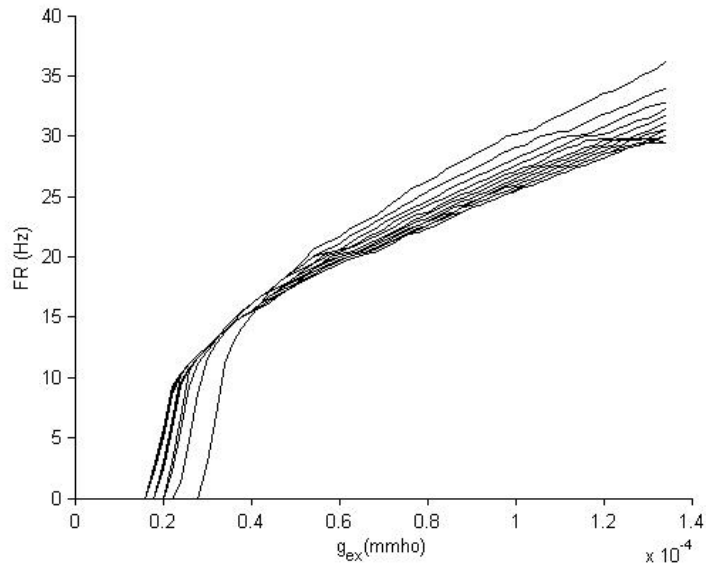
Figure 5.2: Firing rate versus the input excitatory conductance applied to the dendritic compartments for every tenth motor neuron of the pool.

of [122, 50] which specifies the diameter d_{MF}, centre c_{MF} and neuromuscular junction n_{MF} location of each fibre as well as its associated motor unit $\overline{W_{Mus}}$ was used. The main stages of simulating a muscle layout can be summarized as:

- *Assigning motor unit territory diameter:* Both the muscle and the constituent motor unit territories are assumed to have circular cross-sectional areas. The motor unit sizes are sampled from a Poisson distribution.

- *Assigning motor unit territory centre:* The two main assumptions are: (1) there is no necessary correlation between motor unit territory diameter and motor unit territory centre, and (2) motor unit centres are uniformly distributed across the cross-sectional area of a muscle. The algorithm developed in [50] which divides the muscle cross section into a uniform grid was used. This algorithm then iteratively places motor unit territory centres at grid points, perturbed by random offsets, in a randomized manner guaranteeing that any motor unit is equally likely to be placed

in any quadrant.

- *Assigning muscle fibre centre location $\overline{c_{MF}}$:* Muscle fibres are located in a uniform grid such that a uniform density of 400 muscle fibres per mm^2 is achieved.

- *Assigning muscle fibres to motor units ($\overline{W_{Mus}}$):* Each muscle fibre is assigned randomly to one of the motor units which has territory including its location. The likelihood of the ith muscle fibre being assigned to the jth motor unit is estimated as a weighted sum of three factors:

  1. the distance from the motor unit territory centre to the muscle fibre centre
  2. the number of fibres already assigned to the motor unit
  3. the expected number of fibres to be assigned to the motor unit

- *Assigning muscle fibre diameter d_{MF}:* The diameters of the muscle fibres belonging to a given motor unit are sampled from a Gaussian distribution specific to the motor unit. The mean muscle fibre diameter of a motor unit is modified by a range of increments to account for the fact that type-I fibres are more likely to be found in smaller motor units.

- *Assigning neuromuscular junction location n_{MF}:* Because a muscle cross-section is arbitrarily chosen to be in an x-y plane, the location of the neuromuscular junction is modelled to be along the z axis and is drawn from a Gaussian distribution with a zero mean and a standard deviation based on its motor unit territory diameter.

- *Muscle fibre ploughing:* A concentric needle electrode detection surface is modelled as an ellipsoidal cross-sectional area at the tip of the needle oriented at 15.95 degrees relative to the axis of the cannula. When simulating detected EMG signals the needle tip is assumed to be positioned at a specific location $\overline{e_{\text{CN}}}$ within the muscle and all fibres that would intersect with the cannula are therefore assumed to have moved either above or below the cannula, whichever is closer.

The motor neuron pool model is interfaced to this muscle model by assigning motor neurons ordered according to their recruitment threshold to motor units ordered based on their territory diameters.

5.4.5 Muscle Fibre Potential Model

The model used to simulate MFPs is based on the work done in [82]. The concentric needle electrode is assumed to have an ellipsoid detection surface with a major axis of 580 μm and a minor axis of 150 μm. The ellipse is modelled using six line integrals spaced equally across the surface. The MFP of the ith fibre $P_{\mathrm{MF}}(i)$ is calculated by convolving a propagating transmembrane current with a weight function related to the relative geometry of the detection surface and the fibre location:

- **Propagating transmembrane current** amplitude and conduction velocity are dependent on muscle fibre diameter $d_{\mathrm{MF}}(i)$.

- **Electrode weight function** is the average response to a unit impulse current of the six line electrode potential response functions used to model the concentric needle detection surface. It is dependent on the position of the electrode $\overline{e_{\mathrm{CN}}}$, the position of the muscle fibre centre $\overline{c_{\mathrm{MF}}(i)}$, neuromuscular junction $n_{\mathrm{MF}}(i)$, and conductance properties of the extracellular tissue.

The transmembrane currents travelling toward and away from the electrode based on $\overline{e_{\mathrm{CN}}}$ and the neuromuscular junction location $n_{\mathrm{MF}}(i)$ are both modelled. For a given position of the electrode detection surface, a MFP is simulated for each fibre of a motor unit. If any of the simulated MFPs of the motor unit has a second derivative value of greater than 1 kV/s^2, the corresponding MUPT is considered decomposable (i.e. the corresponding motor unit is considered to have been sampled and the firing sequence of its motor neuron is analyzed).

5.4.6 Neuropathy Model

A diffuse neuropathic process is simulated as a loss of motor neurons [51]. Different levels of involvement are modelled as the loss of different fractions γ_{Mus} of the total number of motor neurons. It is assumed that all motor units are equally likely to be affected by the diffuse disease process, therefore lost motor neurons are randomly selected. The

re-innervation process is modelled by re-executing the muscle fibre assignment procedure described in section 5.4.4. In this case, however, a surviving motor neuron can support only a maximum number of additional fibres which is described as a fraction δ_{Mus} of its original size.

5.5 Data Analysis

5.5.1 Estimation of Mean Motor Unit Firing Rates

The acquisition and analysis of the clinical data is described in Section 3.4.1 on Page 55. Only data acquired from the TA muscle was used in this study. The error-filtered estimation (EFE) algorithm described in [130] was used to estimate mean motor unit firing rate. This algorithm has been shown to provide accurate estimates even when the firing sequence of a MUPT is only partially complete or includes erroneous firings.

The EFE algorithm makes use of the fact that the probability distribution function of the IDIs of an incomplete and/or an inaccurate firing sequence has a peak corresponding to the true mean IDI and other peaks at integer multiples of the true mean IDI value. The EFE algorithm iteratively divides the IDI histograms into three regions:

1. a region of small IDIs due to false firings

2. a region of large IDIs due to missed firings

3. a region with true IDIs lying in between.

5.5.2 Measures of Motor unit Activation

A set of features describing a given contraction is estimated from the extracted MUPTs and their associated motor unit mean firing rates:

- **No. of decomposable MUPTs:** The number of active motor units sampled during the contraction

- **Contraction Mean Firing Rate (cont.MFR):** Mean of the motor unit mean firing rates of the motor units sampled during the contraction

- **Contraction Sum Mean Firing Rate (cont.SFR):** Sum of the motor unit mean firing rates of the active motor units sampled during the contraction

- **Contraction Mean Firing Rate Range (cont.Range):** Difference between the maximum motor unit mean firing rate and the minimum motor unit mean firing rate of the active motor units sampled during the contraction

5.5.3 Simulated Data Acquisition

Using the muscle layout model $f_{\text{layout}}(.)$, 60 simulated muscles were generated with each muscle having 120 motor units. 30 of them were modified by the modelled neuropathic process $f_{\text{neuro}}(.)$. γ_{Mus} was set to 0.3 for the first 10 muscles, 0.4 for the second 10, and 0.5 for the last 10. δ_{Mus} was set to 0.5 for all neuropathic simulated muscles. Using the MFP model $f_{\text{MF}(.)}$, decomposable MUPTs detectable by a concentric needle EMG electrode were identified.

The motor neuron pool model $f_{\text{pool}}(.)$ and the motor neuron model $f_{\text{Nr}}(.)$ do not include any stochastic components, therefore there was no need to rerun them for each muscle and/or excitation level. The sequence of inputs applied to all motor neurons in the pool was a ramp sequence of excitatory conductance in mmho:

$$g_{ex}^{(c)}(k) = 1.5 \times 10^{-5} + k \times 10^{-6} \qquad (5.5)$$

where $c \in \{1, 2, 3\}$ is the dendritic compartment index and k is a step in the input. At each step, the $\bar{g}_{ex}$ was maintained constant for all motor neurons for two seconds to simulate an isometric contraction.

The first set of inputs was $k \in \{0, 2, ..100\}$. The average cont.SFR of normal simulated muscles was then calculated at each step. The range of steps for which $0 \leq$ avg. cont.SFR ≤ 100 was found to be $2 \leq k \leq 8$. Another fine tuned set of inputs was then created with $k \in \{2, 2.125, 2.25, ..., 8\}$. It was found that motor neurons of recruitment order $j \leq 85$ were recruited by $k = 8$.

5.6　Results and Discussion

Results from the clinical and simulated EMG studies shown in Figure 5.3 demonstrate an increased cont.MFR for neuropathic muscles, which is consistent to results shown in [29, 48, 45]. The increase is relatively higher for cont.SFR. above 40 Hz.

The acquisition protocol in which the contraction level is increased until 40 to 80 MUPs/s are detected has already been shown to be efficient in extracting QEMG features capturing MUP morphology and morphological stability in Chapter 3. This suggests that these features can be automatically extracted without the need to complete an additional/different acquisition protocol and/or to measure force.

The evidence of neuropathy provided by the newly proposed motor unit activation features is independent from that provided by morphological features. Therefore, a set of features combining both aspects, i.e., morphological and activation features, is expected to yield more accurate categorizations than a set including either of them individually. Moreover, electrodiagnostic clinicians are familiar with motor unit mean firing rate concepts and the EFE algorithm estimates can be easily validated by examining the IDI distributions.

It is worth noting that in practise increasing the cont.SFR of an EMG signal above 100 Hz makes decomposition of the EMG signal into its constituent MUPs more difficult because more MUP superpositions are likely to occur.

Based on our simulation results, when cont.SFR is above 20 Hz around 25% of active motor units are decomposable. This might explain why the results obtained using cont.Range did not show clear discriminablity between normal and neuropathic muscles. It is unlikely in normal muscles that motor neurons reflecting the width of the full range will be sampled.

Three main limitations of the implemented composite model can be summarized as:

- The motor neuron and motor neuron pool models used excluded some temporal details, such as sensory feedback loops and synaptic neurodyanimcs, that could be useful for muscle characterization .

- Needle movement and instrumentation noise caused by a subjects inability to maintain a constant contraction were not modelled.

- The MUP model, as implemented, was not used to analyze MUP morphological features. It is important to investigate potential relationships between aspects of MUP morphology and motor unit activation. These relationships can be studied by calculating a unique MUP for each firing of a motor unit as the summation of the MFPs of the motor unit taking into account neuromuscular junction instability.

The firing sequences of concurrently active motor units are probably too complex to be adequately described using only their mean firing rates. Other measures quantifying the variability of firing rates, synchrony among motor units firings and correlations of their instantaneous firings rates might also yield discriminative information taking into consideration acquisition and analysis limitations. While MUPT features quantify individual motor units, the features proposed in this study quantify a subset of concurrently active motor units sampled in a given muscle or the entire muscle. New methods are being sought to optimize integration of information coming from features describing individual motor units as well as whole muscles.
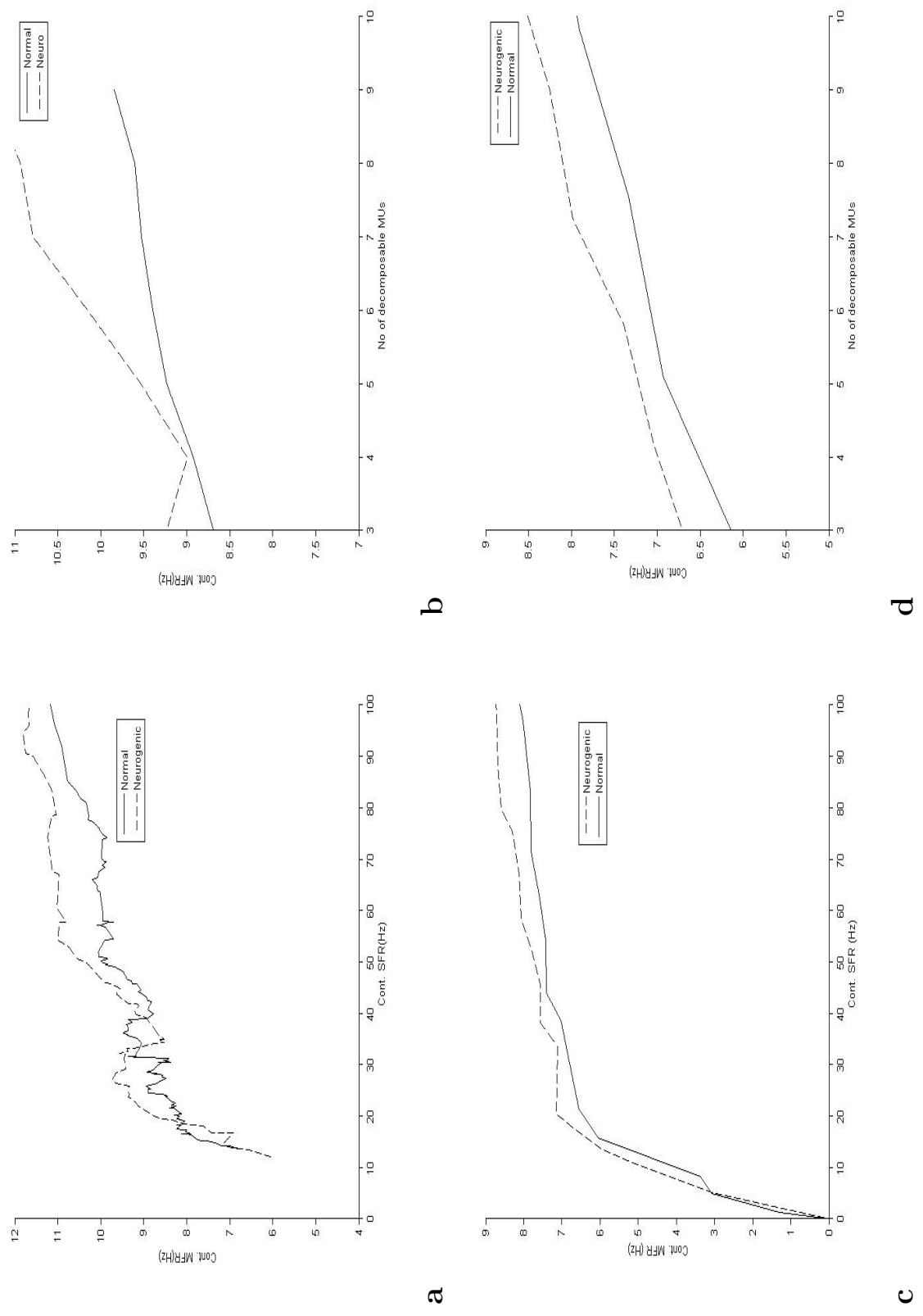
Figure 5.3: (a) and (b) show the variation of Cont. MFR as the Cont. SFR and No. of decomposable motor units change respectively for clinical EMG studies. (c) and (d) show the results as obtained from simulated studies.

Chapter 6

Decision Support: Different Binarization Mappings for Obtaining Transparent Characterization of Neuromuscular Disorders

6.1 Summary

Objective: The aim of this study is to improve available methods for obtaining transparent muscle characterizations from features obtained using QEMG techniques. More specifically, the study investigates the following questions: (1) Can the use of binarization mappings improve muscle categorization accuracies of transparent methods? (2) What are the appropriate binarization mappings in terms of accuracy and transparency?

Results: The obtained results from four different sets of examined limb muscles (342 muscles in total) demonstrate that four out of the ten investigated binarization mappings based on transparent characterization methods outperformed the multi-class characterizers based on Gaussian mixture models and the corresponding binarization mappings based on Gaussian mixture models.

Conclusion: This suggests that the use of an appropriate binarization mapping can overcome the decrease in categorization accuracy associated with quantizing MUPT features, which is often used to obtain transparent characterizations using quantized feature values. This performance gain can be attributed to the use of more relevant features and tuned quantization to obtain more specific binary characterizations.

6.2 Introduction

In the context of this work, muscle characterization is the process of characterizing a muscle using clinical and EMG information to assist with the detection of neuromuscular disorders and to determine whether detected disorders are likely due to myopathic or neurogenic processes. More specifically, the focus of this study is to assess the diagnostic utility of information extracted from EMG signals detected using a concentric needle electrode during isometric voluntary contractions independent of information from other EMG procedures (such as nerve conduction studies and EMG signals detected due to spontaneous and insertional activity) and physical examinations (including sensory testing, motor examination and assessment of stretch reflexes).

As explained in Chapter 2, quantitative analysis starts by segmenting MUPs from an EMG signal and then clustering the segmented MUPs into distinct trains based on the assumption that MUPs from a single motor unit are expected to be more similar to each other than MUPs from other motor units [127].

Each MUPT is represented by an estimated MUP template and the ensemble of MUPs compromising the MUPT. MUPTs can be represented using QEMG features, which describe the morphology of a typical or template MUP, the consistency of the morphologies of the individual MUPs belonging to the same MUPT as well as features describing motor unit recruitment and firing pattern. The representation and feature extraction stages are described in further details in Chapters 3, 4 and 5.

Given the number of possible QEMG features, the dependence among feature values, and the overlap of feature value probability distributions between muscle categories, it is not straightforward how to reach a muscle characterization using a selected set of QEMG features. The focus of this study is to assess various ways of providing an accurate and consistent muscle characterization utilizing QEMG features. The problem is challenging because of the following reasons:

- The level of disease involvement is not uniform among all of the motor units of the same muscle. For example, a neurogenic muscle may have slightly affected, severely affected and normal motor units. There is no clear cut rule that can be applied to determine when to consider a muscle to be affected. Clinicians often consider a muscle to be affected, when the set of EMG signals suggest the presence of a sufficient number of significantly affected motor units. Muscle categorization can be facilitated if the characterization of each motor unit, based on its detected MUPT, can be in the form of a score reflecting disease involvement to allow aggregation into an overall muscle characterization.

- Most of the estimated MUPT features suffer from dependence on the signal detection protocol. The two main sources of variation are focusing (i.e., adjusting the electrode position to acquire suitably sharp MUPs which effectively reflect motor unit morphology and physiology) and the level of contraction.

- The training dataset is annotated at the muscle level; consequently each MUPT label represents the condition of the muscle to which the motor unit belongs rather than the actual condition of the motor unit.

- The dataset is also highly unbalanced due to the fact that it is more likely that an examined muscle is normal than diseased and the number of sampled motor units varies across different muscles.

- Biovariability, poor understanding of the underlying electrophysiological process and variation in detection protocols lead to poor agreement among annotators [63]. The labelling of the training or the testing data therefore cannot be considered certain nor completely accurate.

In addition to these challenges, a formulation of muscle characterization as a learning problem should consider that a diagnostic impression is often a result of accumulating evidence from physical and other electrodiagnostic examinations. Therefore, the output of any candidate algorithm should be a continuous value or set of continuous values, refuting or supporting an outcome, a muscle category or set of muscle categories in our case, with a certain degree of confidence, so that it can be integrated with the outcomes of other examinations that could have either quantitative or qualitative outcomes.

A candidate muscle characterization algorithm should be transparent. This means that the computational inductive reasoning leading to the outcome and the associated degree of confidence should be presented to the electrodiagnostic physician in a form that can be evaluated and therefore validated. Transparency also implies that the outcome of the algorithm and the inductive reasoning underlying it can be translated into/explained by physiological and anatomical disease-induced changes. For example, an increase in size aspect feature values suggests a reinnervation process, while increased instability suggests pathological changes to neuromuscular junctions. There can be a cost associated with using transparent classifiers because they often require feature value quantization which is expected to reduce accuracy relative to non-transparent classifiers that can use continuous feature values.

Class binarization is defined by Fürnkranz [41] as "a mapping of the multi-class learning

problem to several 2-class problems in a way that allows a sensible decoding of the prediction, i.e., allows deriving a prediction for the multi-class problem from the predictions of the set of 2-class classifiers. The learning algorithm used for solving the 2-class problems is called the base classifier". A lot of work has been done in the machine learning community on class binarization to increase accuracy, reduce complexity, and overcome the limitation of some algorithms being only capable of performing binary classification [80, 57, 8].

In the context of this study, the muscle characterization problem is defined as a multi-class problem where a muscle is labelled as normal, myopathic or neurogenic and the main questions addressed can be summarized as:

- Can using a class binarization overcome the cost of using transparent techniques for muscle characterization?

- What is the best binarization mapping in terms of accuracy and transparency?

- What are the most relevant features?

These questions were addressed by investigating muscle categorization accuracies using multi-class characterizers and a comprehensive set of binarization mappings using a probabilistic model and a rule induction algorithm applied to sets of MUPT data extracted from EMG signals detected from four different sets of clinically examined muscles.

6.3   Literature Review

6.3.1   Review of multi-class muscle characterization

During the 1940s and early 1950s, many studies similar to the work of Kugelberg [69] correlated certain disorders to variations in the morphology and frequency content of detected MUPs. In 1955, Buchthal et al. [14] coined the term QEMG and proposed a muscle characterization based on comparison of extracted features to reference data of matching age range, gender, electrode type and other physical parameters.

Pattichis et al. [93] evaluated the performance of an artificial neural network (ANN) trained using both supervised and unsupervised learning. The performances of an ANN and the K-nearest neighbour (KNN) technique were also compared. The feature vector was composed of the standard deviation and mean of seven time domain features. For supervised training, back propagation was utilized, while a self organizing feature map algorithm was used for the unsupervised paradigm. Both ANN paradigms showed comparable performance with diagnostic accuracy of 80%, which substantially exceeded the KNN.

Pfeiffer et al. [97] used linear discriminant analysis to map duration, area, number of turns, and central frequency features into two scores. The mapping was a linear function of the features and was inferred using the training data, so as to maximize the separability among scores for different classes. The utilized algorithm also excluded features that did not improve discrimination. The centroid of each categorization was then estimated. During classification, the posterior probability was computed using Bayes' rule. The likelihood probabilities were estimated using the Euclidean distance from class centroids assuming features were normally distributed with equal covariance for all classes. For the first MUP, the prior probabilities of the classification were based on epidemiological data. The posterior probability of the previous MUP was then used as the prior probability for subsequent MUPs. Experimentation showed diagnostic probabilities above 0.95 in 91% of 223 biceps brachii muscles from 80 patients.

Pino et al. [98] used classification based on event association rules for muscle characterization. During the training phase, repeatable patterns were discovered from quantized feature vectors. A weight of evidence (WOE) measure was then estimated to reflect the support or refutation of each of the patterns for one of the classes. During classification, the summations of the WOE measures for all patterns for the three classes were then used to estimate the posterior probabilities. These MUP characterizations were then aggregated using Bayes' rule or averaged to produce a muscle characterization. Experimentation based on both clinical and simulated data using only four time domain features had performance similar to that achieved by the method described by Pfeiffer et.al. [97].

6.3.2 Review of binarization mappings of muscle characterization

Katsis et al. [62] used a feature vector comprised of the time samples in a 25 ms interval of raw EMG data centred around the peak of a MUP to train three support vector machines in a one-against-one mapping. Katsis et.al. [61] also investigated a different binarization mapping, using an ANN to classify a feature vector, comprised of five features, representing a MUP as normal or diseased. If a diseased MUP was detected in the first stage, a decision tree was used to classify a quantized version of the feature vector as either myopathic or neurogenic. A decision tree was used in the second stage to provide rules for transparency. In both of these studies, the MUP characterizations were not aggregated to produce a muscle characterization. Instead, an expert was asked to label MUP templates estimated by a previous stage of the algorithm.

AbdelMaseeh et al. [3] proposed using a variation of decision directed acyclic graph binarization mappings in which a muscle is classified as neurogenic or myopathic in the first stage. The second stage then uses a classifier specific to each disease category to confirm or refute the disease involvement. Decision directed acyclic graph binarization mappings are formally defined and further studied in this work.

This study tackles the class binarization mapping of muscle characterization more comprehensively than previous efforts. In addition, it defines muscle characterization as a different task than classification, stressing the importance of:

1. The integrability of a characterization obtained from an EMG signal with characterizations obtained from other physical and EMG examinations

2. The capability of validating and interpreting an obtained characterization

3. The non-uniformity of disease involvement across motor units belonging to the same muscle

6.4 Algorithms

6.4.1 Overview

A training set D is constructed from muscle-label pairs $D = \{(M_1, y_1), ..., (M_i, y_i), ..., (M_N, y_N)\}$, where N is the number of pairs. Each muscle M_i is a set of feature vectors $M_i = \{x_j^{(i)} \in \mathbb{R}^d : 1 \leq j \leq n_i\}$. Each vector $x_j^{(i)}$ is of length d, and describes one of the n_i MUPTs sampled from muscle M_i. The label $y_i \in C = \{c_1, ..., c_l, ..., c_L\}$ designates the muscle category of M_i. The elements of the set C may change depending on the definition of the muscle characterization problem. For example, a label $c_l \in C$ might represent normal muscles, muscles affected by a specific disease (say, facioscapulohumeral muscular dystrophy), or muscles affected by a category of related diseases (say, myopathy). It might also represent muscles affected and/or not affected by a group of diseases or categories of related diseases. For example, a label c_l might represent all muscles not affected by myopathic diseases.

Defining a set of unlabelled muscles $V = \{M_1, ..., M_k, ...\}$, the objective of the training phase is inducing a muscle characterizer $f_D : V \rightarrow Z$, i.e., a function induced using the training set D mapping an unlabelled muscle, say M, to its characterization z, which includes:

1. A muscle categorization: Assignment of the label $c \in C$ to the unlabelled muscle.

2. A likelihood vector Φ: A vector of length $|C|$, whose l^{th} element (ϕ_l) is a scalar estimate of the likelihood that the unlabelled muscle M is to be categorized as c_l. Estimation of the likelihood vector is necessary to allow integration of the obtained characterization with characterizations obtained from other physical or EMG examinations. The muscle categorization in this work is obtained from Φ by assigning M to the label estimated to be most likely. Other techniques of obtaining a categorization from Φ are also possible, such as a technique capable of reporting "No Categorization", when no label is clearly more likely than the other labels.

3. Transparency Rules: A transparent characterizer should also report a set of rules θ_l corresponding to each ϕ_l. A system operator can use this set of rules to validate the

estimate, and interpret the characterization, i.e., conceptually link feature values to disease-induced changes.

A muscle characterization might also include measures proportional to the level of disease involvement and metrics assessing signal quality; however those are out of the scope of this study.

The binary characterizer f_B is induced using $B = \{(M_i, y_i) \in D : y_i \in \{c_+, c_-\}\}$. When the output of f_B is obtained for an unlabelled muscle M, it categorizes M as either c_+ or c_- estimating the likelihood vector (ϕ_+, ϕ_-) and the corresponding vector of sets of transparency rules (θ_+, θ_-). A binarization mapping transforms the problem of inducing a multiclass characterizer into inducing a specific class $MAP(F)$ over a set of binary characterizers F, such that a characterization z for an unlabelled muscle can be estimated by evaluating the output of the binary characterizers. An instance of $MAP(F)$, say $\mathcal{X}$, has a set of binary characterizers $F_{\mathcal{X}} = \{f_1, ..., f_s, ..., f_S\}$ induced during the training phase.

The estimation of the characterization of an unlabelled muscle through evaluation of the output of an instance of an ordered binarization mapping and an instance of an unordered binarization mapping are shown in Figures 6.2 and 6.1 respectively. The evaluation of the output of an instance of an unordered binarization mapping is obtained by decoding binary characterizations obtained through evaluating the outputs of all binary characterizers. While, the evaluation of the output of an instance of an ordered binarization mapping is obtained through evaluating the outputs of some or all binary characterizers in a specific order implied by the binarization mapping.

6.4.2 Ordered Binarization Mapping

6.4.2.1 Decision Directed Acyclic Graph Binarization

A rooted binary directed acyclic graph (DAG) is a graph whose edges have an orientation and no cycles, and whose nodes have either zero or two edges directed from them. The root node is the only node with no edges pointing toward it. An instance of a decision directed acyclic graph (DDAG) [99] binarization mapping, say $\triangle$, is implemented using
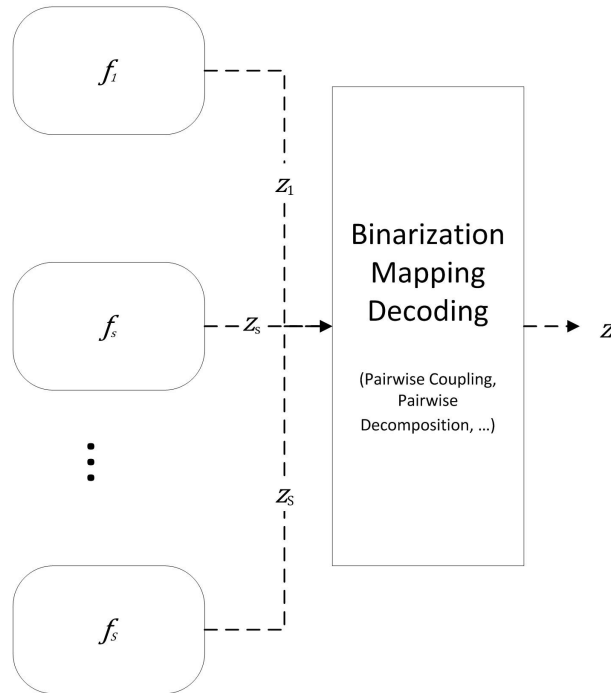
Figure 6.1: An instance of an unordered binarization mapping. Each box represents a different binary characterizer induced during the training phase. The outputs of all binary characterizers are evaluated for the same unlabelled muscle without any specific order. The muscle characterization is then obtained as a function of the resulting binary characterizations.

a DAG, where each of the internal nodes is labelled with a binary characterizer induced during the training phase. The output of $\triangle$ is evaluated by traversing its DAG starting from the root node. At each node, the output of the binary characterizer is evaluated, and the next node is selected based on the categorization of the binary characterizer.

The purpose of this study is to discriminate among normal (given the label c_{nor}), myopathic (given the label c_{myo}) and neurogenic (given the label c_{neu}) muscles. The set of binary characterizers utilized by $\triangle$ in this study therefore consists of three binary charac-

**Ordered
Binarization Mapping**

1- Decision Directed Acyclic Graph

f_{root}

z_{root}

f_{left}

f_{right}

$z = z_{left}$

$z = z_{right}$

2-Staged

f_1

z_1

$z = z_1$

f_2

$z = z_2$
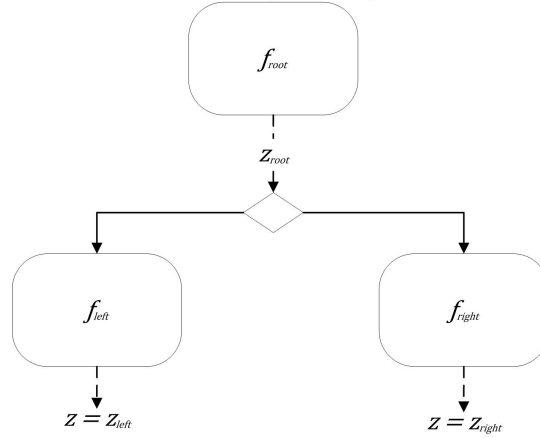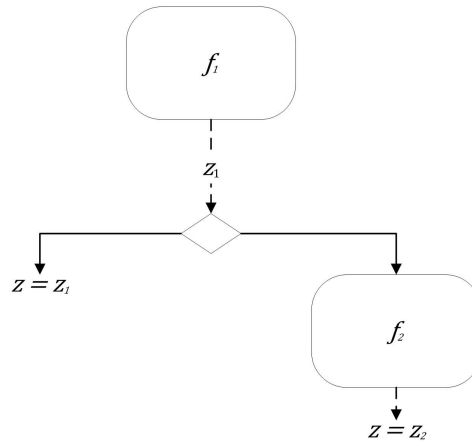
Figure 6.2: Instances of two different classes of ordered binarization mappings. The upper graph represents an instance of a decision directed acyclic graph binarization mapping. The lower graph represents an instance of a staged binarization mapping. The diamond shaped polygon and solid lines represent making a decision as to which binary characterizer to evaluate its output next based on the categorization obtained by the preceding binary characterizer.

terizers $F_\triangle = \{f_{myo-neu}, f_{nor-myo}, f_{nor-neu}\}$. During the training phase, the binary characterizer $f_{myo-neu}$ is induced using $B_{myo-neu} = \{(M_i, y_i) \in D : y_i \in \{c_{myo}, c_{neu}\}\}$, $f_{nor-myo}$ is induced using $B_{nor-myo} = \{(M_i, y_i) \in D : y_i \in \{c_{nor}, c_{myo}\}\}$, and $f_{nor-neu}$ is induced using $B_{nor-neu} = \{(M_i, y_i) \in D : y_i \in \{c_{nor}, c_{neu}\}\}$.

For the purpose of discriminating among normal, myopathic, and neurogenic muscles, three different variations of a DDAG can be obtained by labelling the root node with a different characterizer in $F_\triangle$. The three variations are listed in Table 6.1.

Binarization Mapping	Abbreviation	Root Node	Left Node	Right Node
DDAG Disease First	DDAG_Dis	$f_{myo-neu}$	$f_{nor-myo}$	$f_{nor-neu}$
DDAG Myo First	DDAG_Myo	$f_{nor-myo}$	$f_{nor-neu}$	$f_{myo-neu}$
DDAG Neuro First	DDAG_Neu	$f_{nor-neu}$	$f_{nor-myo}$	$f_{myo-neu}$

Table 6.1: Different variations of DDAG binarization for discrimination among normal, myopathic and neurogenic muscles

6.4.2.2 Staged Binarization Mapping

An instance of a staged binarization mapping, say τ, utilizes a set of binary characterizers $F_\tau = \{f_1, ..., f_s, ..., f_{|C|-1}\}$. The outputs of binary characterizers belonging to F_τ are evaluated in stages. In the first stage, f_1 categorizes an unlabelled muscle M as either c_{1+} or not. If M is categorized as c_{1+}, z (the characterization of M) will be set to the characterization obtained by f_1 and the evaluation process terminates. Otherwise the output of f_2 is evaluated in the second stage and M is categorized as either c_{2+} or not. This keeps going on until $f_{|C|-1}$ categorizes M as one of the two remaining classes.

During the training phase, the binary characterizer $f_s \in F_\tau$ is induced using $B_s = B_{s+} \cup B_{s-}$ where $B_{s+} = \{(M_i, y_i) \in D : y_i = c_{s+}\}$ and B_{s-} is obtained by relabelling $y_i = c_{s-} \ \forall \ \{(M_i, y_i) \in D : y_i \notin \{c_{1+}, c_{2+}, ..., c_{s+}\}\}$, i.e., by relabelling all muscle-label pairs as negative examples, except those belonging to categories considered as positive examples in the current stage or previous stages.

For the purpose of discriminating among normal, myopathic and neurogenic muscles (i.e., $|C| = 3$), an instance of a staged binarization mapping utilizes a set of two binary characterizers $F_\tau = \{f_1, f_2\}$. Similar to a DDAG, a different variation of a staged binarization mapping is obtained by defining a different category $c_l \in \{c_{nor}, c_{myo}, c_{neu}\}$ as c_{1+}. Those variations are listed in Table 6.2.

Binarization Mapping	Abbreviation	c_{1+}
Staged Normal First	S_Nor	c_{nor}
Staged Myopathy First	S_Myo	c_{myo}
Staged Neuropathy First	S_Neu	c_{neu}

Table 6.2: Different variations of staged binarization for discrimination among normal, myopathic and neurogenic muscles

6.4.3 Unordered Binarization Mappings

6.4.3.1 Pair-wise Decomposition Binarization

The set of binary characterizers used by an instance of a pairwise decomposition (PWD) binarization is the same as $F_\triangle$, the set of binary characterizers used by a related instance of a DDAG binarization mapping, given they are induced using the same dataset D.

Let ϕ_{gh} be the likelihood estimate of an unlabelled muscle, M, being categorized as c_g obtained by the binary characterizer induced using $B = \{(M_i, y_i) \in D : y_i \in \{c_g, c_h\}\}$ during the training phase, while $\phi_{hg} = 1 - \phi_{gh}$ is an estimate of the likelihood of the same muscle being categorized as c_h obtained by the same binary characterizer. ϕ_{gh} is an estimate of $P(y = c_g | y = c_g \ or \ y = c_h, M)$. It can be assumed that $\phi_{gh} = P(y = c_g | y = c_g \ or \ y = c_h, M)$ [114, 100] such that:

$$
\begin{aligned}
& P(y = c_g | y = c_g \ or \ y = c_h, M) \\
&= \frac{P(y = c_g | M)}{P(y = c_g | M) + P(y = c_h | M)} \\
&= \frac{P(M | y = c_g) P(y = c_g)}{P(M | y = c_g) P(y = c_g) + P(M | y = c_h) P(y = c_h)}
\end{aligned}
\tag{6.1}
$$

Therefore:

$$\frac{P(y = c_g | y = c_g \ or \ y = c_h, M)}{P(y = c_h | y = c_g \ or \ y = c_h, M)}$$
$$= \frac{P(M | y = c_g) P(y = c_g)}{P(M | y = c_h) P(y = c_h)} \tag{6.2}$$

given that $P(M | y = c_l) > 0 \ \forall \ c_l \in C$.

By applying Bayes' rule, the posterior probability $\phi_g = P(y = c_g | M)$, i.e., the likelihood of the unlabeled muscle being categorized as c_g, can be estimated as:

$$P(y = c_g | M) = \frac{P(M | y = c_g) P(y = c_g)}{\sum_{l=1}^{L} P(M | y = c_l) P(y = c_l)} \tag{6.3}$$

It can be shown [114, 100] that:

$$P(y = c_g | M)$$
$$= \frac{1}{\sum_{l:l \neq g} \frac{1}{P(y = c_g | y = c_g \ or \ y = c_l, M)} - (L - 2)} \tag{6.4}$$

6.4.3.2   Pair-wise Coupling Binarization

The set of binary characterizers used by an instance of a pair-wise coupling (PWC) binarization mapping is the same as $F_{\triangle}$, given they are induced from the same training dataset D.

In contrast to the previous method, it can be assumed that ϕ_{gh} and $P(y = c_g | y = c_g \ or \ y = c_h, M)$ are not equal [53] such that ϕ_g can be estimated by minimizing the Kullback-Leibler kl distance between them.

$$kl = \sum_{g \neq h} [n_{gh} \frac{P(y = c_g | M)}{P(y = c_g | M) + P(y = c_h | M)}$$
$$\log \frac{P(y = c_g | y = c_g \ or \ y = c_h, M)}{\phi_{gh}}] \tag{6.5}$$

where n_{gh} is the total number of training examples labelled c_g or c_h. The point that minimizes the above criteria was shown to satisfy:

$$\sum_{j:j\neq i} n_{gh} P(y = c_g | y = c_g \ or \ y = c_h, M)$$

$$= \sum_{j:j\neq i} n_{gh} \frac{P(y = c_g | M)}{P(y = c_g | M) + P(y = c_h | M)}$$

$$= \sum_{j:j\neq i} n_{gh} \phi_{gh} \tag{6.6}$$

$$\sum_{l=1}^{L} P(y = c_l | M) = 1$$

$$P(y = c_l | M) > 0, \ l = 1, ..., L$$

and $\phi_g = P(y = c_g | M)$ can be obtained by solving the system of equations in 6.6 using an iterative algorithm.

6.4.3.3 Pairwise Resemblance Binarization

The set of binary characterizers used by an instance of a pairwise resemblance (PWR) binarization mapping is the same as $F_\triangle$, given they are induced from the same training dataset D.

It has been pointed out that the ratio $\frac{P(y=c_g|y=c_g \ or \ y=c_h,M)}{P(y=c_h|y=c_g \ or \ y=c_h,M)}$ often differs significantly from $\frac{\phi_{gh}}{\phi_{hg}}$ and that the effects of this inconsistency can be mitigated by the use of a resemblance model [49]. Assuming a set of three muscle categories $C = \{c_1, c_2, c_3\}$, the main assumptions of a resemblance model can be summarized as:

- Each category, say c_1, is divided into virtual classes c_{12} and c_{13}, where c_{12} represents a subset of c_1 labelled muscles that are closer to c_2, and c_{13} represents a subset of c_1 labelled muscles that are closer to c_3.

- Since the main focus is on discrimination between "confusing" muscles, it is assumed that: $\frac{P(y=c_1|y=c_1 \ or \ y=c_2,M)}{P(y=c_2|y=c_1 \ or \ y=c_2,M)} = \frac{P(y=c_{12}|y=c_1 \ or \ y=c_2,M)}{P(y=c_{21}|y=c_1 \ or \ y=c_2,M)}.$

- The last assumption is that $\frac{P(y=c_{12}|y=c_1 \ or \ y=c_2, M)}{P(y=c_{21}|y=c_1 \ or \ y=c_2, M)} = \frac{P(y=c_{31}|y=c_1 \ or \ y=c_3, M)}{P(y=c_{32}|y=c_1 \ or \ y=c_3, M)}$.
  The other ratios of the posteriori probabilities of the virtual classes of a given class can be similarly found.

The posterior category probability can be estimated using [49]:

$$
\begin{aligned}
P(y = c_g|M) \\
= \frac{\prod_{l,l \neq g} P(y = c_g|y = c_l \ or \ y = c_g, M)}{\sum_h \prod_{l,l \neq h} P(y = c_h|y = c_l \ or \ y = c_h, M)}
\end{aligned}
\tag{6.7}
$$

6.4.3.4   One-Against-All Binarization

An instance of a one-against-all (OAA) binarization mapping, say ρ, induced to discriminate among L labels, utilizes a set of binary characterizers F_ρ of length L. A binary characterizer $f_l \in F_\rho$ is associated with the label c_l, since when obtained, it categorizes an unlabelled muscle, M, to be either c_l or not. The data set used for inducing f_l is $B_l = B_{l_+} \cup B_{l_-}$, where $B_{l_+} = \{(M_i, y_i) \in D : y_i = c_l\}$ and B_{l_-} is obtained by labelling $y_i = c_{l_-} \ \forall \ \{(M_i, y_i) \in D : y_i \neq c_l\}$. When the output of f_l is evaluated for a test muscle M, a vector of likelihood estimates (ϕ_l, ϕ_{l_-}) is estimated. The first element of the vector represents the likelihood of M being labeled c_l, while the second element is the likelihood of M not being labeled c_l. A likelihood factor for c_l can be defined as $\xi_l = \frac{\phi_l}{\phi_l + \phi_{l_-}}$.
During the evaluation of the output of ρ using M, all the outputs of all elements of F_ρ are evaluated. The element of the final likelihood vector $\Phi(l)$ estimating the likelihood of an unlabelled muscle, M, being labelled c_l is obtained as:

$$
\Phi(l) = \frac{\xi_l}{\sum_{a=1}^{L} \xi_a}
\tag{6.8}
$$

6.4.4   MUPT Characterization based on Event Association Rules

This and the following subsections describe inducing MUPT characterizers based on event association rules (EAR) and Gaussian mixture models (GMM), as either binary characterizers or as multi-class characterizers. The training set T used for estimating a MUPT

125

characterizer consists of a pool of labelled MUPTs. This is obtained by assigning a muscle label to its constituent MUPTs:

$T = \{(x_1^{(1)}, y_1), ..., (x_{n_1}^{(1)}, y_1), ..., (x_1^{(N)}, y_N), ..., (x_{n_N}^{(N)}, y_N)\}.$

The label assigned to a MUPT might not be the correct MUPT categorization, because some of the motor units belonging to a diseased muscle might not be affected by the disease. The output of a MUPT characterizer (induced using the dataset T) for a feature vector representing a MUPT belonging to the unlabeled muscle $M_k \in V$, say $x_j^{(k)}$ for each category c_l consists of: (1) The estimate $\zeta_j^{(k)}(l)$ of the likelihood of assigning the MUPT to c_l and (2) the corresponding set of transparency rules. It was assumed in this work that $\Phi(l)$, i.e., an estimate of the likelihood of M_k being categorized as label c_l, can be obtained as:

$$\Phi(l) = \frac{1}{n_k} \sum_{j=1}^{n_k} \zeta_j^{(k)} \tag{6.9}$$

where n_k is the number of MUPTs sampled from muscle M_k.

The characterization based on EAR [142, 139, 141] performs statistical analysis on discrete data using contingency tables of dimension $[(d + 1) \times (d + 1)]$. Therefore, each feature, either discrete or continuous, is quantized using Q bins (in this work, $Q = 5$), such that each bin has the same number of elements. For a given labelled feature vector $x_j^{(i)} = (x_j^{(i)}(1), ..., x_j^{(i)}(u), ..., x_j^{(i)}(d)) \in M_i$ representing a MUPT, a corresponding discretized feature vector is created $\chi_j^{(i)} = (\chi_j^{(i)}(1), ..., \chi_j^{(i)}(u), ..., \chi_j^{(i)}(d))$, such that the uth feature can assume an element from a specific alphabet: $\chi_j^{(i)}(u) \in \{\alpha_u(1), ..., \alpha_u(q), ..., \alpha_u(Q)\}$.

In the training set T, a primary event occurs when an element of $\chi_j^{(i)}$ takes a specific value $\chi_j^{(i)}[u] = \alpha_u(q)$. An rth order event φ^r, where $r \leq d$ contains r primary events. An event will be defined as a pattern if it passes a test of statistical significance. The number of expected observations e_{φ^r} is calculated by assuming that the alphabets forming any feature are equally likely and the variables belonging to the same vector are independently sampled.

$$d_{\varphi^r} = \frac{o_{\varphi^r} - e_{\varphi^r}}{\sqrt{v_{\varphi^r}} \sqrt{e_{\varphi^r}}} \tag{6.10}$$

where o_{φ^r} is the number of times the event φ^r was observed in T and $\sqrt{v_{\varphi^r}}$ is the standard deviation of $\frac{o_{\varphi^r} - e_{\varphi^r}}{\sqrt{e_{\varphi^r}}}$.

The discriminatory power of a pattern that includes a label in supporting or refuting a class c_l is estimated using the weight of evidence:

$$WOE_l(\varphi^r) = \log(\frac{P(\varphi^r|y = c_l)}{P(\varphi^r|y \neq c_l)})$$ (6.11)

A rule is formed of a triplet of a pattern, label and WOE.

The evaluation of the output of a MUPT characterizer using $x_j^{(k)}$, a feature vector describing a MUPT belonging to an unlabelled muscle M_k, starts by quantizing the features into $\chi_j^{(k)}$ using the same quantization ranges obtained during the training phase. The rules used for classifying are selected starting from the highest order rule first and accumulating its WOE for each label. All the feature-value pairs of this rule are then excluded and the highest order rule is then found from the remaining feature-value pairs. This continues until no rule can be extracted or no feature-value pairs remain. The algebraic sum of the WOE of all classifying rules supporting or refuting a given category, say c_l, is an estimate of $\zeta_j^{(k)}(l)$. The union of the patterns of the classifying rules represents the corresponding transparency rules.

6.4.5 MUPT Characterization based on Gaussian Mixture Model

In this work, the conditional probabilities were estimated by assuming a multivariate Gaussian probabilistic model such that:

$$P(x_j^{(i)}|y_i = c_l) = \mathcal{N}(x_j^{(i)}|\mu_l, \Psi)$$ (6.12)

where $\mathcal{N}(x_j^{(i)}|\mu_l, \Psi)$ is a multivariate Gaussian probability distribution. Using the training data T, the maximum likelihood estimate of the mean feature vector μ_l and the covariance matrix Ψ_l are obtained for each category. Assuming all categories are equally likely, the averaged covariance matrix Ψ is estimated using:

$$\Psi = \frac{1}{L}\sum_{l=1}^{L}\Psi_l$$ (6.13)

The posterior probability of $x_j^{(k)} \in M_k$, a feature vector describing a MUPT belonging to an unlabelled muscle, is then calculated using Bayes' rule as:

$$\zeta_j^{(v)} = P(y = c_l | x_j^{(k)}) = \frac{P(x_j^{(k)} | y = c_l)}{\sum_l P(x_j^{(k)} | y = c_l)} \tag{6.14}$$

6.5 Empirical Evaluation

6.5.1 Validation

The data was acquired and processed in the same manner as described in Section 3.4.1 on Page 55. Also, this work utilized all features defined in Chapter 3 using the same estimation parameters. Leave-one-out cross-validation (LOOCV) was used. In each iteration, the feature vectors of the MUPTs of a given muscle were used for testing, and feature vectors of the remaining MUPTs were used as training data.

For each class, the class error was calculated as the ratio of the number of incorrectly categorized muscles to the total number of muscles belonging to that class. The overall muscle categorization error was then estimated as the mean value of individual class errors.

6.5.2 Feature Selection

The sequential floating forward search (SFFS) algorithm described in [101] was used to select the feature sets, used by the binary characterizers of the investigated binarization mappings or the multi-class characterizers, which minimized muscle categorization error. Tables 6.3 and 6.4 list overall muscle categorization accuracies obtained by different binarization mappings and multi-class characterizers based on EAR and GMM, utilizing the selected feature sets.

	TA	FDI	DLT	VM	Average
Multi-class	88.95	83.97	76.54	78.79	82.06
Ordered Binarization Mappings					
DDAG_Dis	91.91	86.53	84.47	83.64	**86.64**
DDAG_Myo	91.91	86.53	82.31	**87.99**	**87.19**
DDAG_Neu	91.91	86.53	**84.87**	86.54	**87.46**
S_Nor	89.59	58.03	74.87	74.07	74.14
S_Myo	91.17	86.53	78.14	81.41	84.31
S_Neu	**94.1**	**89.05**	81.54	**87.99**	**88.17**
Unordered Binarization Mappings					
PWD	90.4	84.32	79.81	83.64	84.54
PWC	90.4	63.23	67.23	69	72.47
PWR	90.4	82.93	79.81	83.64	84.2
OAA	84.47	56.07	75.7	73.98	72.56

Table 6.3: Overall muscle categorization accuracies of different binarization mappings and multi-class characterization based on EAR

6.6 Discussion

Characterization based on EAR is transparent, because it provides the underlying evidence supporting its decision in a way that can be understood and evaluated by clinicians. The searched hypothesis space is a set of conjunctive rules associated with a particular class. The main reasons characterization based on EAR was selected over other inductive rule learning algorithms such as IREP [42] or its successor, RIPPER [22], which are also transparent, can be summarized as:

1. the capability of detecting and assessing higher order relationships between different features

2. immunity to noisy patterns

3. the ability to avoid exhaustive search using a reasonable statistical heuristic

	TA	FDI	DLT	VM	Average
Multi-class	91.24	82.02	**83.2**	83.64	85.03
Ordered Binarization Mappings					
DDAG_Dis	90.43	**86.02**	**83.2**	84.99	86.16
DDAG_Myo	90.43	84.89	81.47	84.99	85.45
DDAG_Neu	90.43	84.89	81.47	84.99	85.45
S_Nor	86.69	54.38	69.81	67.4	69.57
S_Myo	90.43	84.32	81.47	**86.44**	85.67
S_Neu	**92.69**	85.54	82.37	83.73	86.08
Unordered Binarization Mappings					
PWD	82.09	81.05	74.68	73.98	77.95
PWC	85.94	75.67	71.41	73.98	76.75
PWR	79.05	81.5	72.12	72.53	76.3
OAA	89.66	75.73	73.97	73.4	78.19

Table 6.4: Overall muscle categorization accuracies of different binarization mappings and multi-class characterization based on GMM

4. the possibility of analyzing mixed-mode data using an appropriate quantization approach

5. the ability to combine WOE measures from different sources of evidence supporting or refuting a given decision to obtain an overall measure supporting or refuting a specific categorization.

However, the current configuration of characterization based on EAR does not easily allow the embedding of prior or domain knowledge. Therefore, the superiority of MUPT characterization based on EAR over other inductive rule learning algorithms remains an open question to be investigated theoretically and empirically.

Investigated binarization mappings were also implemented using GMMs as MUPT characterizers. A GMM is an instance of a Bayesian linear separator that provides a semi-parametric density model. Similar to parametric models, a GMM has structure and

parameters which control the behaviour of the density, with sufficient degrees of freedom to allow arbitrary density modelling [103]. The choice of using GMMs to model MUPT conditional probabilities is justifiable, because the marginal conditional probabilities of each MUPT feature is either normal or log normal and therefore this normality is expected to hold for their joint distributions.

The QEMG features used in this study are also transparent, i.e., an electrodiagnostic physician can validate an estimate of a feature value by examining the MUP template, in the case of morphological features, and the ensemble of MUPs belonging to the same MUPT, in the case of morphological stability features. It has also been shown in Chapter 3 that changes in the values of the features used can be related to disease-induced changes. For example, neurogenic MUP templates have higher values of thickness feature, as more muscle fibres comprise the motor unit due to reinnervation; while myopathic MUP templates have smaller values of thickness feature because of muscle fibre loss. electrodiagnostic physicians are also aware of limitations of the feature values used. For example, the MUP amplitude is known to be highly dependent on the size and number of the few nearest motor unit fibres.

Electrodiagnostic physicians, applying quantitative EMG techniques, may exclude invalid MUPTs or inconsistent MUPs from ensembles of MUPs belonging to the same MUPT used for template and/or stability features estimation and often adjust the onset and end positions of the provided MUP templates used to calculate important feature values. In this work, MUPTs were not manually excluded or edited and MUP template onset and end marker positions were not manually adjusted. The feature values automatically provided by DQEMG [124] were used. The following reasons summarize this decision:

- Editing is a time consuming process, and normally in the course of a needle examination more than one muscle is examined and each muscle examination includes the sampling of motor units at several muscle locations. Therefore, it is important to have QEMG methods that can provide useful information without the need for manual editing to ensure their clinical viability.

- Editing might be biased by prior hypotheses originating from other examinations. They for example might exclude small MUPs to avoid categorizing a slightly involved

muscle as myopathic.

- The need to evaluate the effectiveness of validation procedures implemented in DQEMG [90] and the immunity of different binarization mappings and MUPT characterizers to probable inaccuracies in feature estimates.

Tables 6.3 and 6.4 show that the multi-class characterizer based on GMM outperformed on average the multi-class characterizer based on EAR. However, four out of ten binarization mappings based on EAR outperformed the multi-class characterizer based on GMM. Seven binarization mappings based on EAR, including the aforementioned four mappings, also outperformed the corresponding binarization mappings based on GMM. Furthermore, characterizations based on EAR always performed better than the characterizations based on GMM when one takes the best score across all binarization mappings for each muscle. These results are significant as they suggest that the use of an appropriate binarization mapping can overcome the possible decrease in categorization accuracy resulting from quantizing MUPT features, often used to realize a transparent characterization.

As shown in Tables 6.3 and 6.3, improved categorization accuracies are often obtained using binarization mappings compared to multi-class characterization. Seven out of ten binarization mappings based on EAR outperformed on average the multi-class characterization based on EAR, and five out of ten binarization mappings based on GMM outperformed on average the multi-class characterization based on GMM. The performance gain can be attributed to the fact that binary characterizers use more relevant features to obtain more specific characterizations. Binary characterizers based on EAR also make use of more relevant quantization yielding more accurate statistical significance testing of events.

S_Nor binarization mapping performed significantly worse than the multi-class characterizers and the other binarization mappings based on either GMM or EAR. The categorization accuracy of the first stage discriminating normal versus others was low, because the disease process is progressive and non-uniform across the motor units belonging to the same muscle, which results in many MUPTs belonging to diseased muscles being normal. This can also explain the poor performance of the OAA binarization mapping, as it utilizes the same binary characterizer.

Using characterizers based on EAR, PWD binarization mapping outperformed the multi-class characterizer and was close to the highest performing binarization mappings, which was not the case for PWD using characterizers based on GMM. In PWD, it is assumed that the likelihood estimate obtained by a binary characterizer is equal to the posterior probability of a muscle being categorized as a category given that only two categories are under consideration. This indicates that the likelihood estimates obtained by the binary characterizer based on EAR are closer to the true posterior probability estimates than estimates obtained using binary characterizers based on GMM characterizers. The categorization accuracies for PWR are close to those for PWD, which suggests that the impurities in the diseased muscles can be captured to some extent using the resemblance model adopted by the PWR binarization mapping.

The DDAG variations and the S_Myo and S_Neu binarization mappings had comparable categorization accuracies and exceeded the accuracies of the multi-class characterizers based on either GMM or EAR. It is not straightforward how to decide which one is superior. One important factor to consider is how the electrodiagnostic physician can use the obtained likelihood estimates and sets of transparency rules. For instance, the transparency rules obtained in either of the leaf nodes in the DDAG_DIS enumerate the evidence supporting and refuting the muscle being categorized as diseased versus being categorized as normal. These rules can possibly be used as a basis for a diagnosis.

The SFFS algorithm [101] is not guaranteed to find the optimal feature set, i.e., the feature set having the maximum muscle categorization accuracy. This is the case for all feature selection algorithms based on heuristic search. Nonetheless, the SFFS algorithm was used because:

1. It is computationally efficient. This is crucial, since the initial feature set has 22 features.

2. It allows selected features to be later discarded. A given feature might prove to be useless after another set of features have been selected. It was shown that there is a high interdependence between QEMG features belonging to the same aspect (see Chapter 3).

3. It is tolerant to deviation from monotonic behaviour of classification accuracy as new features are added. Since a conditional exclusion step follows the comparison of feature subsets to features with the same dimension.

Table 6.5 shows the results of feature selection up to the 5th dimension for binary characterizers belonging to $F_{\triangle}$ and the multi-class characterizer based on EAR. It is clear that the results are consistent with the results presented in Chapter 3 using more exhaustive feature selection techniques and both real and simulated muscle studies. The consistency is clear from the following observations:

1. the most relevant feature set is composed of features belonging to different aspects

2. FbrCnt is better than Trn, because FbrCnt is estimated using high-passed filtered data, which emphasizes the contribution of fibres close to the detection surface of the electrode

3. local complexity features related to turns are more important for discrimination of myopathic complexity, while local complexity features related to phases are more relevant for discrimination of neurogenic complexity

4. Duration is highly affected by marker placement and this may be why it is less relevant when no manual editing is performed.

6.7 Conclusion

This work contributes to the development of transparent and accurate methods for obtaining muscle characterizations based on EMG signals detected during isometric contractions. For the characterizations to meet clinical requirements, they should be integratable with characterizations evaluated from other physical and electrophysiological examinations. The characterizations should also include transparency rules that can be used for validation and as a basis for diagnosis. Results of this work demonstrate that the use of binarization mappings can overcome decreases in categorization accuracies associated with transparent

Characterizer	Size	Global Complexity	Local Complexity	Stability
$f_{myo-neu}$	Amplitude	Fibre Count, Shape Width	Phase Complexity	Jiggle
$f_{nor-myo}$	Amplitude	Fibre Count, Shape Width	Turn Amplitude	B Jiggle
$f_{nor-neu}$	Area	Number of Phases, Number of Turns	Phase Complexity	B Jiggle
Multi-class	Area	Shape Width, Number of Phases, Fibre Count	-	B Jiggle

Table 6.5: SFFS selected features up to the 5th dimension for muscle characterizers based on EAR for the TA muscle

characterizers. Future work will focus on the value of transparency rules obtained using EAR compared to rules obtained using other rule induction algorithms. Better ways of estimating muscle characterizations by integrating information obtained from QEMG features extracted from resolved MFPs, decomposed MUPTs, sampled contractions and the whole muscle will also be investigated. Finally, a clinical study evaluating the impacts of applying the proposed methods in practise is strongly recommended.

Chapter 7

Conclusion

7.1 Summary

In this chapter, a summary of the contributions of this thesis and their possible impacts are presented. The chapter also discusses the important directions of future work.

7.2 Summary of Thesis Contributions

The central problem addressed in this thesis is the characterization of neuromuscular disorders by quantitatively analyzing EMG signals acquired using an intra-muscular needle electrode from human skeletal muscle during low to moderate isometric voluntary contraction. Digital signal processing algorithms and machine learning methods were developed to provide accurate, sensitive and transparent muscle characterization in a time span comparable to the the time needed to complete a qualitative analysis using clinically viable acquisition protocols.

EMG Signal Preprocessing

The main contribution to the the preprocessing sub-stage is the adoption of digital filtering techniques (Savitzky-Golay filter) that primarily focus on maintaining the MUP morphology while discarding contaminations from instrumentation noise and other irrelevant bio-electric sources. This is crucial, because MUP morphology is, by far, the most reliant source of information to capture disease induced changes to the muscle structure and function. The preprocessing scheme is also adaptive, where the filter configuration is changed based on each signal optimizing for the Durbin-Watson criteria.

MUP segmentation

The MUP segmentation technique proposed in this thesis is an extensible approach that does not only aim at extracting active segments from the EMG signal, but also attempts to classify the extracted segments based on how well their morphology resemble an isolated MUP. An extensive evaluation using 50 simulated EMG signals calculated using an electro-physiologically sound model shows that the obtained average recall is 0.95 ± 0.066 and the average precision is 0.966 ± 0.035. These results are obtained for MUPs with maximal amplitude that is three times larger than the standard deviation of the added noise.

MUPT Identification

The design philosophy behind the proposed MUPT identification methods is conservative but reasonably effective. It is conservative in a sense that it does not try to assign every segmented MUP, or even identify every MUPT. Instead, the main focus is to identify a subset of MUPTs that can be used to investigate disease induced changes in MUP morphology and how MUP morphology varies across a train. The proposed methods are also specifically tailored to accommodate issues that are particularly relevant to the analysis of clinical EMG signals in the context of characterizing neuromuscular disorders. These issues include:

- **Random intra-train variability**: The use of DTW alignment is effective in estimating morphological similarity measures that are least affected by variability in MUP morphology due to instabilities in neuromuscular transmission.

- **Trending intra-train variability**: The reliance on spectral clustering, that assumes connectivity between cluster members rather than cluster compactness, can track the changes resulting from slow and slight electrode movement.

- **Inter-train MUP morphological similarity**: Similarity graph pruning provides a powerful mean for integrating motor unit firing times into the clustering. In some cases, the firing times can be the last resort in discriminating between trains that happen to have highly morphologically similar MUPs.

A comprehensive evaluation of the proposed methods shows that a high yield of representative MUPTs can be identified accurately in a course of a few seconds. Beyond proposing new methods, the thesis also contributes to the MUPT identification problem by defining a new framework for evaluation. This framework quantifies superposition degree of influence, train representativeness, information yield and potential identification errors including misassignment, train splitting and merging.

Morphological and Morphological Stability Features

The thesis proposes ten new features capturing MUP morphology and how it varies across the MUPs belonging to the same train. The newly proposed features are shown to be discriminative across different disease categories. More importantly, the thesis introduces the novel concept of grouping quantitative EMG features into groups, where each group is reflecting a different aspect of MUP morphology. This aspect grouping is investigated by creating simulated EMG studies and applying an in-depth statistical feature selection algorithm.

In any of its iterations, the feature selection algorithm selects all subsets of features that performed equivalently in a statistical sense. This prevents the search from discarding feature combinations at early stages due to subtle performance differences. The results are

also validated using clinical EMG studies and a feature selection algorithm based on a different search approach. Results also confirm that a muscle characterization based on a selected feature set that is limited to have each aspect represented by only one feature does not result in a decrease in categorization accuracies. Instead, it enables the making of a more structured, more transparent and simpler clinical decision.

Features for Characterizing Neuromuscular Junction Stability

The thesis introduces a new QEMG feature called NF-MUP-Jitter that is sensitive to disturbances in the neuromuscular junction function. The estimation of this feature relies on segmenting single fibre MUP segments, i.e., parts of the MUP, where a contribution from one of the muscle fibres is not significantly changed by contributions from other fibres. Aligning and evaluating the morphological consistency of these segments are achieved using regional dynamic time warping. For the purpose of segmenting single fibre MUP segments from the MUP, a SVM classifier is trained using simulated MUPTs with known NF-MUP-Jitter values.

An evaluation based on 680 simulated MUPTs shows that the average error in estimating NF-MUP-Jitter is 8.9%. One or more single fibre MUP segments can be detected in 85.3% of MUPTs. The key advantage of this feature is that it can be estimated quickly (the average analysis time for a MUPT is 3.6 seconds) from an automatically decomposed EMG signal acquired using conventional clinical protocol and equipment. These improvements shall facilitate the characterization of NMDs affecting the neuromuscular junction operation using EMG techniques substantially, when compared to estimating jitter based on traditional single fibre EMG.

Firing Patterns Features

The thesis shows initial evidence supporting the possibility of detecting neurogenic disorders by investigating quantitative features summarizing the firing patterns of sampled concurrently active motor units. These quantitative features are driven from mean firing rates that are estimated from MUPTs extracted from partially decomposed EMG signals.

The MUPTs are sampled using an acquisition protocol that does not demand measurement nor control of the contraction level. The evidence is based on clinical data acquired from more than 800 MUPTs sampled from the TA muscle. For a further insight and confirmation, a model with a modularized architecture is built blending state of the art mathematical and numerical models that predict motor neuron pool neurodynamics and muscle electrophysiology.

Muscle Characterization

The thesis provides a mathematical formulation of the muscle characterization problem emphasizing its nature as a multiple instance learning problem and delineating its different outputs. The thesis evaluates remodelling the muscle characterization problem to ten different binarization mappings. The performance of each is investigated using a through feature selection procedure based on both statistical and rule induction classifiers. The results obtained using more than 340 clinical studies confirm that using an appropriate binarization mapping can result in obtaining higher categorization accuracy and more clinically relevant transparency rules.

7.3   Directions for Future Work

Each of the preceding five chapters concludes with suggestions for future directions related to the methods and evaluation techniques discussed within the chapter. This section focuses on more general and long term directions for future work.

7.3.1   Evaluation of Clinical Utility

A set of clinical studies should be performed to evaluate the proposed system with respect to the following criteria:

- How well will the system generalize across age groups or race/ethnicities?

- Do the proposed characterizations contribute to equivocal cases?

- How often do clinicians need to edit the identified trains by excluding and/or including MUPs?

- How suitable is the proposed system for tracking prognosis?

- How correlated are the estimated features and induced rules to the level of disease involvement?

7.3.2   Refining and Monitoring the Acquisition Protocol

The yield and quality of the information extracted from an EMG signal is determined by the nature of the acquired signal. For instance, signals acquired at a low contraction force with inappropriate needle positioning will result in few (one to three) representative MUPTs being identified. On the other hand, increasing the level of contraction results in a lesser chance of observing isolated MUPs. This will also demand a more complicated and time consuming analysis, and will result in less representative MUPTs.

The first phase of this sought study shall focus on the biophysial basis of intramuscular EMG signals by utilizing and extending the mathematical, computational and phenomenological models of EMG to find convincing answers to basic, yet unresolved, questions including:

- What characteristics should a MUP possess before it can be considered suitable for characterization of neuromuscular disorders?

- How many MUPs need to be sampled from each train to be able to confidently quantify the variability in neuromuscular transmission?

- How much electrode movement can be tolerated?

- How important is it to measure and control the level of contraction?

This should be followed by development of signal analysis techniques that are capable of providing real-time signal quality indexes. An operating electrodiagnostic clinician should use these indexes to adjust the needle position and to provide instruction to the test subject (For example, to increase or decrease the contraction level). The sought analysis techniques should also provide a feedback to the operating clinician on when enough high quality signal for characterization of neuromuscular disorders are acquired.

7.3.3 Characterization using Clinically Relevant Multi-level Transparency Rules

The information yield of decomposition based methods is constantly increasing, i.e., decomposing more MUPTs and extracting more and finer clinically relevant details. This will lead to characterization being based on higher order and more transparency rules. The first thing to consider along this line of investigation is to induce lower order rules and not to increase the order of an induced rule, unless it will lead to a statistically significant improvement in the confidence in the likelihood estimates.

The second sought improvement is to develop means of transparency rules ranking and selection that allows integration of domain knowledge without compromising categorization accuracy or confidence in likelihood estimates. For instance, selecting a rule that includes two features belonging to the same aspect should be avoided unless it significantly changes the results.

The last objective is to deal with the relational nature of the features, meaning that the estimated features can not be expressed using a single fixed length feature vector [65]. QEMG features describe all of the following levels of the neuromuscular structure: (1) Muscle, (2) Contraction, (3) MUPT, and (4) MFPs.

Therefore, a One-to-Many relational description of a muscle data rather than a tabular representation is more accurate. Most of the conventional machine learning approaches are suitable for tabulated data. This limits the integration of features describing other levels and therefore most of the previous work [98] use aggregation methods to move from the MUPT level to the muscle level.

A desired muscle characterization based on a multi-level clinically relevant transparency rules should be expressed verbally. For instance:

"The likelihood of this muscle being categorized as neurogenic rather than normal is 80 %. This is because 90% of the decomposed potential trains have medium to high instability and high complexity. 72 % of the resolved NF-MUPs have large sizes".

Appendix A

Morphological Features Describing Near Fibre MUPs

A.1 Summary

In this appendix, a preliminary investigation of the utility of features describing the morphology of NF-MUPs is presented. Statistical results and provided examples suggest that a better discrimination between normal and affected muscles is achievable using NF-MUP global complexity features compared to MUP global complexity features.

A.2 Introduction

The objective of this appendix is to compare the utility of size and global complexity aspect features, specifically area and turns, acquired using standard clinical bandwidths

---

Portions of this appendix previously appeared in D. Stashuk, M. AbdelMaseeh, and B. Smith. Looking under the blanket for better measures of motor unit potential size and complexity. *Muscle & Nerve*, 48(4):669–669, 2013

144

versus features from NF-MUPs templates obtained using low-pass double differentiation. A visual reasoning behind why NF-MUPs are potentially more capable of providing better MUP complexity features is presented in Figure A.1.

The middle column shows templates and raster plot of a MUPT sampled from a normal muscle. The left column of a MUPT sampled from a myopathic muscle, while the right column is of a MUPT sampled from a neurogenic muscle. Examining the MUP templates presented in the first row, the three MUPs are of similar size and look similarly complex, given that all of them are comprised of two or three turns. On the other hand, the NF-MUPs presented in the third row show that diseased NF-MUPs have larger numbers of distinctive and dispersed turns and therefore are more complex compared to the normal MUP. In any of the MUPTs, the raster of isolated NF-MUPs validate that the detected turns can be tracked consistently, to some extent, across the raster of NF-MUPs and that they are jittering with respect to each other.

A.3   Empirical Analysis

The data was acquired using the same procedure described in Section 3.4.1 on Page 55. However, only studies from the TA muscle were utilized in this study. Area and number of turns features were extracted from the MUP templates. These MUP templates were then high-pass filtered using a second order low-pass differentiator and a new estimate of the area (NF-area) and the number of turns (NF-Turns) were extracted.

The histograms in Figure A.2 show a better separability between normal and diseased MUPTs distributions when NF-turns are used compared to turns. It is also clear that not much separation exists between myopathic and neurogenic MUPTs distributions using either turns or NF-turns, which is expected as both types of MUPs are predicted to be more complex.

The discriminability of the investigated features across different classes was also investigated using muscle-level features obtained by averaging the feature values across MUPTs sampled from the same muscle. Muscle-level features can overcome the non-uniformity of disease involvement across the motor units belonging to the same muscle. This means
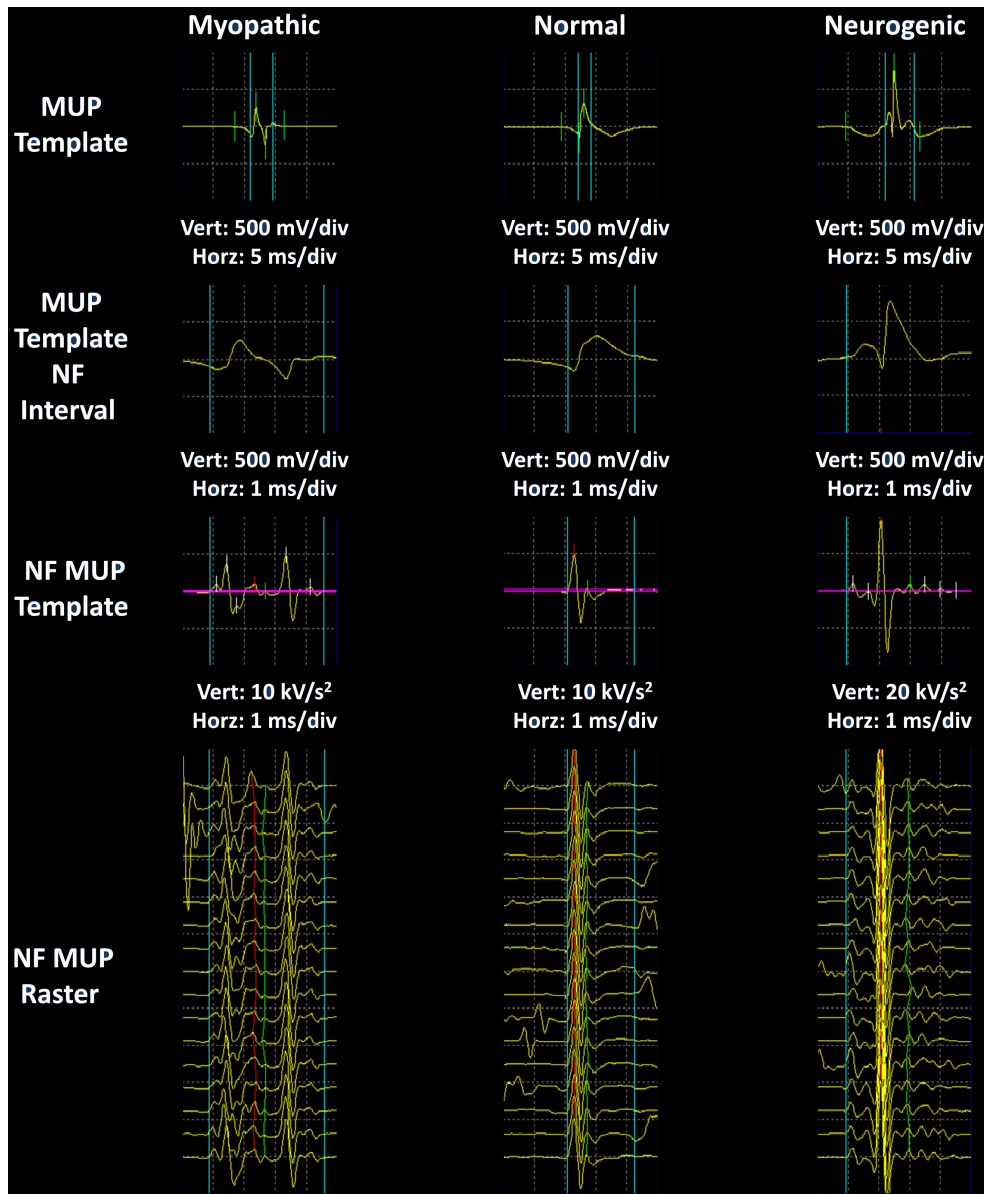
Figure A.1: Example MUP templates, NF-MUP templates and NF-MUP raster plots

that some of the motor units sampled in an affected muscle can be slightly affected or not
affected at all.
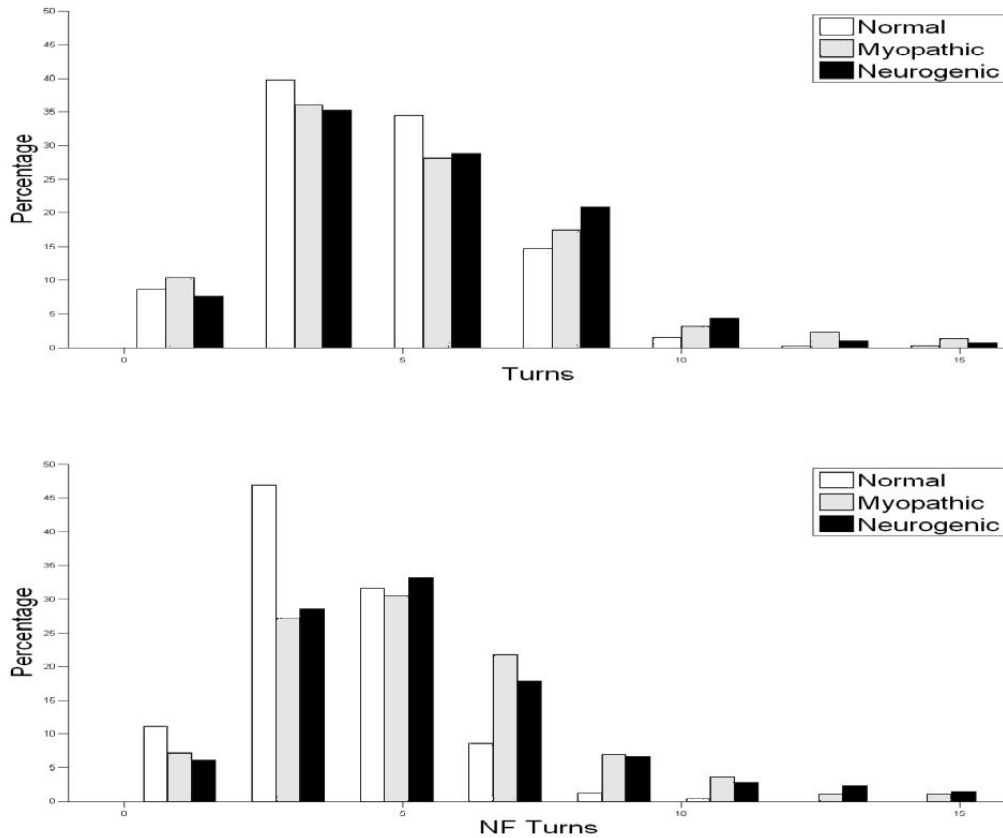
Figure A.2: Histograms of Turns and NF-Turns show better discrimination between normal and disease categories using NF-Turns compared to using turns

The area under curve (AUC) metric of the receiver operating characteristics curve [75] was used to evaluate discriminability of four corresponding muscle-level features and the results are shown in Table A.1. The main reason for using AUC is that it is a non-parametric test. This is beneficial, since the number of muscles in the used dataset are low, especially for myopathic muscles and therefore it is not possible to assume how the muscle-level features are conditionally distributed.

The three most obvious observations in Table A.1 are: (1) the NF-Turns feature is more indicative of disease than the Turns feature (2) Not much discrimination between disease

Feature	Myo vs Normal	Neuro vs Normal	Neuro vs Myo
Area	0.85	0.94	0.97
NF-Area	0.63	0.88	0.88
Turns	0.61	0.72	0.58
NF-Turns	0.79	0.9	0.62

Table A.1: The area under a receiver operating curve (AUC) estimates the discriminiabilty of a muscle-level feature across two categories. AUC values for all two category decisions are presented.

categories can be obtained using either turns or NF-turns (3) Area is more discriminative than NF-Area for the three decisions. The last observation can be attributed to the fact that discarding contributions for distant muscle fibres might lead to a less representative feature of the number of fibres in a motor unit.

Feature Set	Myo vs Normal	Neuro vs Normal	Neuro vs Myo	Multi-category
Area	79.1	85.2	88.7	76.2
NF-Area	57	80.8	79.9	58.5
Area , Turns	70.4	85.2	88.7	70.4
Area, NF-Turns	91.3	85.2	88.7	85.1

Table A.2: Classification accuracies for two and multi-category decisions using various feature combinations

The ability of NF-turns to improve the discrimination provided by size aspect features was investigated using classification based on event association discussed in Section 6.4.4 on Page 125. Similar to the paradigm adopted in Chapter 6, the utility of a feature set was equated to the classification accuracy. Table A.2 shows that a feature set comprised of Area and NF-Turns increased categorization accuracy for a binary characterizer discriminating myopathic and normal muscles by almost 10% over using Area only, while no improvement was achieved for the other two decisions. The multi-class categorization

accuracy implemented using a decision directed acyclic graph (diseased-first) binarization mapping discussed in Chapter 6 using a feature set comprised of NF-Turns and Area was 9% higher than using Area only. No similar improvement was obtained when a feature set composed of area and turns was used. Similar to what is shown in Table A.1, the classification accuracies obtained using Area is higher than NF-Area.

The improvement in the ability to discriminate myopathic from normal muscles achieved by the feature set comprised of Area and NF-Turns can be attributed to the fact that it is more likely to find small NF-MUPs that have larger numbers of NF-Turns. The turns, since they are estimated from the raw MUPs, are less capable of revealing MUP complexity, especially for small MUPs that are more likely to be found in myopathic muscles. This is potentially due to the fact that the morphology of a MUP is blurred by low frequency components contributed by distant fibres obscuring complexity details. Equal accuracies were obtained for discrimination between neurogenic and normal when a feature set composed of Area, Area and Turns, or Area and NF-Turns. This suggests that no additional evidence of neuropathy is provided by either of the complexity features.

In summary, Area is more useful then NF-area. However, NF-turns are more useful than turns. In general, NF-MUPs contain more useful complexity information that can be automatically extracted and used to better distinguish better between normal muscles and muscles affected by myopathic and neurogenic disorders.

References

[1] M. AbdelMaseeh, T. Chen, P. Poupart, B. Smith, and D. Stashuk. Transparent muscle characterization using quantitative electromyography: Different binarization mappings. *Neural Systems and Rehabilitation Engineering, IEEE Transactions on*, 22(3):511–521, May 2014.

[2] M. AbdelMaseeh, T. Chen, and D. Stashuk. Extraction and classification of multichannel electromyographic activation trajectories for hand movement recognition. *Neural Systems and Rehabilitation Engineering, IEEE Transactions on*, PP(99):1–1, 2015.

[3] M. Abdelmaseeh, P. Poupart, B. Smith, and D. Stashuk. Muscle categorization using quantitative needle electromyography: A 2-stage Gaussian mixture model based approach. In *Proceedings of the 2012 11th International Conference on Machine Learning and Applications - Volume 01*, ICMLA '12, pages 548–553, 2012.

[4] M. AbdelMaseeh, B. Smith, and D. Stashuk. Detecting neuropathy using measures of motor unit activation extracted from standard concentric needle electromyographic signals. In *Engineering in Medicine and Biology Society (EMBC), 2014 36th Annual International Conference of the IEEE*, pages 4066–4070, Aug 2014.

[5] M. AbdelMaseeh, B. Smith, and D. Stashuk. Detecting neuropathy using measures of motor unit activation extracted from standard concentric needle electromyographic signals. In *Engineering in Medicine and Biology Society (EMBC), 2014 36th Annual International Conference of the IEEE*, pages 4066–4070. IEEE, 2014.

[6] M. Abdelmaseeh, B. Smith, and D. Stashuk. Feature selection for motor unit potential train characterization. *Muscle & Nerve*, 49(5):680–690, 2014.

[7] M. AbdelMaseeh, B. Smith, and D. Stashuk. An automated decomposition algorithm of electromyographic signals tailored for characterization of neuromuscular disorders. Submitted for publication, December 2015.

[8] E. L. Allwein, R. Schapire, and Y. Singer. Reducing multiclass to binary: a unifying approach for margin classifiers. *J. Mach. Learn. Res.*, 1:113–141, Sep 2001.

[9] C. Bishop. *Pattern Recognition and Machine Learning (Information Science and Statistics)*. Springer-Verlag New York, Inc., Secaucus, NJ, USA, 2006.

[10] M. Brand and K. Huang. A unifying theorem for spectral embedding and clustering. In *Proceedings of the Ninth International Workshop on Artificial Intelligence and Statistics*, 2003.

[11] A. Buchman and M. Garratt. Determining neuromuscular jitter using a monopolar electrode. *Muscle & Nerve*, 15(5):615–619, 1992.

[12] F. Buchthal and S. Clemmesen. On the differentiation of muscle atrophy by electromyography. *Acta Psychiatrica Scandinavica*, 16(2-3):143–181, 1941.

[13] F. Buchthal, C. Guld, and P. Rosenfalck. Action potential parameters in normal human muscle and their dependence on physical variables. *Acta Physiologica Scandinavica*, 32(2-3):200–218, 1954.

[14] F. Buchthal, C. Guld, and P. Rosenfalck. Action potential parameters in different human muscles. *Acta Psychiatrica Scandinavica*, 30(1-2):125–131, 1955.

[15] F. Buchthal and P. Pinelli. Analysis of muscle action potentials as a diagnostic aid in neuro-muscular disorders. *Acta Medica Scandinavica*, 142(S266):315–327, 1952.

[16] C. Campos, A. Malanda, L. Gila, V. Segura, I. Lasanta, and J. Artieda. Quantification of jiggle in real electromyographic signals. *Muscle & Nerve*, 23(7):1022–1034, 2000.

[17] C. Campos, A. Malanda, L. Gila, V. Segura, I. Lasanta, and J. Artieda. Quantification of jiggle in real electromyographic signals. *Muscle & Nerve*, 23(7):1022–1034, 2000.

[18] T. Chen, M. Abdelmaseeh, and D. Stashuk. Affine and regional dynamic time warpng. *arXiv preprint arXiv:1505.06531*, 2015.

[19] A. Cherian, N. Baheti, and T. Iype. Electrophysiological study in neuromuscular junction disorders. *Annals of Indian Academy of Neurology*, 16(1):34, 2013.

[20] C. Christodoulou and C. Pattichis. Unsupervised pattern recognition for the classification of EMG signals. *Biomedical Engineering, IEEE Transactions on*, 46(2):169–178, 1999.

[21] F. Chung. *Spectral graph theory*. American Mathematical Soc., 1997.

[22] W. Cohen. Fast effective rule induction. In *Proceedings of the Twelfth International Conference on Machine Learning*, pages 115–123, 1995.

[23] C. Cortes and V. Vapnik. Support-vector networks. *Machine learning*, 20(3):273–297, 1995.

[24] R. Daube and D. Rubin. Needle electromyography. *Muscle & Nerve*, 39(2):244–270, 2009.

[25] C. De Luca and Z. Erim. Common drive of motor units in regulation of muscle force. *Trends Neurosci.*, 17(7):299–305, Jul 1994.

[26] C. De Luca and J. Kline. Statistically rigorous calculations do not support common input and long-term synchronization of motor-unit firings. *Journal of neurophysiology*, 112(11):2729–2744, 2014.

[27] F. Dodge and J. Cooley. Action potential of the motorneuron. *IBM Journal of Research and Development*, 17(3):219–229, 1973.

[28] W. Donath and A. Hoffman. Lower bounds for the partitioning of graphs. *IBM Journal of Research and Development*, 17(5):420–425, 1973.

[29] L. Dorfman, J. Howard, and K. McGill. Motor unit firing rates and firing rate variability in the detection of neuromuscular disorders. *Electroencephalography and Clinical Neurophysiology*, 73(3):215 – 224, 1989.

[30] D. Dumitru, D. Stegeman, and M. Zwarts. Electrical sources and volume conduction. In D. Dumitru, A. Amato, and M. Zwarts, editors, *Electrodiagnostic Medicine*, chapter 2. Hanley & Belfus, 4th edition, Jul 2000.

[31] J. Durbin and G. Watson. Testing for serial correlation in least squares regression. i. *Biometrika*, 37(3-4):409–428, 1950.

[32] J. Ekstedt. Human single muscle fibre action potentials. *Acta Physiol Scand*, 61:1–96, 1964.

[33] M. Ertaş, M. Baslo, N. Yildiz, J. Yazici, and A. Őge. Concentric needle electrode for neuromuscular jitter analysis. *Muscle & Nerve*, 23(5):715–719, 2000.

[34] D. Farina, A. Crosetti, and R. Merletti. Evaluation of intra-muscular EMG signal decomposition algorithms. *Journal of Electromyography and Kinesiology*, 11(3):175 – 187, 2001.

[35] D. Farina, A. Crosetti, and R. Merletti. A model for the generation of synthetic intramuscular EMG signals to test decomposition algorithms. *Biomedical Engineering, IEEE Transactions on*, 48(1):66–77, Jan 2001.

[36] D. Farina, H. Rehbaum, A. Holobar, I. Vujaklija, J. Ning, C. Hofer, S. Salminger, H. van Vliet, and O. Aszmann. Noninvasive, accurate assessment of the behavior of representative populations of motor units in targeted reinnervated muscles. *Neural Systems and Rehabilitation Engineering, IEEE Transactions on*, 22(4):810–819, July 2014.

[37] C. Farkas, A. Hamilton-Wright, A. Parsaei, and D. Stashuk. A review of clinical quantitative electromyography. *Critical Reviews in Biomedical Engineering*, 38(5):467–485, 2010.

[38] J. Florestal, P. Mathieu, and A. Malanda. Automated decomposition of intramuscular electromyographic signals. *IEEE Trans. Biomed. Engineering*, 53(5):832–839, 2006.

[39] M. Forsman, R. Kadefors, Q. Zhang, L. Birch, and G. Palmerud. Motor-unit recruitment in the trapezius muscle during arm movements and in VDU precision work. *International Journal of Industrial Ergonomics*, 24(6):619 – 630, 1999.

[40] A. Fuglsang-Frederiksen, T. Smith, and H. Høgenhaven. Motor unit firing intervals and other parameters of electrical activity in normal and pathological muscle. *Journal of the Neurological Sciences*, 78(1):51 – 62, 1987.

[41] J. Fürnkranz. Round robin rule learning. In *Proceedings of the 18th International Conference on Machine Learning (ICML-01):146– 153*, pages 146–153. Morgan Kaufmann, 2001.

[42] J. Fürnkranz and G. Widmer. Incremental reduced error pruning. In William W. Cohen and H. Hirsh, editors, *Proceedings of the 11th International Conference on Machine Learning*, pages 70–77, 1994.

[43] A. Gerber, R. Studer, R. de Figueiredo, and G. Moschytz. A new framework and computer program for quantitative EMG signal analysis. *Biomedical Engineering, IEEE Transactions on*, (12):857–863, 1984.

[44] S. Greenberg and A. Amato. *EMG Pearls*. Pearls series. Hanley & Belfus, 2004.

[45] L. Grimby, K. Holm, and k. Sjöuström. Abnormal use of remaining motor units during locomotion in peroneal palsy. *Muscle & Nerve*, 7(4):327–331, 1984.

[46] O. Grygorash, Yan Z., and Z. Jorgensen. Minimum spanning tree based clustering algorithms. In *Tools with Artificial Intelligence, 2006. ICTAI '06. 18th IEEE International Conference on*, pages 73–81, Nov 2006.

[47] I. Guyon and A. Elisseeff. An introduction to feature extraction. In Isabelle Guyon, Masoud Nikravesh, Steve Gunn, and Lotfi Zadeh, editors, *Feature Extraction*, vol-

ume 207 of *Studies in Fuzziness and Soft Computing*, pages 1–25. Springer Berlin / Heidelberg, 2006.

[48] J. Halonen, B. Falck, and H. Kalimo. The firing rate of motor units in neuromuscular disorders. *Journal of Neurology*, 225(4):269–276, 1981.

[49] T. Hamamura, H. Mizutani, and B. Irie. A multiclass classification method based on multiple pairwise classifiers. In *Document Analysis and Recognition, 2003. Proceedings. Seventh International Conference on*, pages 809–813, 2003.

[50] A. Hamilton-Wright and D. Stashuk. Physiologically based simulation of clinical EMG signals. *Biomedical Engineering, IEEE Transactions on*, 52(2):171–183, Feb. 2005.

[51] A. Hamilton-Wright, D. Stashuk, and T. Doherty. Simulation of disease effects on muscle structure, activation and acquired electromyography. *Muscle & Nerve*, 28(S12), 2003.

[52] J. Harper. *Clinical Neurophysiology*, chapter Single Fibre ELectromyograph. Contemporary Neurology Series. Oxford University Press, USA, 2009.

[53] T. Hastie and R. Tibshirani. Classification by pairwise coupling. In *Proceedings of the 1997 conference on advances in neural information processing systems 10*, NIPS '97, 1998.

[54] k. He. Automated measurement of neuromuscular jitter based on EMG signal decomposition. Master's thesis, University of Waterloo, Waterloo, Ontario, Canada, 2007.

[55] E. Henneman. Relation between size of neurons and their susceptibility to discharge. *Science*, 126(3287):1345–1347, 1957.

[56] N. Hirsch. Neuromuscular junction in health and disease. *British journal of anaesthesia*, 99(1):132–138, 2007.

[57] C. Hsu and C. Lin. A comparison of methods for multiclass support vector machines. *Neural Networks, IEEE Transactions on*, 13(2):415 –425, Mar 2002.

[58] T. Jebara and V. Shchogolev. B-matching for spectral clustering. In *Machine learning: Ecml 2006*, pages 679–686. Springer, 2006.

[59] N. Jiang, P. Parker, and K. Englehart. Modeling of muscle motor unit innervation process correlation and common drive. *IEEE Trans Biomed Eng*, 53(8):1605–1614, Aug 2006.

[60] S. Kanoun and N. Ali. A new digital signal processing technique for the estimation of motor unit action potential templates. In *Computer Engineering Systems, 2009. ICCES 2009. International Conference on*, pages 537–542, Dec 2009.

[61] C. Katsis, T. Exarchos, C. Papaloukas, Y. Goletsis, D. Fotiadis, and I. Sarmas. A two-stage method for MUAP classification based on EMG decomposition. *Computers in Biology and Medicine*, 37(9):1232 – 1240, 2007.

[62] C. Katsis, Y. Goletsis, A. Likas, D. Fotiadis, and I. Sarmas. A novel method for automated EMG decomposition and MUAP classification. *Artificial Intelligence in Medicine*, 37(1):55 – 64, 2006.

[63] R. Kendall and R. Werner. Interrater reliability of the needle examination in lumbosacral radiculopathy. *Muscle & Nerve*, 34(2):238–241, Aug 2006.

[64] E. Keogh and C. Ratanamahatana. Exact indexing of dynamic time warping. *Knowledge and information systems*, 7(3):358–386, 2005.

[65] H. Khosravi and B. Bina. A survey on statistical relational learning. In *Advances in Artificial Intelligence*, pages 256–268. Springer, 2010.

[66] S. Kim, S. Park, and W. Chu. An index-based approach for similarity search supporting time warping in large sequence databases. In *Data Engineering, 2001. Proceedings. 17th International Conference on*, pages 607–614, 2001.

[67] J. Kimura. *Electrodiagnosis in diseases of nerve and muscle: principles and practice.* Oxford university press, 2013.

[68] T. Kohonen. The self-organizing map. *Neurocomputing*, 21(13):1 – 6, 1998.

[69] E. Kugelberg. Electromyography in muscular dystrophies; differentiation between dystrophies and chronic lower motor neurone lesions. *J. Neurol. Neurosurg. Psychiatr.*, 12:129–136, May 1949.

[70] G. Loudon, N. Jones, and A. Sehmi. New signal processing techniques for the decomposition of EMG signals. *Med Biol Eng Comput*, 30(6):591–599, Nov 1992.

[71] T. Luu. Approach to evaluating clustering using classification labelled data. Master's thesis, University of Waterloo, 2011.

[72] S. Ma. Measuring neuromuscular jitter in motor unit potentials. Master's thesis, University of Waterloo, Waterloo, Ontario, Canada, 2003.

[73] B. Mambrito and C. De Luca. Acquisition and decomposition of the EMG signal. In *Computer-aided electromyography*, volume 10, pages 52–72. 1983.

[74] B. Mambrito and C. De Luca. A technique for the detection, decomposition and analysis of the EMG signal. *Electroencephalography and Clinical Neurophysiology*, 58(2):175 – 188, 1984.

[75] H. Mamitsuka. Selecting features in microarray classification using ROC curves. *Pattern Recognition*, 39(12):2393 – 2404, 2006.

[76] K. McGill, K. Cummins, and L. Dorfman. Automatic decomposition of the clinical electromyogram. *Biomedical Engineering, IEEE Transactions on*, (7):470–477, 1985.

[77] K. McGill and L. Dorfman. High-resolution alignment of sampled waveforms. *Biomedical Engineering, IEEE Transactions on*, BME-31(6):462–468, June 1984.

[78] K. McGill and L. Dorfman. Automatic decomposition electromyography (ADEMG): validation and normative data in brachial biceps. *Electroencephalography and Clinical Neurophysiology*, 61(5):453 – 461, 1985.

[79] K.C. McGill and H. Marateb. Rigorous a posteriori assessment of accuracy in EMG decomposition. *Neural Systems and Rehabilitation Engineering, IEEE Transactions on*, 19(1):54–63, Feb 2011.

[80] J. Milgram, M. Cheriet, and R. Sabourin. "one against one" or "one against all": which one is better for handwriting recognition with SVMs? In *Tenth International Workshop on Frontiers in Handwriting Recognition*, Oct 2006.

[81] S. Nandedkar, P. Barkhaus, D. Sanders, and E. Stålberg. Analysis of amplitude and area of concentric needle EMG motor unit action potentials. *Electroencephalography and Clinical Neurophysiology*, 69(6):561 – 567, 1988.

[82] S. Nandedkar, D. Sanders, E. Stålberg, and S. Andreassen. Simulation of concentric needle EMG motor unit action potentials. *Muscle & Nerve*, 11(2):151–159, 1988.

[83] S. Nandedkar and E. Stålberg. Simulation of single muscle fibre action potentials. *Medical and Biological Engineering and Computing*, 21(2):158–165, 1983.

[84] S. Nandedkar, E. Stålberg, and D. Sanders. Quantitative EMG. In D. Dumitru, A. Amato, and M. Zwarts, editors, *Electrodiagnostic Medicine*, chapter 8. Hanley & Belfus, 4th edition, July 2000.

[85] J. Navallas, A. Malanda, and J. Rodriguez-Falces. Maximum likelihood estimation of motor unit firing pattern statistics. *Neural Systems and Rehabilitation Engineering, IEEE Transactions on*, 22(3):460–469, May 2014.

[86] A. Ng, M. Jordan, and Y. Weiss. On spectral clustering: Analysis and an algorithm. *Advances in neural information processing systems*, 2:849–856, 2002.

[87] M. Nikolic and C. Krarup. EMGTools, an adaptive and versatile tool for detailed EMG analysis. *Biomedical Engineering, IEEE Transactions on*, 58(10):2707–2718, 2011.

[88] National Institute of Neurological Disorders and Stroke. Amyotrophic lateral sclerosis fact sheet. 2008.

[89] S. Pan and Q. Yang. A survey on transfer learning. *Knowledge and Data Engineering, IEEE Transactions on*, 22(10):1345–1359, 2010.

[90] H. Parsaei and D. Stashuk. SVM-Based validation of motor unit potential trains extracted by EMG signal decomposition. *Biomedical Engineering, IEEE Transactions on*, 59(1):183 –191, Jan 2012.

[91] J. Patten. *Neurological differential diagnosis*. Springer Science & Business Media, 1982.

[92] C. Pattichis and M. Pattichis. Time-scale analysis of motor unit action potentials. *Biomedical Engineering, IEEE Transactions on*, 46(11):1320 –1329, nov. 1999.

[93] C. Pattichis, C. Schizas, and L. Middleton. Neural network models in EMG diagnosis. *Biomedical Engineering, IEEE Transactions on*, 42(5):486 –496, May 1995.

[94] J. Payan. The blanket principle: A technical note. *Muscle & Nerve*, 1(5):423–426, 1978.

[95] G. Pfeiffer and K. Kunze. Turn and phase counts of individual motor unit potentials: correlation and reliability. *Electroencephalogr Clin Neurophysiol*, 85(3):161–165, Jun 1992.

[96] G. Pfeiffer and K. Kunze. Frequency analysis and duration of motor unit potentials: reliability and diagnostic usefulness. *Electroencephalogr Clin Neurophysiol*, 89(6):365–374, Dec 1993.

[97] G. Pfeiffer and K. Kunze. Discriminant classification of motor unit potentials (MUPs)successfully separates neurogenic and myopathic conditions. a comparion of multi- and univariate diagnostical algorithms for MUP analysis. *Electroencephalography and Clinical Neurophysiology Electromyography and Motor Control*, 97(5):191 – 207, 1995.

[98] L. Pino, D. Stashuk, and Timothy J. Doherty. Motor unit potential characterization using "pattern discovery". *Medical Engineering Physics*, 30(5):563 – 573, 2008.

[99] J. Platt, N. Cristianini, and J. Shawe-taylor. Large margin DAGs for multiclass classification. In *Advances in Neural Information Processing Systems*, pages 547–553. MIT Press, 2000.

[100] D. Price, S. Knerr, L. Personnaz, and G. Dreyfus. Pairwise neural network classifiers with probabilistic outputs. In *Neural Information Processing Systems*, volume 7, pages 1109–1116, 1994.

[101] P. Pudil, J. Novovičová, and J. Kittler. Floating search methods in feature selection. *Pattern Recognition Letters*, 15(11):1119 – 1125, 1994.

[102] W. Rall. Theory of physiological properties of dendrites. *Annals of the New York Academy of Sciences*, 96(4), 1962.

[103] D. Reynolds, T. Quatieri, and R. Dunn. Speaker verification using adapted Gaussian mixture models. *Digital Signal Processing*, 10:19 – 41, 2000.

[104] P. Rousseeuw. Silhouettes: a graphical aid to the interpretation and validation of cluster analysis. *Journal of computational and applied mathematics*, 20:53–65, 1987.

[105] L. Rowland. Diseases of the motor unit. In E. R. Kandel, J. H. Schwartz, and T. M. Jessell, editors, *Principles of Neural Science*, chapter 35. McGraw-Hill Medical, 4th edition, July 2000.

[106] J. Saboisky, D. Stashuk, A. Hamilton-Wright, A. Carusona, L. Campana, J. Trinder, D. Eckert, A. Jordan, D. McSharry, D. White, S. Nandedkar, W. David, and A. Malhotra. Neurogenic changes in the upper airway of patients with obstructive sleep apnea. *Am. J. Respir. Crit. Care Med.*, 185(3):322–329, Feb 2012.

[107] H. Sakoe and S. Chiba. Dynamic programming algorithm optimization for spoken word recognition. *Acoustics, Speech and Signal Processing, IEEE Transactions on*, 26(1):43–49, Feb 1978.

[108] D. Sanders. Clinical impact of single-fiber electromyography. *Muscle & Nerve*, 25(S11):S15–S20, 2002.

[109] D. Sanders and E. Stålberg. AANEM minimonograph# 25: Single-fiber electromyography. *Muscle & nerve*, 19(9):1069–1083, 1996.

[110] P. Sarrigiannis, R. Kennett, S. Read, and M. Farrugia. Single-fiber EMG with a concentric needle electrode: Validation in myasthenia gravis. *Muscle & Nerve*, 33(1):61–65, 2006.

[111] A. Savitzky and M. Golay. Smoothing and differentiation of data by simplified least squares procedures. *Analytical Chemistry*, 36(8):1627–1639, 1964.

[112] R. Schafer. On the frequency-domain properties of Savitzky-Golay filters. In *Digital Signal Processing Workshop and IEEE Signal Processing Education Workshop (DSP/SPE), 2011 IEEE*, pages 54–59, Jan 2011.

[113] J. Shi and J. Malik. Normalized cuts and image segmentation. *Pattern Analysis and Machine Intelligence, IEEE Transactions on*, 22(8):888–905, 2000.

[114] W. Siedlecki. A formula for multi-class distributed classifiers. *Pattern Recognition Letters*, 15(8):739 – 742, 1994.

[115] M. Sonoo and E. Stålberg. The ability of MUP parameters to discriminate between normal and neurogenic MUPs in concentric EMG: analysis of the MUP thickness and the proposal of size index. *Electroencephalography and Clinical Neurophysiology Evoked Potentials Section*, 89(5):291–303, 1993.

[116] E. Stålberg. Propagation velocity in single human muscle fibres. *Acta Physiol Scand*, suppl 287:1–112, 1964.

[117] E. Stålberg. Jitter analysis with concentric needle electrodes. *Annals of the New York Academy of Sciences*, 1274(1):77–85, 2012.

[118] E. Stålberg, J. Ekstedt, and A. Broman. The electromyographic jitter in normal human muscles. *Electroencephalography and Clinical Neurophysiology*, 31(5):429 – 438, 1971.

[119] E. Stålberg, B. Falck, M. Sonoo, S. Stålberg, and M. Åström. Multi-MUP EMG analysisa two year experience in daily clinical work. *Electroencephalography and Clinical Neurophysiology/Electromyography and Motor Control*, 97(3):145–154, 1995.

[120] E. Stålberg, S. Nandedkar, D. Sanders, and B. Falck. Quantitative motor unit potential analysis. *Journal of clinical neurophysiology*, 13(5):401–422, 1996.

[121] E. Stålberg and M. Sonoo. Assessment of variability in the shape of the motor unit action potential, the jiggle, at consecutive discharges. *Muscle & Nerve*, 17(10):1135–1144, 1994.

[122] D. Stashuk. Simulation of electromyographic signals. *J Electromyogr Kinesiol*, 3(3):157–173, 1993.

[123] D Stashuk. Mean, median and mode estimation of motor unit action potential templates. In *Engineering in Medicine and Biology Society, 1996. Bridging Disciplines for Biomedicine. Proceedings of the 18th Annual International Conference of the IEEE*, volume 4, pages 1498–1499. IEEE, 1996.

[124] D. Stashuk. Decomposition and quantitative analysis of clinical electromyographic signals. *Medical Engineering Physics*, 21(67):389 – 404, 1999.

[125] D. Stashuk. Detecting single fiber contributions to motor unit action potentials. *Muscle & Nerve*, 22(2):218–229, 1999.

[126] D. Stashuk. Detecting single fiber contributions to motor unit action potentials. *Muscle & Nerve*, 22(2):218–229, 1999.

[127] D. Stashuk. EMG signal decomposition: how can it be accomplished and used? *Journal of Electromyography and Kinesiology*, 11(3):151 – 173, 2001.

[128] D. Stashuk, M. AbdelMaseeh, and B. Smith. Looking under the blanket for better measures of motor unit potential size and complexity. *Muscle & Nerve*, 48(4):669–669, 2013.

[129] D. Stashuk and Y. Qu. Adaptive motor unit action potential clustering using shape and temporal information. *Medical and Biological Engineering and Computing*, 34(1):41–49, 1996.

[130] D. Stashuk and Y. Qu. Robust method for estimating motor unit firing-pattern statistics. *Medical and Biological Engineering and Computing*, 34(1):50–57, 1996.

[131] R. Studer, R. de Figueiredo, and G. Moschytz. An algorithm for sequential signal estimation and system identification for EMG signals. *Biomedical Engineering, IEEE Transactions on*, BME-31(3):285–295, March 1984.

[132] R. Traub. A model of a human neuromuscular system for small isometric tensions. *Biological Cybernetics*, 26(3), 1977.

[133] R. Traub. Motorneurons of different geometry and the size principle. *Biol Cybern*, 25(3):163–176, Feb 1977.

[134] S. Usui and I. Amidror. Digital low-pass differentiation for biological signal processing. *Biomedical Engineering, IEEE Transactions on*, BME-29(10):686–693, Oct 1982.

[135] G. Vivó-Truyols, J. Torres-Lapasió, A. van Nederkassel, H. Vander Heyden, and D. Massart. Automatic program for peak detection and deconvolution of multi-overlapped chromatographic signals: Part i: Peak detection. *Journal of Chromatography A*, 1096(12):133 – 145, 2005.

[136] U. Von Luxburg. A tutorial on spectral clustering. *Statistics and computing*, 17(4):395–416, 2007.

[137] J. N. Walton. The electromyogram in myopathy: analysis with the audio-frequency spectrometer. *J. Neurol. Neurosurg. Psychiatr.*, 15(4):219–226, Nov 1952.

[138] X. Wang. Automatically measuring neuromuscular jitter. Master's thesis, University of Waterloo, Waterloo, Ontario, Canada, 2005.

[139] Y. Wang and A. Wong. From association to classification: inference using weight of evidence. *Knowledge and Data Engineering, IEEE Transactions on*, 15(3):764–767, 2003.

[140] D. Wiechers. Single fiber EMG evaluation in denervation and reinnervation. *Muscle & Nerve*, 13(9):829–832, 1990.

[141] A. Wong and Y. Wang. Discovery of high order patterns. In *Systems, Man and Cybernetics, 1995. Intelligent Systems for the 21st Century., IEEE International Conference on*, volume 2, pages 1142 –1147, Oct 1995.

[142] A. Wong and Y. Wang. Pattern discovery: a data driven approach to decision support. *Systems, Man, and Cybernetics, Part C: Applications and Reviews, IEEE Transactions on*, 33(1):114 –124, Feb 2003.

[143] B. Yi, H. Jagadish, and C. Faloutsos. Efficient retrieval of similar time sequences under time warping. In *Data Engineering, 1998. Proceedings., 14th International Conference on*, pages 201–208, 1998.

[144] E. Zalewska and I. Hausmanowa-Petrusewicz. Evaluation of MUAP shape irregularity-a new concept of quantification. *Biomedical Engineering, IEEE Transactions on*, 42(6):616 –620, June 1995.